



**HAL**  
open science

# Orthogonal Precoder for Dynamic Spectrum Access in Wireless Networks

Leonardo Sampaio Cardoso

► **To cite this version:**

Leonardo Sampaio Cardoso. Orthogonal Precoder for Dynamic Spectrum Access in Wireless Networks. Other. Supélec; Universidade federal do Ceará, 2011. English. NNT : 2011SUPL0018 . tel-00839860

**HAL Id: tel-00839860**

**<https://theses.hal.science/tel-00839860>**

Submitted on 1 Jul 2013

**HAL** is a multi-disciplinary open access archive for the deposit and dissemination of scientific research documents, whether they are published or not. The documents may come from teaching and research institutions in France or abroad, or from public or private research centers.

L'archive ouverte pluridisciplinaire **HAL**, est destinée au dépôt et à la diffusion de documents scientifiques de niveau recherche, publiés ou non, émanant des établissements d'enseignement et de recherche français ou étrangers, des laboratoires publics ou privés.



N° d'ordre : 2011-18-TH

# THÈSE DE DOCTORAT

## SPÉCIALITÉ: PHYSIQUE

École doctorale “Sciences et Technologies de l’Information, des  
Télécommunications et des Systèmes”

*Présenté par:*

**Leonardo S. CARDOSO**

Sujet:

Précodage Orthogonal pour l’Accès Dynamique au Spectre dans les Réseaux Sans Fils  
(*Orthogonal Precoder for Dynamic Spectrum Access in Wireless Networks*)

Soutenue le 18 novembre 2011 devant les membres du jury (liste provisionnelle):

M. Mérouane Debbah,	Chaire Alcatel-Lucent/Supélec - Gif	Directeur de Thèse
Mme. Mari Kobayashi,	Département Télécom/Supélec - Gif	Co-encadrant
M. F. Rodrigo P. Cavalcanti,	DETI/UFC	Co-encadrant (co-tutelle)
M. Luis da Silva,	Virginia Tech	Rapporteur
Mme. Maria-Gabriella di Benedetto,	Université de Rome La Sapienza	Rapporteur
M. Markus Mueck,	ETSI	Examinateur
M. Jean-Marie Gorce,	INSA - Lyon	Examinateur
M. Pierre Duhamel,	LSS - Gif	Représentant Orsay
M. Jacques Palicot,	SCEE/Supélec - Rennes	Invité
M. Charles C. Cavalcanti,	DETI/UFC	Invité
M. João César M. Mota,	DETI/UFC	Invité



## Acknowledgments

**T**HE DEVELOPMENT of a Ph.D. work can be a very humbling experience, since it is a period of self discovery and limits surpassing. Of course one can trail this path alone, but the help of others make the ride much more enjoyable and fulfilling. This truth also applies to myself and to this Ph.D. work, which has been made possible by the presence of many brilliant people.

I would like to start by expressing my deepest gratitude to my three Ph.D. advisors:

**Prof. Merouane Debbah**, for his technical support, crucial for the positive outcome of this work; for all the advices and encouragements not spared in the moments of doubt and deception; for all his unconditional support during the adversities this thesis has brought along; for his friendship;

**Prof. F. Rodrigo P. Cavalcanti**, for his belief in my qualities as a researcher, encouraging me when opportunities or doubts arrived; for his insightful technical discussions that often enlightened aspects of my work to which I was oblivious; for his friendship;

**Dr. Mari Kobayashi**, for her technical support, passing on techniques and tools essential for the work; for redirecting my efforts in a methodical and scholarly way, which allowed me to stay focused, even when overwhelmed by the complexity of the problems at hand.

The last months of this Ph.D. work were essential for its success, and its closing could not have been accomplished without the supportive and insightful comments from the thesis Jury.

I also want to thank my colleagues and friends for all the insightful discussions, collaborations and caring that contributed (directly or indirectly) to many of my research results. Among them I would like to highlight the names of **Raul de Lacerda**, **Marco Maso**, **Ejder Bastug**, **Jakob Hoydis**, **Najett Neji**, **Samir M. Perlaza**, **Veronica Belmega**, **Salam Akoum**, **Subhash Lakshminarayana**, **Romain Couillet**, **Marios Kountouris**, **Sylvain Azarian**, **Luca Rose**, **Karim Tadrist**, **Antonia Masucci**, **Alonso Silva**, **Florence Faucitano**, **Amor Nafka**, **Wassim Jouini** and **Sharon Betz**. Without their collaboration, judicious comments, technical discussions, publication reviews or even mere words of support, this thesis would have not been possible. On the same note, I would also like to thank **Prof. Jacques Palicot**, **Prof. Pascal Bianchi**, **Prof. Jamal Najim**, **Walid Hachem** and **Prof. Mylène Maïda** for their collaboration and technical discussions.

I would like to demonstrate my appreciation of all the financial, material and logistics support received from **Alcatel-Lucent**, the **Alcatel-Lucent Chair in Flexible Radio**, **Supélec**, the **Universidade Federal do Ceará**, **GTEL** and **CAPES-COFECUB**.

## IV

I wish I could easily express all the joy I feel for having been part of the Alcatel-Lucent Chair in Flexible Radio, especially of being one of its “founding fathers”. Clearly, the ambiance of friendship and hard work cultivated in the “Chair” (as we call it in the intimacy), have taught me that the pursue of high quality work is not incompatible with being playful and fun. In fact it is quite the contrary: strong human bonds foster collective creativity and group work. I hope that this kind of ambiance goes on and becomes one of the trademarks of this wonderful group.

I also wish to express my deepest indebtedness to my family for all the affection as well as personal and logistical support. Coming from a family rooted in the academia served as a great inspiration to pursue research and carry out a Ph.d.

Last, but definitely not least, one very especial thought goes to my companion **Justine**, who, with great caring, understanding and support helped me through (various) moments of turbulence.

*Thank you all — Merci beaucoup — Muito obrigado.*

– Leonardo S. Cardoso

# Résumé

Le déferlement mondial des services de télécommunications, impose, aux réseaux qui les supportent, d'augmenter de plus en plus leurs capacités afin de subvenir aux besoins de ses utilisateurs dont le nombre ne cesse de croître. Le spectre radio, ressource de base pour les communications sans fils, ne suit malheureusement pas cette croissance. Même si des marges réutilisables sont disponibles, leur accès est limité par des politiques strictes de gestion du spectre radio-fréquentiel. Pour remédier à cette situation, les organismes régulateurs des télécommunications se dirigent vers un paradigme de gestion plus flexible, en autorisant de nouvelles méthodes basées sur l'accès dynamique au spectre (DSA - *dynamic spectrum access*) et les radio cognitives (CR - *cognitive radio*).

Dans ce travail doctoral, est proposée une nouvelle technique pour traiter la problématique de la disponibilité du spectre radio-fréquentiel. Appelée multiplexage fréquentiel par sous-espace de Vandermonde (VFDM - *Vandermonde-subspace frequency division multiplexing*), elle permet à deux technologies d'accès radio (RATs - *radio access technologies*) de fonctionner côte-a-côte dans un environnement de petites cellules CR. Ceci se fait en partageant la bande radio tout en protégeant des interférences les systèmes pour lesquels le spectre radio avait été originellement réservé. VFDM transmet les données pré-codées dans le noyau du canal interférant entre l'émetteur opportuniste et le récepteur originel en utilisant la sélectivité en fréquence des canaux et duplexage temporel (TDD - *time division duplexing*).

Le travail de cette thèse propose une approche exhaustive du développement de la technologie VFDM, en allant des bases théoriques jusqu'à la démonstration de faisabilité. Ainsi, les bases théoriques proposées ont été en premier lieu analysées. Puis, en partant de ces bases théoriques, VFDM a été graduellement développé vers une chaîne émetteur-récepteur complète. Des résultats significatifs sont apparus à mi-chemin dans la phase de développement, comme par exemple, l'établissement de stratégies de précodage optimales ou la mise en évidence d'aspects critiques lors de l'implémentation.

Sous certaines conditions, VFDM permet aux réseaux secondaires opportunistes d'être utilisés en même temps que le réseau originel, aux seules contraintes de la connaissance des canaux et de l'accroissement de la complexité du système. Au travers des résultats obtenus en simulation, il a été démontré que des taux de transfert de données significatifs peuvent être atteints, et ce, malgré que les capacités de VFDM soient toujours limitées par la taille du sous-espace de Vandermonde du canal interfèrent primaire-secondaire. Finalement, la chaîne émetteur-récepteur développée démontre la faisabilité de cette méthode.



# Resumo

À medida que serviços de comunicações pessoais (PCS, do inglês *personal communications services*) são instalados em todo o mundo, maior é a pressão por redes de maior capacidade para acomodar uma base de usuários em crescimento exponencial. Por outro lado, o espectro de rádio, recurso básico em comunicações sem fio, não é capaz de crescer na mesma proporção. Ainda que o uso do espectro atual deixe margens para reutilização, isto é limitado pela a atual política de gestão do espectro, que é fixa. Para remediar este problema, agências de regulação de espectro estão migrando um paradigma de gestão flexível, aproveitando novas técnicas de acesso dinâmico ao espectro (DSA, do inglês *dynamic spectrum access*) baseados em rádio cognitivo (CR, do inglês *cognitive radio*).

Neste trabalho de doutorado, uma nova tecnologia de CR-DSA é apresentada visando aliviar o problema de escassez de espectro. Propomos a multiplexagem por divisão em frequência usando sub-espço de Vandermonde (VFDM, do inglês *Vandermonde-subspace frequency division multiplexing*), que permite a duas tecnologias de acesso de rádio (RAT, do inglês *radio access technology*) coexistirem em um ambiente de CR baseado no conceito de pequenas células (do inglês *small-cells*) e compartilhando a banda ao mesmo tempo que protege o sistema legado de interferência. VFDM transmite dados pré-codificados no espaço nulo do canal interferente cruzado (canal do transmissor secundário ao receptor primário), presumindo seletividade de frequência e duplexação por divisão em tempo (TDD, do inglês *time division duplexing*).

Este trabalho de doutorado propõe uma abordagem exaustiva para o desenvolvimento do VFDM: indo desde a base teórica até o desenvolvimento de uma prova de conceito. Inicialmente, o fundamento teórico, base da técnica em si, foi apresentada e analisada. Então, o VFDM foi gradualmente desenvolvido a partir de um conceito matemático até um transceptor completo. Durante esse desenvolvimento, vários resultados intermediários importantes foram desenvolvidos, como a extensão do VFDM ao caso multi-usuário e aspectos críticos de implementação.

Sob algumas restrições, o VFDM se mostra capaz de permitir que uma rede secundária oportunista coexista com a uma rede primária legada, a partir do conhecimento canal e sob o custo de maior complexidade. Por meio de exemplos numéricos, é demonstrado que taxas significativa são possíveis de serem alcançadas, embora o desempenho do VFDM seja limitado pelo tamanho do subespaço nulo do canal interferente entre o transmissor secundário e o receptor primário. Finalmente, a implementação do transceptor VFDM é mostrada, fornecendo uma prova de conceito da técnica.



# Abstract

The global deployment of personal communications services (PCS) is pushing for more and more network capacity to accommodate an exponentially growing user base. Radio spectrum, the basic resource in radio communications, unfortunately does not follow this growth. Even though the current spectrum usage leaves margins for re-use, it is limited by the current fixed spectrum management policies. To remediate this issue, spectrum regulators are switching to a flexible management paradigm, leveraging new dynamic spectrum access (DSA) schemes based on cognitive radio (CR).

In this PhD work, a novel CR-DSA technology is introduced to address spectrum scarcity problem. Called Vandermonde-subspace frequency division multiplexing (VFDM), it allows two radio access technologies (RATs) to operate side-by-side in a small-cell CR setting, sharing the band while protecting the legacy system from interference. VFDM transmits data pre-coded on the null-space of the interfering cross channel (channel from the opportunistic transmitter to the legacy receiver), assuming frequency selectivity and time division duplexing (TDD) communications.

This PhD work proposes a rather exhaustive approach to the development of VFDM: to go from the theoretical basis up to a proof-of-concept development. Initially the theoretical background, basis of the technique itself was introduced and analyzed. Then, VFDM was gradually developed from a pure mathematical concept up to a full transceiver. During this development, several important mid-way results were developed, such as the multi-user strategy for pre-coding and critical implementation aspects.

VFDM, under certain constraints, has been shown to allow a secondary opportunistic network to successfully be installed along with a legacy primary one at merely the cost of channel knowledge and added complexity. By means of numerical examples, it has been shown that significant rates can be attained, even though VFDM's performance is constrained by the size of the Vandermonde-subspace of the interfering channel between the secondary transmitter and primary receiver. Finally, a working VFDM transceiver implementation is shown, providing a proof-of-concept of the technique.



# Contents

<b>List of Figures</b>	<b>XV</b>
<b>List of Tables</b>	<b>XIX</b>
<b>List of Acronyms</b>	<b>XXI</b>
<b>List of Notations</b>	<b>XXV</b>
<b>1 Introduction</b>	<b>1</b>
1.1 Brain-empowered Radios . . . . .	2
1.1.1 Non-cognitive Radio . . . . .	2
1.1.2 Software Defined Radio . . . . .	3
1.1.3 The Next Step in Flexibility . . . . .	5
1.1.4 Dynamic Spectrum Access . . . . .	6
1.2 Small-Cells . . . . .	7
1.3 Contribution . . . . .	9
1.4 Scientific Production . . . . .	9
1.5 Thesis Outline . . . . .	11
<b>I Design and Performance</b>	<b>13</b>
<b>2 VFDM</b>	<b>15</b>
2.1 Problem and State of the Art . . . . .	15
2.2 System Model . . . . .	17
2.3 Precoder Design . . . . .	18
2.4 Optimal Receiver . . . . .	20

2.4.1	Performance . . . . .	21
2.5	Sub-optimal Linear Receivers . . . . .	22
2.5.1	Performance . . . . .	24
2.6	VFDM vs. Spectrum Sensing Resource Sharing . . . . .	27
2.7	Closing Remarks . . . . .	27
<b>3</b>	<b>Towards Multiple Users</b>	<b>29</b>
3.1	Multi-User: Initial Considerations . . . . .	29
3.2	Multi-Primary — Single-Secondary System Model . . . . .	32
3.3	Precoder Design . . . . .	33
3.4	Achievable Rates . . . . .	34
3.4.1	Numerical Results . . . . .	36
3.5	Closing Remarks . . . . .	38
<b>4</b>	<b>Network MIMO VFDM</b>	<b>39</b>
4.1	Multi-Primary — Multi-Secondary System Model . . . . .	39
4.2	Pre-coder Design . . . . .	42
4.2.1	Practical Transmit Schemes . . . . .	43
4.2.2	RIBF Flexible Network Solution . . . . .	44
4.2.3	Numerical Analysis . . . . .	46
4.3	Comparison with existing solutions . . . . .	48
4.4	Closing Remarks . . . . .	50
<b>II</b>	<b>Practical Aspects and Implementation</b>	<b>51</b>
<b>5</b>	<b>Practical Aspects</b>	<b>53</b>
5.1	Channel State Awareness and Estimation . . . . .	53
5.2	Single User Channel Estimation Protocol . . . . .	54
5.2.1	Channel Estimation Protocol Overview . . . . .	55
5.2.2	Primary System . . . . .	56
5.2.3	Secondary System . . . . .	56
5.2.4	Performance Under Imperfect channel state information (CSI) . . . . .	58
5.3	MU-VFDM's Performance Under Imperfect CSI . . . . .	60

5.3.1	Performance under imperfect CSI . . . . .	60
5.4	Synchronization . . . . .	62
5.5	System-Level Aspects . . . . .	64
5.5.1	VFDM Cell Border Issue . . . . .	65
5.5.2	Mobility . . . . .	66
5.5.3	MU-VFDM Subset Selection . . . . .	67
5.6	Closing Remarks . . . . .	67
<b>6</b>	<b>Prototype Implementation</b>	<b>69</b>
6.1	SDR4all Platform . . . . .	69
6.2	Considerations and VFDM Scenario . . . . .	71
6.3	Base-Band Transceiver Implementation . . . . .	72
6.4	Experimental Setup . . . . .	76
6.5	Illustrative Results . . . . .	77
6.5.1	Decoding . . . . .	80
6.6	Closing Remarks . . . . .	82
<b>III</b>	<b>Conclusions, Perspectives and Appendices</b>	<b>83</b>
<b>7</b>	<b>Conclusions and Perspectives</b>	<b>85</b>
7.1	Conclusions . . . . .	86
7.1.1	Single-user VFDM . . . . .	86
7.1.2	Multi-user VFDM . . . . .	86
7.1.3	Practical Aspects and Implementation . . . . .	87
7.2	Perspectives . . . . .	88
<b>A</b>	<b>OFDM Implementation</b>	<b>99</b>
A.0.1	Data Bearing Mode . . . . .	100
A.0.2	Channel Sounder Mode . . . . .	101
A.0.3	Reception Trigger . . . . .	102
A.1	Metrics and Outputs . . . . .	102



# List of Figures

1.1	Digital radio device blocks. . . . .	3
1.2	Digital radio device blocks. . . . .	4
1.3	Cognitive cycle. . . . .	5
1.4	Typical small-cell deployment. . . . .	8
2.1	Cognitive interference channel model. . . . .	16
2.2	VFDM's spectral efficiency for $N = 64$ , $L \in \{8, 16, 32\}$ and $\alpha=0$ . . . . .	23
2.3	VFDM's spectral efficiency for $N = 64$ , $L = 16$ and $\alpha \in \{0, 0.1, 0.5, 1\}$ . . . . .	23
2.4	VFDM's $R_{\text{opt}}$ and $R_{\text{lin}}$ for the MMSE, ZF and MF equalizers for $N = 64$ , $L = 16$ and $\alpha = 0$ . . . . .	25
2.5	VFDM's $P_e$ for the MMSE, ZF and MF equalizers for $N = 64$ , $L = 16$ and $\alpha = 0$ . . . . .	26
2.6	Comparative probability of bit error ( $P_e$ ) for the MMSE and ZF equalizer for varying interference levels $\alpha = \{0, 0.5, 1\}$ ( $N = 64$ , $L = 16$ ). . . . .	26
2.7	VFDM's spectral efficiency for $N = 64$ , $L = 16$ and $\alpha \in \{0, 1\}$ , compared to OFDM with $(3/4 - 1/4)$ shared resources. . . . .	28
2.8	VFDM's sum (primary + secondary) spectral efficiency for $N = 64$ , $L = 16$ and $\alpha \in \{0, 1\}$ , compared to OFDM with $(3/4 - 1/4)$ shared resources. . . . .	28
3.1	Multi-user scenarios. . . . .	31
3.2	OFDMA downlink cognitive interference channel model. . . . .	32
3.3	Sum rate of the primary system in a 8-user OFDMA configuration compared to the secondary receiver's rate ( $N = 128$ , $L = 32$ and bandwidth of 1.92 MHz). . . . .	36
3.4	Rate of the secondary system for increasing number of primary receivers and several SNR values ( $N = 128$ , $L = 32$ and bandwidth of 1.92 Mhz). . . . .	37

3.5	Rate of the primary system for different number of users compared to the secondary receiver's rate ( $N = 128, L = 32$ and bandwidth of 1.92 MHz).	38
4.1	OFDMA downlink cognitive interference channel model.	40
4.2	Rate of the small-cells for different techniques, $\mathcal{K} = 3$ ( $N = 128, L = 32$ and bandwidth of 1.92 Mhz).	47
4.3	Achievable Rate of the SBSs with the RIBF flexible network solution, $K = 3, \beta = 3$ ( $N = 128, L = 32$ and bandwidth of 1.92 Mhz).	47
4.4	Rate of the SBSs with the RIBF flexible network solution for different numbers of Small Cells, $\beta = 2$ , ( $N = 128, L = 32$ and bandwidth of 1.92 Mhz).	48
4.5	Capacity of multi-user Vandermonde-subspace frequency division multiplexing (MU-VFDM) vs. complete separation scheme, $\mathcal{K} = 2, \beta = 4$ , ( $N = 24, L = 6$ and bandwidth of 0.48 Mhz).	49
5.1	VFDM's relation to the coherence time.	54
5.2	VFDM's relation to the coherence time.	55
5.3	Channel estimation and transmission time for the primary system.	56
5.4	Spectral efficiency for the primary (OFDM) system with varying SNR levels $\{0, 10, 20\}$ dB ( $N = 64, L = 16$ ).	59
5.5	Spectral efficiency for the secondary (VFDM) system with varying SNR levels $\{0, 10, 20\}$ dB ( $N = 64, L = 16$ ).	59
5.6	Primary system performance under imperfect CSI, $K = 3, \beta = 1$ , ( $N = 24, L = 6$ ).	61
5.7	Secondary system performance with imperfect CSI, $K = 3, \beta = 1$ , ( $N = 24, L = 6$ and bandwidth of 0.48 Mhz).	62
5.8	VFDM when unsynchronized w.r.t. the primary receiver.	63
5.9	Interference caused by off sync reception of the VFDM precoded message at the primary system.	63
5.10	Cell border issue with VFDM.	65
5.11	Effect of mobility on the coherence time and VFDM's performance.	66
6.1	SDR4all overall layout.	71
6.2	Laptops and USRPs.	71
6.3	Cognitive interference channel scenario, focusing on secondary and its links.	72
6.4	VFDM Transmission chain.	73
6.5	VFDM frame structure.	74

6.6	VFDM Reception chain. . . . .	75
6.7	Laboratory environment used in the VFDM transmission tests. . . . .	76
6.8	Original Lena picture fed into the transmitter. . . . .	77
6.9	Example receive frame. . . . .	78
6.10	Empirical CDF of the preamble SNR ( $N = 128$ and $L = 16$ ). . . . .	79
6.11	Empirical CDF of the preamble SNR ( $N = 64$ and $L = 8$ ). . . . .	79
6.12	Outcome of the selected transmission. . . . .	80
6.13	Empirical CDF of the payload BER ( $N = 128$ and $L = 16$ ). . . . .	81
6.14	Empirical CDF of the payload BER ( $N = 64$ and $L = 8$ ). . . . .	81
A.1	General OFDM transmission chain frame configuration. . . . .	99
A.2	OFDM frame structure for data bearing mode . . . . .	100
A.3	OFDM frame structure for channel sounder mode . . . . .	101



# List of Tables

2.1	Simulation parameters . . . . .	22
5.1	Imperfect CSI simulation parameters. . . . .	58
6.1	Parameters for the hardware part. . . . .	70
6.2	Parameters for the VFDM transceiver. . . . .	77
A.1	Parameters for the data bearing mode. . . . .	101
A.2	Parameters for the channel sounder mode. . . . .	102



# List of Acronyms

<b>16-QAM</b>	16 - quadrature amplitude modulation
<b>A/D</b>	analog-to-digital
<b>ADSL</b>	asynchronous digital subscriber line
<b>AGC</b>	automatic gain control
<b>ASIC</b>	application-specific integrated circuit
<b>AWGN</b>	additive white gaussian noise
<b>BB</b>	base-band
<b>BC</b>	broadcast channel
<b>BD</b>	block diagonalization
<b>BER</b>	bit error rate
<b>BPSK</b>	binary phase shift keying
<b>CDF</b>	cumulative distribution function
<b>CQI</b>	channel quality indicator
<b>CR</b>	cognitive radio
<b>CSI</b>	channel state information
<b>CSMA/CA</b>	carrier sense multiple access with collision avoidance
<b>D/A</b>	digital-to-analog
<b>DFT</b>	discrete Fourier transform
<b>DPC</b>	dirty paper coding

<b>DSA</b>	dynamic spectrum access
<b>DSP</b>	digital signal processing
<b>FDD</b>	frequency division duplexing
<b>FPGA</b>	field-programmable gate array
<b>FTTH</b>	fiber-to-the-home
<b>GSM</b>	global system for mobile communications
<b>HF</b>	high frequency
<b>HSPA</b>	high speed packet access
<b>IDFT</b>	inverse discrete Fourier transform
<b>IEEE</b>	Institute of Electrical and Electronics Engineers
<b>IF</b>	intermediate frequency
<b>i.i.d.</b>	independent and identically distributed
<b>IRBD</b>	iterative regularized block diagonalization
<b>ISM</b>	industrial, scientific and medical
<b>KKT</b>	Karush-Kuhn-Tucker
<b>LOS</b>	line of sight
<b>LS</b>	least squares
<b>LTE</b>	long term evolution
<b>MCS</b>	modulation and coding scheme
<b>MF</b>	matched filter
<b>MIMO</b>	multiple input, multiple output
<b>MMSE</b>	minimum mean square error
<b>MU-VFDM</b> ing	multi-user Vandermonde-subspace frequency division multiplex-
<b>MUE</b>	macro-cell user equipment
<b>OFDM</b>	orthogonal frequency division multiplexing
<b>OFDMA</b>	orthogonal frequency division multiple access

<b>ORBF</b>	opportunistic random beamforming
<b>PAN</b>	personal area network
<b>PAPR</b>	peak to average power ratio
<b>PCS</b>	personal communications services
<b>PLL</b>	phase-locked loop
<b>QoS</b>	quality of service
<b>QPSK</b>	quadrature phase shift keying
<b>RAT</b>	radio access technology
<b>RF</b>	radio frequency
<b>RIBF</b>	regularized inverse beamforming
<b>SDR</b>	software defined radio
<b>SDR4all</b>	SDR4all
<b>SINR</b>	signal to interference plus noise ratio
<b>SMMSE</b>	successive minimum mean square error
<b>SNR</b>	signal to noise ratio
<b>SUE</b>	small-cell user equipment
<b>SUS-ZFBF</b>	semi-orthogonal user selection zero force beamforming (ZFBF)
<b>SVD</b>	singular value decomposition
<b>TDD</b>	time division duplexing
<b>TDMA</b>	time division multiple access
<b>TCP/IP</b>	transmission control protocol / internet protocol
<b>UE</b>	user equipment
<b>USB</b>	universal serial bus
<b>USRP</b>	universal software radio peripheral
<b>UWB</b>	ultra wide band
<b>VFDM</b>	Vandermonde-subspace frequency division multiplexing
<b>WIFI</b>	wireless fidelity

<b>ZF</b>	zero forcing
<b>ZFBF</b>	zero force beamforming

# List of Notations

$a$	Scalar
$i, j, k$	Indexes
$i$	imaginary unit ( $i^2 = -1$ )
$\mathbf{a}$	Vector (All vectors are columns unless otherwise stated)
$\mathbf{A}$	Matrix
$[\mathbf{A}]_{mn}$	Matrix element at $m^{\text{th}}$ row and the $n^{\text{th}}$ column
$\mathbf{a}_m$	Column (or row) vector $m$ of matrix $\mathbf{A}$
$\mathbf{I}_N$	Identity matrix of size $N$
$\mathbf{0}$	Matrix (or vector) of zeros (depending on the context)
$\mathbf{A}^{\text{H}}$	Transpose conjugate of $\mathbf{A}$
$\mathbf{A}^{-1}$	Inversion of $\mathbf{A}$
$\mathbf{A}^{\dagger}$	Pseudo-inversion of $\mathbf{A}$
$\mathcal{T}(\mathbf{a})$	Toeplitz matrix from vector $\mathbf{a}$ (refer to (2.3) for details)
$\mathbf{A} \otimes \mathbf{B}$	Kronecker product between matrices $\mathbf{A}$ and $\mathbf{B}$
$\mathbb{E}[\cdot]$	Expectation operator
$ \cdot $	Determinant operator
$\bigoplus_{i=1}^N (\cdot)$	Direct sum operator
$\text{tr}(\cdot)$	Trace operator
$\angle(\cdot)$	Angle operator
$\mathbb{C}$	Set of all complex numbers
$\mathcal{R}$	Set of all real numbers



# Chapter 1

## Introduction

**A**N IMPORTANT aspect that characterizes the start of the twenty-first century is the explosion in the adoption of telecommunications platforms and the associated PCS. This wide spread adoption of PCS is in part a response to the birth of new communication platforms, such as social networks, micro-blogging and photo and video sharing, to cite a few. These communication platforms have, for the better or worse, undeniably transformed the way we socially interact [1, 2, 3]. Its power can be clearly seen in its influence to the news media [4], global lifestyle and even politics, as exemplified by popular uprisings of early 2011<sup>1</sup> [5]. This widespread adoption of PCS gained momentum in the 1990s, when it went from being a privilege of a few rich to a widespread commodity item, enjoying what is probably known to be the highest technology adoption rate ever seen in the recent history.

To cope with this fast-paced demand, regulatory agencies, service operators, infrastructure manufacturers and academic communities have strived to keep up the speed in offering frequent updates to the communications technology pool. This constant and fast evolution is necessary to accommodate the higher capacities and data rates demanded by the market. In spite of this constant growth, in the end, physics dictates the limit. The development of new high speed RATs, basis of the known communication platforms, has been constrained by a severe radio spectrum shortage.

Have we finally exhausted our spectral resources? Not really. Studies have shown that the currently allocated radio spectrum is underutilized [6]. The culprit for this dead-end is the fixed spectrum management model, that reserves static frequency bands for single licensees (or group of licensees) [7] at a time. Fixed spectrum management is the current model adopted by regional radio spectrum regulatory agencies, created to enforce spectrum use policies in a time when the radio spectrum was seen mostly as property-based real-estate.

---

<sup>1</sup>This is a reference to the use of social networks in the popular uprisings against totalitarian regimes, for example, the ones in Tunisia and Libia, which took place in the first quarter of 2011.

In a response to the spectrum scarcity issue, regulatory agencies are studying the adoption of flexible rules for spectrum usage (e.g., [8]). In flexible spectrum management, RATs will support spectrum sharing. Ideally, full coordination between systems is targeted, repeating the success of the industrial, scientific and medical (ISM) bands model. In the ISM bands, devices from different vendors and/or for different applications, use co-existence techniques to share frequency bands. The widely popular IEEE 802.11 family [9] of standards serve as an example that such a coexistence is possible, by using carrier sense multiple access with collision avoidance (CSMA/CA) along with channel selection based on inactivity. Nevertheless, at least for the moment, full coordination is not the silver bullet as it lacks a way to properly enforce the spectrum pre-defined usage rules. This is critical for commercially-based wireless services, that need to provide QoS guarantees, as well as for sensitive wireless applications, such as emergency services. At first, a mixed policy seems more likely to be adopted. In such a policy, a licensee network has the full rights to the spectrum while an opportunistic network tries to re-use the resources in a way not to cause negative impacts on the communications of the licensee one. This mixed policy approach to the spectrum management is the fundamental regulatory background advocated and exploited in this thesis.

## 1.1 Brain-empowered Radios

Cognitive radio (CR) is seen as the enabling technology for spectrum sharing in the licensee-opportunistic network setting, enabling an efficient spectrum usage. In a nutshell, CRs are wireless communication devices able to *sense* the environment, *reason* to become situation aware and *adapt* accordingly. Even though CR, was initially introduced by Mitola [10], the term *brain-empowered*, borrowed in the title of this section, was coined by Haykin in a work [11] that concretely placed CRs in the line-of-sight of the wireless communications academy.

But what is it that makes CR different from standard radios? What does a CR radio look like? As those questions still lack clear answers, some clues indicate the path towards the possibilities. To understand the leading steps into the creation of CRs, it is wise to start by defining a standard or — non-cognitive — radio.

### 1.1.1 Non-cognitive Radio

Roughly, a standard digital wireless radio, transmitter or receiver, can be modularized as shown in figure 1.1, where three main blocks are seen (e.g. [12]):

- **base-band (BB)**. Base-band signal processing encompasses all discrete-time signal duties such as channel coding/decoding, filtering and bit-mapping, to cite a few. It is usually executed by dedicated circuitry, such as application-specific integrated circuits (ASICs), digital signal processing (DSP) units and field-programmable gate arrays (FPGAs);

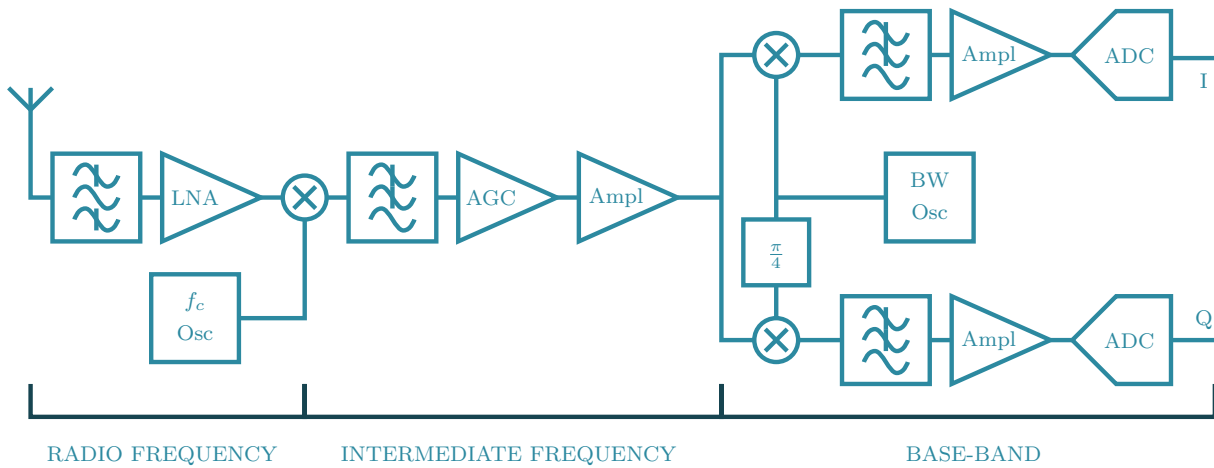


Figure 1.1: Digital radio device blocks.

- **intermediate frequency (IF).** At the IF block the signal is formatted to the transmission waveform, sampling, analog-to-digital (A/D), digital-to-analog (D/A) and automatic gain control (AGC). This step is usually undertaken by a mix of digital and analog components;
- **radio frequency (RF).** The RF block is where the signal is brought up to the actual transmission frequency and bandwidth, with continuous-time signal tasks such as carrier frequency modulation, filtering and transmission power adjustment. Analog RF radio components are usually used at this point.

This design, proven over decades of use, has remained untouched mainly due to the limitations imposed by the RF components available. With the demands for higher data rates, RATs started moving from narrow to wide-band communications. This pushed new challenges to the problem of managing radio communications, ensuring at the same time new restrictive quality of service (QoS) criteria. In wide-band radios, propagation fluctuations need to be compensated for at a faster pace, with the adjustment of several parameters such as modulation and coding scheme (MCS) or transmitted power (for example, the high speed packet access (HSPA) and long term evolution (LTE) [13]). The use of flexible base-band techniques and dedicated ASICs, made this architecture possible.

### 1.1.2 Software Defined Radio

The idea of parametrizing the radio was taken to the limit by Mitola, in a work [14] that introduces the concept of *software radio*, nowadays also known as software defined radio (SDR). In this work, Mitola argues that processing power has become affordable enough to allow base-band processing to be offloaded to general purpose processors, bringing flexibility in radios to a whole new level. Such a flexibility allows a SDR to switch RATs as required, using the same hardware platform, following channel conditions or

geographical based standardization. It can also adaptively change the frequency band and antenna configurations to steer beams towards the receiver and can be updated to newer (or debugged) versions of base-band signal processing improving the hardware life-cycle.

Despite this seminal work, the concept of SDR was already known since the late 1980s. It was initially used in military applications, to create an adaptive radio that could switch bands and standards, such as the Speakeasy series of projects [15] developed by the United States military.

Ideally, a SDR would keep the RF components to a minimum, performing all BB, IF and even some RF tasks in software. Such a SDR configuration would look like the one presented in figure 1.2. In practice, the wider the band, the harder it is to implement such a scheme due to several hardware limitations such as non-linearity of amplifiers and filters. Instead, today's SDRs implement only the required parts in software.

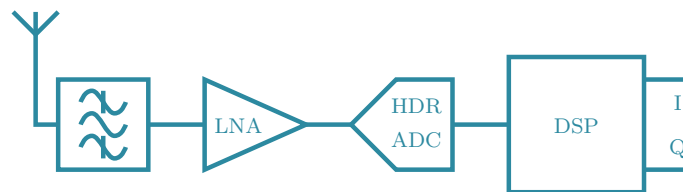


Figure 1.2: Digital radio device blocks.

In the simplest case, only a part of the BB tasks is executed in software. This allows for off-the-shelf components to be used, reducing price and complexity but severely limiting the flexibility of the SDR. An example of such a simple SDR is presented and further detailed in chapter 6. Being commonplace, SDRs like this are usually used in band-limited radios that need some flexibility.

On more complex SDRs, not only the BB, but also the IF is executed in software. In order to do so, expensive high dynamic range, high speed A/D-D/A converters need to be used as well as a processing hardware capable of handling real-time processing at high sample rates. The obvious gain in flexibility comes from the flexible in-software band selection and decimation/filtering. This scheme still requires some RF components to modulate the signal onto the carrier frequency, perform high frequency (HF) filtering and amplification.

In spite of all the flexibility enabled by the SDR concept, wide band radios sometimes require fast adaptation in order to attain the best performance possible in the face of fast changing propagation environments. Some adaptation loops require intervention coming from core network equipment such as base-stations and can amount up to unbearable delays. What if the radios themselves could decide on their own on how to adapt? Such a concept is presented in the following.

### 1.1.3 The Next Step in Flexibility

Initially, a 1999 work by Mitola et. al. [10], passed largely unnoticed by the academic community. Bridging the concepts of artificial intelligence and software radio, Mitola proposed a new class of radio devices called *cognitive radios*. These intelligent radios could make sense of the environment around it to adapt its own parameters. The concept seemed too far fetched at the time, since the processing power required to enable even simple artificial intelligence, was out of reach for consumers.

In the initial proposition, CRs would be capable of detecting a wide range of environments, situations and propagation conditions in order to extract the best performance, pre-allocate resources or even save energy. As an example, Mitola proposes a futuristic scenario in [10], where a businessman takes a taxi cab to a conference center. In this example, his CR enabled device is able to handle issues concerning his connectivity beforehand and also provide insights to the network about future load implications of his travel. This computer-science vision of CRs did not immediately spark the interest of the wireless communication researchers.

It took some years for CRs to be explored from a communications theory perspective, rapidly put forward as the solution to spectrum scarcity. In 2005, Haykin is among the first to propose the use of CRs for allowing spectrum reuse [11]. In this work, he proposed a cognitive cycle, resembling the one in figure 1.3, where the radio senses the environment and then adapts the transmission configuration parameters of a software radio. This proposal was a break-off from the current radio adaptation schemes that were mainly centralized, with commands issued through control channels from base-stations.

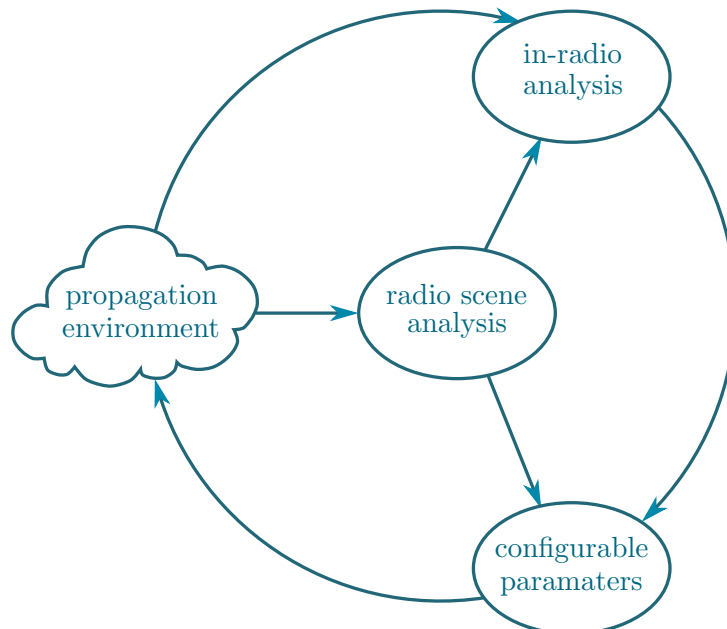


Figure 1.3: Cognitive cycle.

In CR jargon, a *primary system* is the legacy RAT which is already in operation, the

licensee of the spectrum. A primary system can be a PCS system, such as a global system for mobile communications (GSM) cellular system, or a broadcast network, such as analog television or radio. These primary systems are also usually seen as immutable, normally due to high costs involved in changing their underlying technologies. A *secondary system*, on the other hand, is the cognitive opportunistic system, aiming at finding free resources from the primary system to transmit its own data. Specific access rules are determined by a set of policies, called spectrum etiquette, usually decided by the regional regulatory agencies. The primary — secondary denomination will be used throughout this work.

For a while, the majority of communications theory oriented CR research were devoted to spectrum sensing [11, 16]. Spectrum sensing is a necessary step to detect the so called white spaces: inactivity times in the spectrum exploitable by opportunistic radios. The spectrum sensing is then classified as part of the "radio scene analysis" block in figure 1.3. Nevertheless, implementing a spectrum sensing based opportunistic CR has been proven harder than initially thought. It was only after almost a decade of research that white-space radios are starting to be tested for internet access [17, 18]. One of the main problems is that, in realistic scenarios, spectrum sensing is underperforming due to the presence of multi-path fading [11, 19, 20, 16]. An extension of this technique, called cooperative spectrum sensing, successfully copes with the multi-path fading problem [16, 21, 22, 23, 24, 25, 26] by exploiting spatial diversity but introduces complicated signaling between terminals.

Another candidate technique for CR is the interference temperature [11, 20, 24]. In this technique, a secondary transmitter sends its signal with a limited amount of power so that the interference at the primary receiver is contained under a certain acceptable level. However, the interference temperature is hard to compute as secondary transmitters generally do not know all the details related to the the primary receivers required by such a computation.

### 1.1.4 Dynamic Spectrum Access

All of these techniques for opportunistic spectrum usage are encompassed in DSA category (also known as dynamic spectrum sharing). DSA involves techniques other than spectrum sensing and each technique comes with its own diverse characteristics, making it difficult to discern in between them. To make some sense out of this collection of techniques, several studies (e.g. [20], [27] and [28]) have grouped them into various paradigms, relating them by interference management approach, awareness, coordination level and hierarchy. It has been more or less accepted in the literature that such paradigms are of three types: *underlay*, *overlay* and *interweave*.

#### Underlay

In the underlay paradigm, a cognitive radio-based system is assumed to know the interference it causes on a legacy system, therefore, keeping its interference under a certain

threshold. Implementations of this paradigm include beam steering [28] and interference temperature [29, 30, 31] based CRs, or simply ultra wide band (UWB) spread spectrum [32].

### Overlay

In the overlay paradigm, knowledge of the legacy system's characteristics are obtained in order to actively mitigate the interference from the cognitive radio. Dirty paper coding (DPC) [33], opportunistic interference alignment [34] and spectrum shaping [35, 36] are examples of the overlay paradigm.

### Interweave

Finally, the interweave (or open sharing) paradigm, relies on full opportunism among systems, inspired by the operation in the ISM bands. In this paradigm, systems make use of activity information to adaptively access the spectrum, avoiding collisions among systems. The interweave paradigm can be implemented by opportunistic spectrum access through spectrum sensing [11].

Aside from the interweave paradigm, a hierarchical access model is usually considered, in which a primary system possesses the lease to the spectrum (in the case of a legacy cellular operator, for example) while a secondary system uses its cognitive capabilities to opportunistically access the spectrum.

## 1.2 Small-Cells

A new trend in cellular communications is currently on the rise: the deployment of smaller base stations to aid in capacity and coverage [37, 38]. Such smaller base stations, called *femto-* [38] or *small-cells*<sup>2</sup> [37], can be user deployed in a uncontrolled manner and need to intelligently adapt to coexist with macro base stations. A typical small-cell deployment can be seen in figure 1.4, where a service area, already covered by a macro-cell, is densely incremented with small-cells on lamp posts, trees and building facades. These low consumption radio transceivers can be powered frugally (e.g. with solar panels), and are cheap enough to produce to be considered disposable. The idea is that if one of them ceases to work for any reason, the others around it will adapt to compensate for its loss. Intelligence, real-time situation awareness and distributed operation will be used to compensate for any change in the environment, propagation conditions or service load peaks. Small-cells are also envisioned to be connected through a high capacity back-bone, such as an asynchronous digital subscriber line (ADSL) or fiber-to-the-home (FTTH) line, or

---

<sup>2</sup>Throughout this work, we refer to the term *small-cells* to refer to any kind of technology that employs cells which are physically smaller than micro- and pico-cells, in an intelligent and user-deployed way aiming at maximizing coverage and capacity.

even by wireless means, in order to be able to communicate to its peers and coordinate its efforts.



Figure 1.4: Typical small-cell deployment.

Small-cells fundamentally differ in several ways from two previous technologies that also aim at enhancing capacity and coverage:

- *micro-cells*. Micro-cells [39] were a popular way to solve localized higher capacity demands (hotspot) in the end of the 1990s. The installation of micro-cells was hand-tailored for the situation at hand and required the intervention of cellular operators to allocate the resources as to avoid clashes with the other previously deployed macro base stations. This was usually done by channel partitioning or power control, which lowered the spectral efficiency.
- *heterogeneous networks*. Co-existence of cellular and IEEE 802.11 (also known as WIFI) [40] has been proposed during the 2000s. In this proposal, a secondary RAT (in this case IEEE 802.11) is added in order to offload the cellular network. The main problem with this heterogeneous RATs approach is that it introduces many new issues related to the disparity between the RATs, such as quality of service disruption and vertical handoffs, to cite a few. For more details, see [41].

Unlike both previous contenders, small-cells, aim at intelligently re-using the same band as the macro-cells, therefore, maximizing the spectral efficiency. It also promotes the use of the same RAT adopted by the cellular network, with minor changes if any.

So what is the trick behind small-cells, that allow it to operate unmanaged, side-by-side with cellular, while sharing the same band and RAT? Intelligent resource management, based on CRs and situation awareness. Indeed, if the whole radio network is seen from the cognitive radio perspective, i.e., macro base stations and its users, acting as the primary system, are protected from interference while, femto-cells and its users, acting as the secondary system, can accept interference from the macro base stations. Then, DSA [28, 20], comes forward as a candidate solution.

The technique introduced in this work focuses on the DSA overlay paradigm and profits from the knowledge of the macro-cell's (primary system<sup>3</sup>) characteristics to actively mitigate the interference from the small-cells (secondary system<sup>4</sup>).

## 1.3 Contribution

In this thesis, we concentrate on the downlink DSA problem, seen both from the CR (primary-secondary) and small-cells network perspective. The main contributions of this thesis are:

- Propose a novel downlink DSA technique based on a class of orthogonal precoders called VFDM, able to deal with co-channel interference from opportunistic to legacy radio systems;
- Analyze VFDM under the light of information theory in the simple cognitive interference channel scenario, deriving its achievable spectrum efficiency;
- Propose an extension of the downlink VFDM and its pre-coder for the small-cell multi-user scenario using tools from network-multiple input, multiple output (MIMO) systems;
- Understand the practical implementation issues VFDM poses and find implementation parameters;
- Implement a one-way VFDM test-bed based on actual transmissions on a hardware platform to serve as a proof-of-concept of the technique.

## 1.4 Scientific Production

The work in this dissertation is the result of several publications. Some of these publications have triggered patents which are still in analysis phase. The main results of this thesis are well summarized in the following journal articles:

---

<sup>3</sup>In the remainder of this thesis we will use either *macro-cell* or *primary system* to denote the licensee system that should be protected from interference.

<sup>4</sup>In the remainder of this thesis we will use either *small-cell* or *secondary system* to denote the opportunistic system that should not cause interference.

### Journal articles

- Leonardo S. Cardoso, Mari Kobayashi, Francisco Rodrigo P. Cavalcanti and Mérouane Debbah, "*Vandermonde-subspace Frequency Division Multiplexing for Two-Tiered Cognitive Radio Networks*", submitted to IEEE Transactions on Wireless Communications, 2012.
- Marco Maso, Leonardo S. Cardoso, Mérouane Debbah and Lorenzo Vangelista "*Orthogonal Precoder for Heterogeneous Two-tiered Networks*", submitted to IEEE Transactions on Communications, 2012.
- Leonardo S. Cardoso, Ejder Bastug, Marco Maso, Mérouane Debbah and Ozgur Ozdemir "*Implementation of a Cognitive Radio Second Tier System for OFDM*", In preparation. To be submitted to EURASIP Journal on Wireless Communications and Networking, 2012.
- Leonardo S. Cardoso, Marco Maso and Mérouane Debbah "*Survey on Physical Layer for Cognitive Radio*", In preparation. To be submitted to IEEE Communications Magazine, 2012.

### Conference Proceedings

- Leonardo S. Cardoso, Mari Kobayashi, Mérouane Debbah and Øyvind Ryan, "*Vandermonde Frequency Division Multiplexing for Cognitive Radio*", Signal Processing Advances for Wireless Communications (SPAWC) 2008, Recife, Brazil.
- Leonardo S. Cardoso, Raul de Lacerda, Pierre Jallon and Mérouane Debbah "*SDR4all: a Tool for Making Flexible Radio a Reality*", Proceedings of COGNITIVE Systems with Interactive Sensors 2009 - COGNITIVE Systems with Interactive Sensors 2009, France.
- Hongzhi Wang, Wassim Jouini, Rachid Hachemani, Jacques Palicot, Leonardo S. Cardoso and Mérouane Debbah "*Blind bandwidth shape recognition for standard identification using USRP platforms and SDR4all tools*", AICT 2010, Barcelona, Spain.
- Hongzhi Wang, Wassim Jouini, Amor Nafkha, Jacques Palicot, Leonardo S. Cardoso and Mérouane Debbah, "*Blind Standard Identification with Bandwidth Shape and GI Recognition using USRP Platforms and SDR4all Tools*", Crowncom'10, Cannes, France, 2010.
- Leonardo S. Cardoso, Francisco R. P. Cavalcanti, Mari Kobayashi and Mérouane Debbah, "*Vandermonde-Subspace Frequency Division Multiplexing Receiver Analysis*", PIMRC'10, Istanbul, Turkey, 2010.
- Leonardo S. Cardoso, Marco Maso, Mari Kobayashi and Mérouane Debbah, "*Orthogonal LTE two-tier Cellular Networks*", ICC'11, Kyoto, Japan, 2011.

During this thesis some contributions were also made in other related subjects:

### **Spectrum sensing using random matrix theory**

A novel algorithm was proposed to perform spectrum sensing based on the statistics of a Wishart matrix created from the received signal. This work has culminated in two conference papers and one book chapter:

- Leonardo S. Cardoso, Mérouane Debbah, Pascal Bianchi, Jamal Najim, "Cooperative Spectrum Sensing Using Random Matrix Theory", ISWPC'08, Santorini, Greece.
- Leonardo S. Cardoso, Pascal Bianchi, Jamal Najim, Mérouane Debbah, Mylène Maida "Écoute Coopérative de Spectre pour la Radio Cognitive" , GRETSI'09, Dijon, France.
- Leonardo S. Cardoso, Merouane Debbah, Samson Lasauce, Mari Kobayashi and Jacques Palicot "Spectrum Sensing in Cognitive Radio Networks" in book: "Cognitive Radio Networks: Architectures, Protocols and Standards", Edited by Yan Zhang, Jun Zheng and Hsiao-Hwa Chen, Taylor&Francis Group, Auerbach Publications, ISBN: 978-1-4200-7775-9, 2010.

### **Resource allocation in heterogeneous networks**

The author has participated in writing a book chapter on radio resource management for heterogeneous networks. This book chapter dealt mainly with aspects of access selection and vertical handover decision and resource allocation.

- Alex P. da Silva, Leonardo S. Cardoso, Vicente A. de Sousa "Common Resource Management for Multiaccess Technologies", in book: "Optimizing Wireless Communication Systems", Edited by Francisco Rodrigo P. Cavalcanti and Sören Andersson, Springer, ISBN: 978-1-4419-0154-5, July 2009.

## **1.5 Thesis Outline**

This thesis is organized as:

**Part I:** We dive into the theoretical aspects of the orthogonal precoder construction describing its characteristics for single and multi-user settings. This development is done as follows:

**Chapter 2.** Introduction of VFDM pre-coder in the cognitive interference channel scenario and its initial theoretical analysis. An analysis of feasible receiver architectures is also made. The results in this chapter come from [23], [42] and [43];

**Chapter 3.** Discussion of a first step towards a multi-user approach, where only the primary system has multiple users. The results presented in this chapter come from [44];

**Chapter 4.** Introduction of the full multi-user VFDM scheme based on network MIMO. The results presented in this chapter come from [45];

**Part II:** In this part, the practical challenges and steps required in order to implement the VFDM transceiver are discussed. The VFDM prototype is gradually developed through the following steps:

**Chapter 5.** Determination of the best training symbol size with respect to the coherence time is presented. The results presented in this chapter come from [43, 45];

**Chapter 6.** Description of SDR4all, a hardware platform developed during the course of this PhD work and employed in the implementation of a VFDM transceiver, along with some preliminary performance results. The discussions presented in this chapter come from [46];

**Part III:** In this part, the closing to this thesis takes place:

**Chapter 7.** Concluding remarks and perspectives.

**Appendix A.** An orthogonal frequency division multiplexing (OFDM) transceiver chain, implemented during the course of this thesis and currently available in the SDR4all (SDR4all) toolbox, is presented as the starting point for the implementation of the VFDM chain.

# Part I

## Design and Performance



## Chapter 2

# Vandermonde-subspace Frequency Division Multiplexing

**I**N THE PREVIOUS chapter we have seen that small-cells are envisioned to use cognition and awareness to adapt to the environment in order to provide better spectral efficiency. We also remarked that one open problem of small-cells is the interference generated to macro-cells. In this chapter, we aim at proposing one physical layer solution to this problem. Vandermonde-subspace frequency division multiplexing (VFDM) is an overlay dynamic spectrum access (DSA) technique for cognitive radio networks that relies on the frequency dimension. VFDM is based on a linear pre-coder that allows a secondary transmitter to precode its signal on the null-space of the interfering channel, thereby incurring zero interference at the primary receiver. VFDM exploits the unused resources created by frequency selectivity and the use of guard symbols in block transmission systems at the primary system.

### 2.1 Problem and State of the Art

To understand the overlay DSA problem, consider the cognitive interference channel scenario depicted in figure 2.1, where all transmitters and receivers have a single antenna. The cognitive interference channel is characterized as a primary system (the pair TX1-RX1), that communicates a message  $\mathbf{s}_1$  over a licensed band, while a secondary system (the pair TX2-RX2), exploits the band opportunistically to communicate its own message  $\mathbf{s}_2$ , while avoiding harmful interference to the primary receiver. The primary system, being the legal licensee of the band, does not need to avoid interference to the secondary system.

If both primary and secondary systems can fully cooperate by sharing information through an unlimited backhaul, i.e. they belong to the same operator, then primary and secondary systems can be considered as part of a network multiple input, multiple

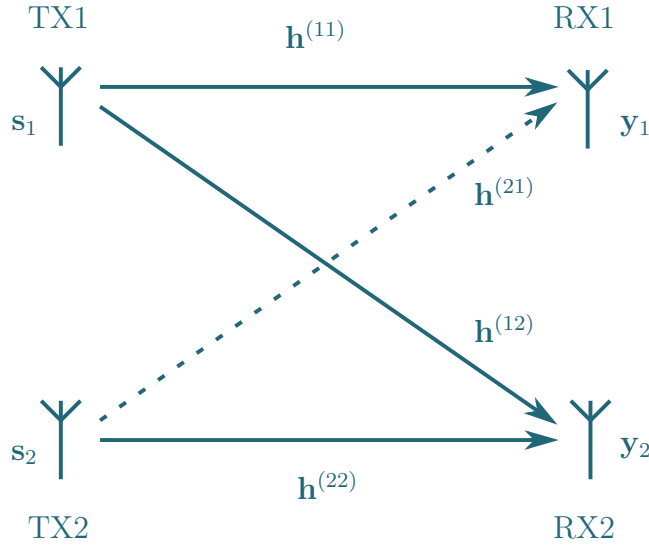


Figure 2.1: Cognitive interference channel model.

output (MIMO) system. In this case, if all the messages ( $\mathbf{s}_1$  and  $\mathbf{s}_2$ ) are known prior to transmission at all the transmitters (TX1 and TX2), then the cognitive interference channel can be generalized to a  $2 \times 2$  MIMO broadcast channel for which dirty paper coding (DPC) has been shown to be capacity achieving [47]. In this case, interference is suppressed on both cross links ( $\mathbf{h}^{(12)}$  and  $\mathbf{h}^{(21)}$ ). The asymmetric case, where interference is suppressed on only one cross link ( $\mathbf{h}^{(21)}$ ), particular for the cognitive interference channel of figure 2.1, has also been shown to achieve capacity by DPC [33]. Furthermore, a zero forcing (ZF) scheme [48] can be used in the fully cooperative network MIMO case to null the interference towards the unintended receivers.

In this work, we consider that there is *no cooperation* between the primary and secondary systems. In this case, a new way of managing interference from a secondary network to a primary one that does not rely on the classical schemes (DPC, ZF and network MIMO) is needed. The motivation for the non-cooperative case is clear for the opportunistic case, where a secondary system is not maintained by the same entity as the primary. Nevertheless, we extend the non-cooperation assumption to the case where primary and secondary systems are part of the same operator. This can be justified by the fact that an operator might want to add new radio infrastructure (either in a planned or random deployment) keeping the already installed infrastructure untouched. Such an addition could be seen as a *second tier cognitive radio network* that operates on the same band, and is available to newer generation software defined radio (SDR) handsets. These handsets could, with little or no change, switch between both tiers following pre-defined policies, such as network congestion, interference levels or background oriented services (i.e., notification messages, background software update, etc). Furthermore, less cooperation between tiers, means less bandwidth consuming signaling between base-stations, which frees backhaul resources for user data. This is critical, especially if this second tier network is composed of new technologies, such as femto-cells and small-cells. Finally, we

stress that the single antenna interference channel is the target of this work. If multiple antennas were to be adopted at the secondary transmitter, then the spatial dimension could be used to manage interference at the primary receiver, by means of techniques such as ZF precoding.

## 2.2 System Model

For the specific purposes of this work, we consider the frequency selective version of the cognitive interference channel of figure 2.1, comprised of  $L + 1$  tap frequency selective channels between transmitter  $i$  and receiver  $j$ ,  $\mathbf{h}^{(ij)}$ . The channels entries are unit-norm, independent and identically distributed (i.i.d.), complex circularly symmetric and Gaussian  $\mathcal{CN}(0, \mathbf{I}_{L+1}/(L + 1))$ . Furthermore, the channels are i.i.d. over any pair  $i, j$ .

We consider that both the primary and secondary systems employ an  $N + L$  size block transmission in order to cope with block-interference. At the primary system, classical orthogonal frequency division multiplexing (OFDM) of  $N$  subcarriers with a cyclic prefix of size  $L$  is used. The choice of OFDM for the primary system is merely to provide a practical setting, but the results presented in this work can be extended to any block transmission system that employs guard symbols (discarded at the reception). For the secondary system, an OFDM-like block transmission scheme is adopted, where the leading  $L$  symbols are also discarded. We assume that the signals are synchronized at the reception (both at the primary and secondary systems) at symbol-level. Then, the received signals at both the primary and secondary receivers are given by

$$\mathbf{y}_1 = \mathbf{F} (\mathcal{T}(\mathbf{h}^{(11)})\mathbf{x}_1 + \mathcal{T}(\mathbf{h}^{(21)})\mathbf{x}_2 + \mathbf{n}_1) \quad (2.1)$$

$$\mathbf{y}_2 = \mathbf{F} (\mathcal{T}(\mathbf{h}^{(22)})\mathbf{x}_2 + \mathcal{T}(\mathbf{h}^{(12)})\mathbf{x}_1 + \mathbf{n}_2), \quad (2.2)$$

where  $\mathcal{T}(\mathbf{h}^{(ij)}) \in \mathcal{C}^{N \times (N+L)}$  is matrix with a Toeplitz structure constructed from the channel's coefficients given by

$$\mathcal{T}(\mathbf{h}^{(ij)}) = \begin{bmatrix} h_L^{(ij)} & \dots & h_0^{(ij)} & 0 & \dots & 0 \\ 0 & \ddots & & \ddots & \ddots & \vdots \\ \vdots & \ddots & \ddots & & \ddots & 0 \\ 0 & \dots & 0 & h_L^{(ij)} & \dots & h_0^{(ij)} \end{bmatrix}, \quad (2.3)$$

$\mathbf{F} \in \mathcal{C}^{N \times N}$  is a unitary discrete Fourier transform (DFT) matrix with  $[\mathbf{F}]_{k+1, l+1} = \frac{1}{\sqrt{N}} e^{-i2\pi \frac{kl}{N}}$  for  $k, l = 0, \dots, N - 1$ , and  $\mathbf{x}_i$  denotes the transmit vector of user  $i$  of size  $N + L$  subject to the individual power constraint given by

$$\text{tr}(\mathbb{E}[\mathbf{x}_i \mathbf{x}_i^H]) \leq (N + L)P_i \quad (2.4)$$

and  $\mathbf{n}_i \sim \mathcal{CN}(0, \sigma_n^2 \mathbf{I}_N)$  is an  $N$ -sized additive white gaussian noise (AWGN) noise vector. The transmit power per symbol is  $P_i$ . For the primary system, we consider OFDM-modulated symbols

$$\mathbf{x}_1 = \mathbf{A} \mathbf{F}^{-1} \mathbf{s}_1 \quad (2.5)$$

where  $\mathbf{A}$  is a  $(N+L) \times N$  a cyclic prefix precoding matrix that appends the last  $L$  entries of  $\mathbf{F}^{-1}\mathbf{s}_1$  and  $\mathbf{s}_1$  is a symbol vector of size  $N$  and unitary norm. Regarding the secondary user, the transmit vector is given by

$$\mathbf{x}_2 = \mathbf{E}\mathbf{s}_2, \quad (2.6)$$

where  $\mathbf{E} \in \mathcal{C}^{(N+L) \times L}$  is a linear precoder and  $\mathbf{s}_2$  is a unitary norm symbol vector.  $\mathbf{E}$  will be presented in the next section.

As previously stated, the secondary system tries to cancel its interference to the primary one, while the primary system remains oblivious to the presence of the secondary one. This is effectively achieved when

$$\mathbf{F}\mathcal{J}(\mathbf{h}^{(21)})\mathbf{E}\mathbf{s}_2 = \mathbf{0} \quad \forall \mathbf{s}_2, \quad (2.7)$$

which is obtained by substituting (2.5) and (2.6) into (2.1) and making the interference part equal to zero. The signal received at the primary system becomes

$$\mathbf{y}_1 = \mathbf{H}_{11}\mathbf{s}_1 + \boldsymbol{\nu}_1, \quad (2.8)$$

where  $\mathbf{H}_{11} = \mathbf{F}\mathcal{J}(\mathbf{h}^{(11)})\mathbf{A}\mathbf{F}^{-1}$  is an  $N \times N$  diagonal overall channel matrix for the primary system and  $\boldsymbol{\nu}_1$  the Fourier transform of the noise  $\mathbf{n}_1$ , has the same statistics as  $\mathbf{n}_1$ .

The primary system does not cooperate with the secondary one, which performs single user decoding at the secondary receiver. Therefore, we take

$$\boldsymbol{\eta} = \mathbf{H}_{12}\mathbf{s}_1 + \boldsymbol{\nu}_2, \quad (2.9)$$

as the interference plus noise component, obtained when substituting (2.5) and (2.6) into (2.2), where  $\mathbf{H}_{12} = \mathbf{F}\mathcal{J}(\mathbf{h}^{(12)})\mathbf{A}\mathbf{F}^{-1}$  is an  $N \times N$  diagonal overall channel matrix for the primary system and  $\boldsymbol{\nu}_2$  the Fourier transform of the noise  $\mathbf{n}_2$ , has the same statistics as  $\mathbf{n}_2$ . The use of a DFT and the removal of the leading  $L$  symbols at the secondary receiver makes it possible to consider a diagonal  $\mathbf{H}_{12}$ , which in turn, allows a simplification of the subsequent analysis w.r.t.  $\boldsymbol{\eta}$ . The signal received at the secondary system becomes

$$\mathbf{y}_2 = \mathbf{H}_{22}\mathbf{s}_2 + \boldsymbol{\eta}, \quad (2.10)$$

where  $\mathbf{H}_{22} = \mathbf{F}\mathcal{J}(\mathbf{h}^{(22)})\mathbf{E}$  denotes the overall  $N \times L$  secondary channel. Finally, from (2.8) and (2.10), we remark that VFDM successfully converts the frequency-selective interference channel (2.1) and (2.2) (or X interference channel) into an one-side vector interference channel (or Z interference channel) where the primary receiver sees interference-free  $N$  parallel channels, while the secondary receiver sees interference from the primary transmitter.

## 2.3 Precoder Design

To achieve its best performance, the secondary system must be designed with two goals in mind: 1) maximize the achievable rate at the secondary system; 2) enforce the interference

protection at the primary system. In mathematical terms, this is equivalent to finding  $\mathbf{S}_2$  and  $\mathbf{E}$  that solve the following optimization problem

$$\begin{aligned} \max_{\mathbf{s}_2, \mathbf{E}} & \left( \frac{1}{N+L} \log_2 |\mathbf{I}_N + \mathbf{S}_\eta^{-1/2} \mathbf{F} \mathcal{T}(\mathbf{h}^{(22)}) \mathbf{E} \mathbf{S}_2 \mathbf{E}^H \mathcal{T}(\mathbf{h}^{(22)})^H \mathbf{F}^H \mathbf{S}_\eta^{-H/2}| \right) \\ \text{s.t.} & \begin{cases} \text{tr}(\mathbf{E}^H \mathbf{E} \mathbf{S}_2) \leq (N+L)P_2 \\ \mathcal{T}(\mathbf{h}^{(21)}) \mathbf{E} = \mathbf{0}. \end{cases}, \end{aligned} \quad (2.11)$$

where  $\mathbf{S}_2$  is the covariance matrix of  $\mathbf{s}_2$ ,  $\mathbf{S}_\eta = \mathbf{H}_{12} \mathbf{S}_1 \mathbf{H}_{12}^H + \sigma_n^2 \mathbf{I}_N$  is the covariance matrix of  $\boldsymbol{\eta}$ , the first constraint comes from (2.4) and the second constraint comes from (2.7). We approximate  $\boldsymbol{\eta}$  to a zero-mean Gaussian random vector. Note that, the objective function in (2.11) does not take into consideration the rate at the primary system. This is the case since, by guaranteeing zero interference from the secondary system, the primary system can achieve maximum capacity through the optimization of its own input power allocation [49].

A closed form solution for (2.11) is not known. A similar problem has been addressed in [50] (based on [51]) where a numerical solution, using convex relaxation and generalized inverses, is used to find the optimal steering vectors and transmit powers. In this work, a suboptimal solution is proposed by exploiting the fact that the second constraint gives a clue on the design conditions of  $\mathbf{E}$ . Due to the particular structure of  $\mathcal{T}(\mathbf{h}^{(21)})$ , it is not difficult to show that a matrix  $\mathbf{E}$ , capable of yielding  $\mathcal{T}(\mathbf{h}^{(21)}) \mathbf{E} = \mathbf{0}$ , has to evaluate the polynomial

$$S(z) = \sum_{i=0}^L h_i^{(21)} z^{L-i},$$

at its roots  $\{a_1, \dots, a_L\}$ . Interestingly, the Vandermonde matrix is known for its property to evaluate a polynomial at certain values [52]. In fact, it is straightforward to see that

$$\mathbf{V} = \begin{bmatrix} 1 & \dots & 1 \\ a_1 & \dots & a_L \\ a_1^2 & \dots & a_L^2 \\ \vdots & & \vdots \\ a_1^{N+L-1} & \dots & a_L^{N+L-1} \end{bmatrix}, \quad (2.12)$$

defines the null-space of  $\mathcal{T}(\mathbf{h}^{(21)})$  and, without loss of generality, we can further choose the columns of  $\mathbf{E}$  as any linear combination based on the columns of  $\mathbf{V}$ , such that

$$[\mathbf{E}]_k = \sum_{l=1}^L [\boldsymbol{\Gamma}]_{k,l} \mathbf{v}_l \quad (2.13)$$

where  $[\boldsymbol{\Gamma}]_{k,l}$  is the  $(k^{\text{th}}, l^{\text{th}})$  element of  $\boldsymbol{\Gamma} \in \mathcal{R}^{L \times L}$ , a coefficient matrix. From (2.13) we can finally define  $\mathbf{E}$  as

$$\mathbf{E} \triangleq \mathbf{V} \boldsymbol{\Gamma}. \quad (2.14)$$

Note that by carefully tuning  $\mathbf{\Gamma}$  we can effectively select any suitable  $\mathbf{E}$  precoder inside of the null-space of  $\mathcal{T}(\mathbf{h}^{(21)})$ . Since the precoder is based on a Vandermonde generated subspace and its orthogonality w.r.t.  $\mathcal{T}(\mathbf{h}^{(21)})$  enables the users to transmit simultaneously over the same frequency band, we have decided to name this scheme *Vandermonde-subspace frequency division multiplexing* (VFDM).

In practice,  $\mathbf{E}$  is constructed by selecting  $\mathbf{\Gamma}$  such that a set of  $L$  orthonormal columns, that lie inside of the Vandermonde-subspace of  $\mathcal{T}(\mathbf{h}^{(21)})$ , is found. This can be accomplished by finding the QR decomposition [53] of  $\mathbf{V} = \mathbf{E}\mathbf{\Gamma}^{-1}$ , where  $\mathbf{\Gamma}^{-1}$  is an upper triangular matrix and  $\mathbf{E}$  is orthonormal. Since  $\mathbf{V}$  will be nonsingular with a high probability,  $\mathbf{E}$  is unique and can be numerically obtained by performing a Gram-Schmidt process [53] on the columns of  $\mathbf{V}$ . Another way to construct  $\mathbf{E}$  is by singular value decomposition (SVD) of  $\mathcal{T}(\mathbf{h}^{(21)})$  [54], where if  $\mathcal{T}(\mathbf{h}^{(21)}) = \mathbf{U}_{\mathcal{T}}\mathbf{\Lambda}_{\mathcal{T}}\mathbf{V}_{\mathcal{T}}^H$ , then

$$\mathbf{E} = [ \mathbf{v}_{\mathcal{T}N} \mid \cdots \mid \mathbf{v}_{\mathcal{T}(N+L)-1} \mid \mathbf{v}_{\mathcal{T}N+L} ],$$

and  $\mathbf{V}_{\mathcal{T}}$  has the form  $[ \mathbf{v}_{\mathcal{T}1} \mid \mathbf{v}_{\mathcal{T}2} \mid \cdots \mid \mathbf{v}_{\mathcal{T}N+L} ]$ .

Finally we stress that, since the single antenna interference channel is the target of this work. If multiple antennas were to be adopted at the secondary transmitter, then the spatial dimension could be used to manage interference to the primary receiver, by means of techniques such as ZF precoding.

## 2.4 Optimal Receiver

In order to determine the achievable rates at the secondary system, we introduce a simplification: instead of trying to solve (2.11) over both  $\mathbf{S}_2$  and  $\mathbf{E}$ , we choose a  $\mathbf{\Gamma}$  matrix that provides a well-behaved  $\mathbf{E}$  with orthonormal columns, and optimize only on  $\mathbf{S}_2$ . The optimization problem now becomes

$$\max_{\mathbf{S}_2} \quad \left( \frac{1}{N+L} \log_2 |\mathbf{I}_N + \mathbf{S}_\eta^{-1/2} \mathbf{H}_{22} \mathbf{S}_2 \mathbf{H}_{22}^H \mathbf{S}_\eta^{-H/2}| \right) \quad (2.15)$$

$$\text{s.t.} \quad \text{tr}(\mathbf{E}^H \mathbf{E} \mathbf{S}_2) \leq (N+L)P_2, \quad (2.16)$$

where we have dropped the second restriction since it becomes implicit from the precoder design.

At this point some remarks are of order. Since the channels  $\mathbf{h}^{(21)}$  and  $\mathbf{h}^{(22)}$  are statistically independent, the probability that  $\mathcal{T}(\mathbf{h}^{(21)})$  and  $\mathcal{T}(\mathbf{h}^{(22)})$  have the same null-space is zero. Hence, we can expect that the secondary user's symbols  $\mathbf{s}_2$  will be transmitted reliably. Furthermore, since the precoder does not depend on the transmitted symbols and due to the orthogonality between the channel and the precoder, the orthogonality condition (2.7) always holds irrespectively of the secondary system's input power  $P_2$  and its link. Clearly, perfect knowledge of the  $\mathbf{h}^{(21)}$  channel state information (CSI) is required at the secondary transmitter in order to adapt the precoder to the channel fluctuations.

In addition to that, perfect knowledge of the interference plus noise covariance  $\mathbf{S}_\eta$  of the secondary receiver is also required at the secondary transmitter. Practical aspects on how to perform channel estimation is given in detail in section 5.3.

The new optimization problem in (2.15) is also convex, but the presence of the term  $\mathbf{E}^H \mathbf{E}$  in the constraint (2.16) requires a prior manipulation step in order to obtain a water-filling solution. Let us initially define

$$\mathbf{G} = \mathbf{S}_\eta^{-1/2} \mathbf{H}_{22},$$

with  $\mathbf{G} \in \mathcal{C}^{N \times L}$  to be an equivalent channel. We then take the SVD of the equivalent channel  $\mathbf{G} = \mathbf{U}_G \mathbf{\Lambda}_G^{1/2} \mathbf{V}_G^H$ , where  $\mathbf{U}_G \in \mathcal{C}^{N \times N}$  and  $\mathbf{V}_G \in \mathcal{C}^{L \times L}$  are unitary matrices and  $\mathbf{\Lambda}_G \in \mathcal{R}^{N \times L}$  contains a top diagonal with the  $r \leq L$  eigenvalues of  $\mathbf{G}^H \mathbf{G}$ , with  $[\mathbf{\Lambda}_G]_{i,i} \geq 0$ . Finally, we let  $\mathbf{S}_2 = \mathbf{V}_G \mathbf{D}_2 \mathbf{V}_G^H$  with  $\mathbf{D}_2 \in \mathcal{R}^{L \times L}$  being  $\text{diag}[d_1, \dots, d_L]$ , and  $\mathbf{Q} = \mathbf{V}_G^H \mathbf{E}^H \mathbf{E} \mathbf{V}_G$ . Using these new definitions (2.15) and (2.16) become

$$\begin{aligned} \max_{\mathbf{P}_2} \quad & \left( \frac{1}{N+L} \log \left| \mathbf{I}_N + \mathbf{U}_G \mathbf{\Lambda}_G^{1/2} \mathbf{D}_2 \mathbf{\Lambda}_G^{H/2} \mathbf{U}_G^H \right| \right) \\ \text{s.t.} \quad & \text{tr}(\mathbf{Q} \mathbf{D}_2) \leq (N+L)P_2, \end{aligned}$$

which can be further rewritten in scalar form as

$$\begin{aligned} \max_{d_i} \quad & \sum_{i=1}^L \log_2(1 + d_i [\mathbf{\Lambda}_G]_{i,i}) \\ \text{s.t.} \quad & \sum_{i=1}^L d_i [\mathbf{Q}]_{i,i} \leq (N+L)P_2. \end{aligned} \tag{2.17}$$

The optimization problem in its new form (2.17) can be solved using the Karush-Kuhn-Tucker (KKT) conditions which lead to the classical water-filling solution [55]. The solution to (2.17) is given by  $\mathbf{S}_2 = \mathbf{V}_G \mathbf{D}_2 \mathbf{V}_G^H$ , where the  $i^{\text{th}}$  component of the matrix  $\mathbf{D}$  is the weighted water-filling solution given by

$$d_i = \left[ \frac{\mu}{[\mathbf{Q}]_{i,i}} - \frac{1}{[\mathbf{\Lambda}_g]_{i,i}} \right]_+, \tag{2.18}$$

where  $\mu$ , known as the ‘‘water level’’, is determined to fulfill the total power constraint  $(N+L)P_2$ . Since we have chosen  $\mathbf{\Gamma}$  such that  $\mathbf{E}$  is orthonormal, it follows that  $\forall i, [\mathbf{Q}]_{i,i} = 1$ , and therefore, the maximum achievable spectrum efficiency for the secondary system is finally given by

$$R_{\text{opt}} = \frac{1}{N+L} \sum_{i=1}^L \log_2(1 + d_i [\mathbf{\Lambda}_G]_{i,i}). \tag{2.19}$$

### 2.4.1 Performance

To illustrate the performance of VFDM’s optimal receiver, numerical results were produced through Monte Carlo based simulations. The parameters used herein are inspired

by IEEE 802.11a [9]. All channels and noise are generated according to the definitions made in section 2.1. Transmit powers are considered to be unitary for both primary and secondary system, and the signal to noise ratio (SNR) is controlled by varying the noise variance  $\sigma_n^2$ .  $\mathbf{E}$  is generated by a Gram-Schmidt process on the columns of  $\mathbf{V}$ , as described in section 2.3. For some of the presented results, in order to control the secondary system's performance with respect to the interference coming from the primary system, an interference weighting factor  $\alpha$  has been added to (2.9) such that

$$\boldsymbol{\eta} = \alpha \mathbf{H}_{12} \mathbf{s}_1 + \boldsymbol{\nu}_2. \quad (2.20)$$

A summary of the simulation parameters is presented in table 2.1.

parameter	value
Number of carriers ( $N$ )	64
Cyclic prefix size ( $L$ )	16
Channels	$\mathcal{CN}(0, \mathbf{I}_{L+1}/(L+1))$
Additive noise	$\mathcal{CN}(0, \sigma_n^2 \mathbf{I}_N)$
$\mathbf{E}$ construction	Gram-Schmidt process
Interference factor ( $\alpha$ )	$\alpha \in \{0, 0.1, 0.5, 1\}$

Table 2.1: Simulation parameters

In figure 2.2, VFDM's average achievable spectrum efficiency using an optimal receiver is given for  $N = 64$  and three sizes of channel  $L \in \{8, 16, 32\}$  taps. In order to isolate the performance of the secondary system,  $\alpha$  is taken to be zero. The spectrum efficiency is seen to suffer a higher penalty for smaller values of  $L$ , since this directly translates into a smaller number of available precoding dimensions.

In figure 2.3, the effect of interference coming from the primary system on the spectral efficiency performance of VFDM is shown. As expected, the secondary system quickly becomes interference limited the higher the  $\alpha$ . Nevertheless, it is interesting to see that even in the worse case scenario, VFDM is still able to offer non-negligible rates.

## 2.5 Sub-optimal Linear Receivers

Up to this point, the performance analysis of VFDM considered optimal decoding, which is not feasible in practice. In this section, we shift our focus to linear equalizers, moving one step closer to the implementation of a practical VFDM system. We analyze the choice of three classical linear equalizers: minimum mean square error (MMSE), ZF and matched filter (MF) in the performance of VFDM.

To construct the linear equalizer for VFDM, let us initially consider the estimated symbols at the secondary receiver  $\hat{\mathbf{s}}_2$  as

$$\hat{\mathbf{s}}_2 = \mathbf{C} \mathbf{y}_2, \quad (2.21)$$

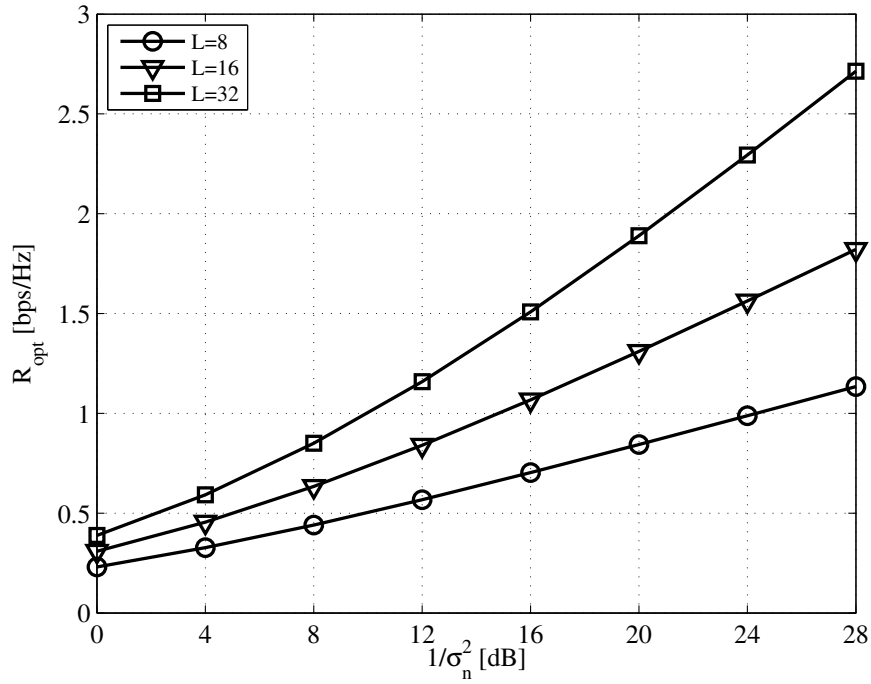


Figure 2.2: VFDM's spectral efficiency for  $N = 64$ ,  $L \in \{8, 16, 32\}$  and  $\alpha=0$ .

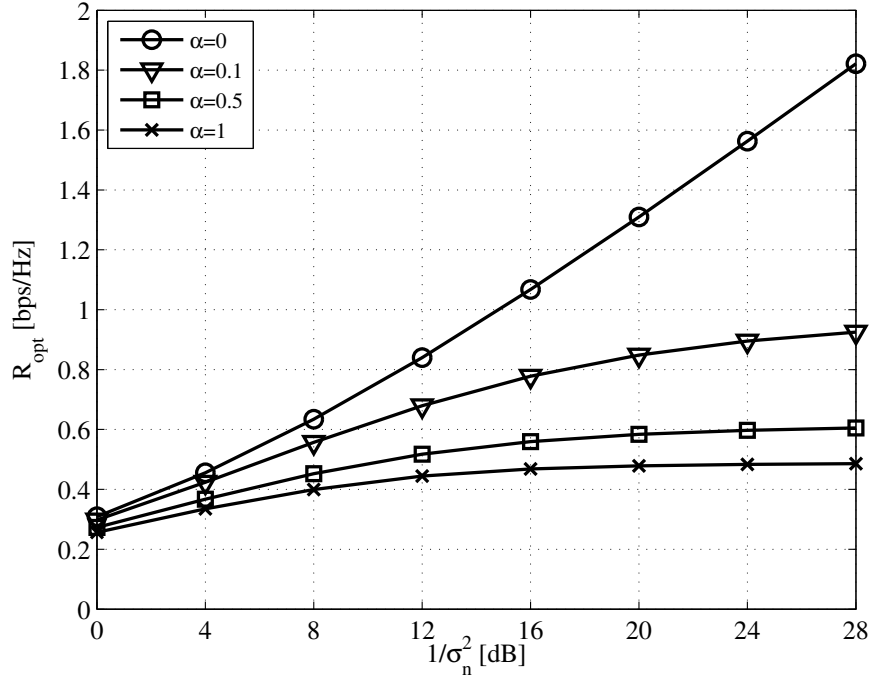


Figure 2.3: VFDM's spectral efficiency for  $N = 64$ ,  $L = 16$  and  $\alpha \in \{0, 0.1, 0.5, 1\}$ .

where  $\mathbf{C}$  is the linear equalizer. Starting from the definition of MMSE [55, 56, 57],  $\mathbf{C}$  can

be written as

$$\mathbf{C}_{\text{MMSE}} = \mathbf{H}_{22}^{\text{H}} (\mathbf{S}_{\eta} + \mathbf{H}_{22} \mathbf{H}_{22}^{\text{H}})^{-1}, \quad (2.22)$$

for which the secondary receiver needs an estimate for  $\mathbf{H}_{22}$  and the covariance of the noise plus interference  $\mathbf{S}_{\eta}$ . Again, from the definition, the ZF filter [55, 56, 57] can be written as

$$\mathbf{C}_{\text{ZF}} = \mathbf{H}_{22}^{\dagger},$$

which, in the case of the rectangular overall channel matrix  $\mathbf{H}_{22}$ , the inversion becomes the pseudo-inverse operation (defined by  $\mathbf{H}_{22}^{\dagger} = (\mathbf{H}_{22}^{\text{H}} \mathbf{H}_{22})^{-1} \mathbf{H}_{22}^{\text{H}}$ ). Finally, for the MF [55, 56, 57], the equalizer is given by

$$\mathbf{C}_{\text{MF}} = \mathbf{H}_{22}^{\text{H}}. \quad (2.23)$$

Differently from the MMSE case, the ZF and MF cases require only an estimate for the overall channel  $\mathbf{H}_{22}$ , thus, ignoring the noise and interference effect on the equalization procedure.

For the three equalizers, the effective signal to interference plus noise ratio (SINR) is given as

$$\gamma_k = \frac{|\mathbf{c}_k^{\text{H}} \mathbf{h}_{22k}|^2}{\sigma^2 |\mathbf{c}_k \mathbf{c}_k^{\text{H}}|^2 + \sum_{m=1}^N |\mathbf{c}_k^{\text{H}} \mathbf{h}_{12m}|^2 + \sum_{n=1; j \neq k}^L |\mathbf{c}_k^{\text{H}} \mathbf{h}_{22n}|^2}, \quad (2.24)$$

where  $\gamma_k$  is the SINR contribution of the  $k^{\text{th}}$  received symbol,  $\mathbf{c}_k$  is the  $k^{\text{th}}$  column of  $\mathbf{C}$  and  $\mathbf{h}_{(\cdot)k}$  is the  $k^{\text{th}}$  column of  $\mathbf{H}_{(\cdot)}$ .

### 2.5.1 Performance

In order to better understand the performance of VFDM based linear receivers, Monte Carlo simulations were executed, following the same configuration parameters as in section 2.4.1.

In figure 2.4 the spectral efficiency is given for all three equalizers as well as the optimal receiver, for reference. The spectral efficiency for the linear receivers  $R_{\text{lin}}$  is obtained by substituting  $\gamma_k$  into the general capacity expression

$$R_{\text{lin}} = \frac{1}{N + L} \sum_{k=1}^L \mathbb{E} [\log_2 (1 + \gamma_k)].$$

Again, we isolate the performance of the secondary system by setting  $\alpha$  to zero. The optimal receiver clearly outperforms the three other equalizers with an almost constant gap of about 2 dB with respect to MMSE and around 4 dB with respect to the ZF. Even though there is no interference coming from the primary system, the MMSE takes

into consideration the characteristics of the noise, which explains its best performance among the three linear receivers. The MF presents the worst performance, with capacity saturating at around 16 dB.

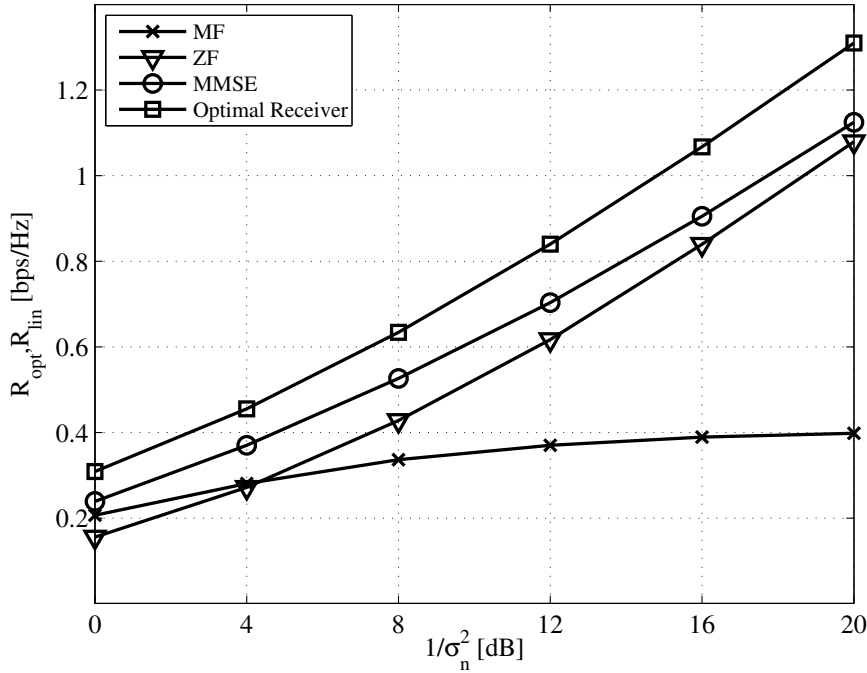


Figure 2.4: VFDM's  $R_{\text{opt}}$  and  $R_{\text{lin}}$  for the MMSE, ZF and MF equalizers for  $N = 64$ ,  $L = 16$  and  $\alpha = 0$ .

The previous findings are confirmed when seen from the probability of error  $P_e$  perspective, as shown in figure 2.5. In this figure, the probability of error given by

$$P_e = \frac{1}{L} \sum_{k=1}^L \mathbb{E}[Q(\sqrt{\gamma_k})],$$

is calculated considering the transmission of a quadrature phase shift keying (QPSK) constellation [58] and  $Q(\cdot)$  is the  $Q$ -function. This time, we concentrate only on the linear receivers and, once again,  $\alpha$  is set to zero, to isolate the their performance. MMSE outperforms the two other equalizers with a constant gap of about 4 dB compared to the ZF.

In figure 2.6, we concentrate only on the best performing linear receivers (ZF and MMSE) to minimize the clutter. This time,  $P_e$  curves are presented for increasing interference ( $\alpha \in \{0, 0.5, 1\}$ ) factors. As expected, the presence of interference severely degrades the performance of both equalizers.

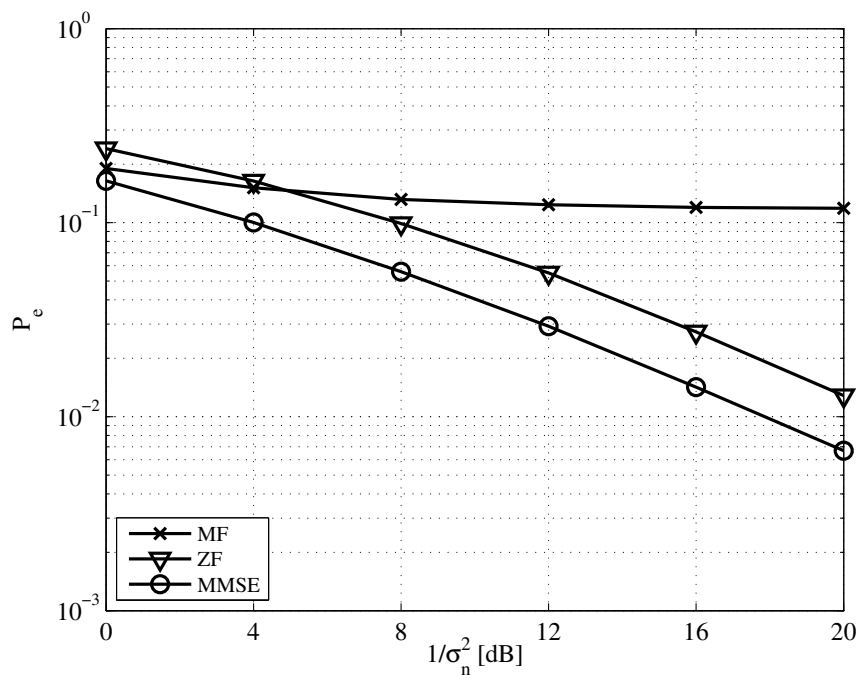


Figure 2.5: VFDM's  $P_e$  for the MMSE, ZF and MF equalizers for  $N = 64$ ,  $L = 16$  and  $\alpha = 0$ .

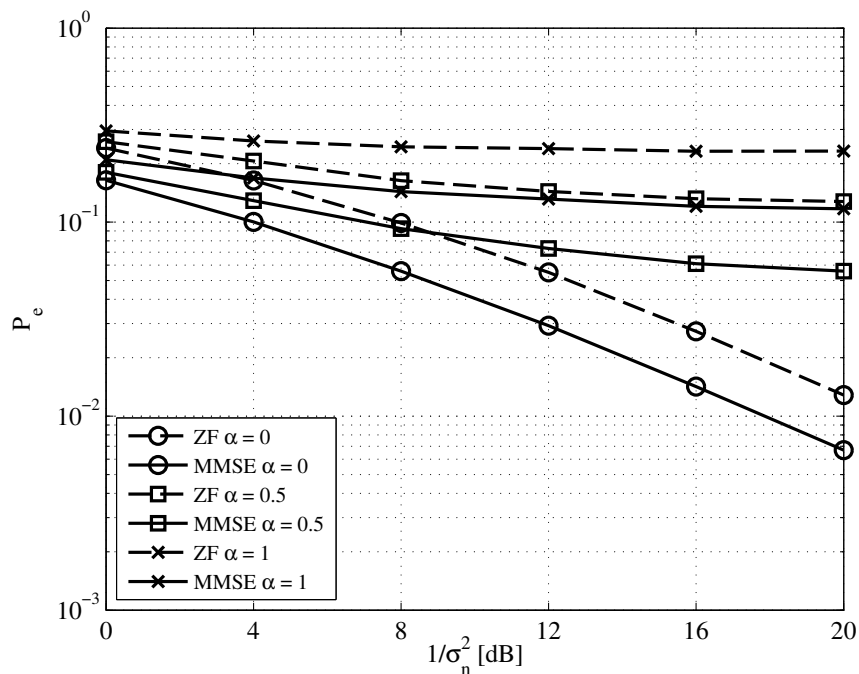


Figure 2.6: Comparative probability of bit error ( $P_e$ ) for the MMSE and ZF equalizer for varying interference levels  $\alpha = \{0, 0.5, 1\}$  ( $N = 64$ ,  $L = 16$ ).

## 2.6 VFDM vs. Spectrum Sensing Resource Sharing

In many works (e.g., [59]), cognitive radio systems exploit the fact that, primary systems based on multiple carriers select only a subset of channels according to specific channel quality indicators (CQIs). Through the detection of free carriers, by means of spectrum sensing, a secondary system can transmit at the same time on those unused carriers. Herein, the performance of VFDM is compared with that of a hypothetical reference interference free system. We assume such a system to be OFDM-based, dividing its carriers in a 3/4, for the *reference primary system*, to 1/4, for the reference secondary system. The 3/4—1/4 choice was done merely for fairness in terms of resource sharing, since the simulated VFDM system transmits  $L = 16$  symbols while OFDM transmits  $N = 64$ , hence the 1/4 proportion). Nevertheless, the results and conclusions that follow, hold for any carrier proportion choice. In figure 2.7, we see that, although the VFDM secondary system has a comparable performance to the OFDM 1/4 reference secondary system, a good performance can be assured for the latter since there is no interference coming from the OFDM 3/4 reference primary system. Nevertheless, the VFDM based secondary system is subject to interference from the regular OFDM based primary system and can experience a severely degraded performance for  $\alpha = 1$ . This good performance for the reference secondary system comes at the cost of a loss of performance at the reference primary system, a limitation not seen for the regular OFDM based primary system. This finding becomes even more evident when seen from the sum spectral efficiency point of view in figure 2.8, where the spectral efficiency of both the primary and secondary systems are summed up. In this result, it becomes evident that OFDM—VFDM surpasses the performance of the OFDM with shared resources (3/4 — 1/4), even with secondary VFDM system under full interference from the primary ( $\alpha = 1$ ).

## 2.7 Closing Remarks

We have seen that VFDM can indeed, depending on the resources available, outperform a spectrum sensing based secondary system that exploits the unused carriers by the primary system. This interesting result motivates the continuation of the development of VFDM in the next chapter, this time extending the number of users the  $\mathbf{E}$  pre-coder can cancel the interference to.

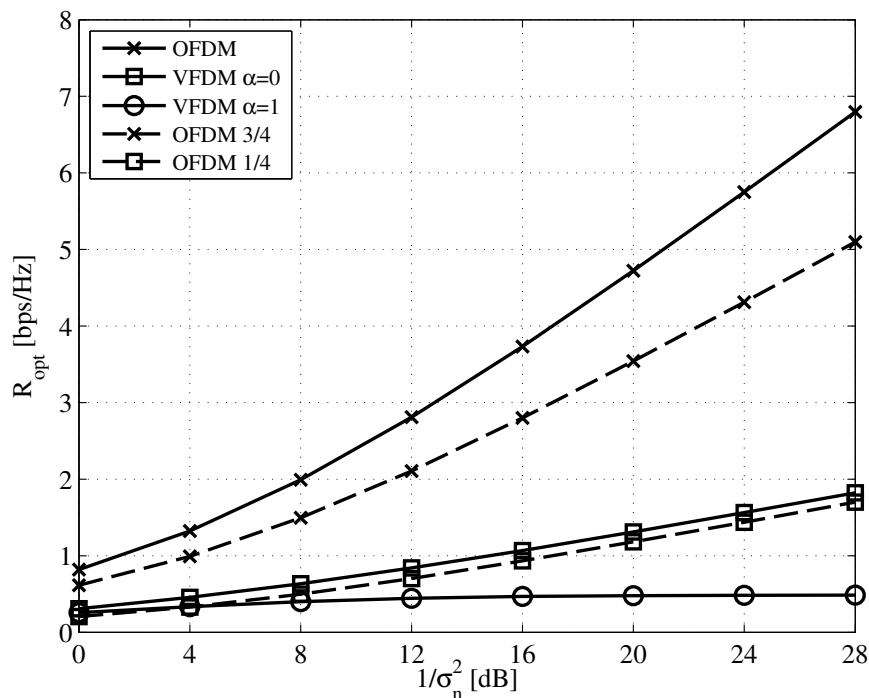


Figure 2.7: VFDM's spectral efficiency for  $N = 64$ ,  $L = 16$  and  $\alpha \in \{0, 1\}$ , compared to OFDM with (3/4 — 1/4) shared resources.

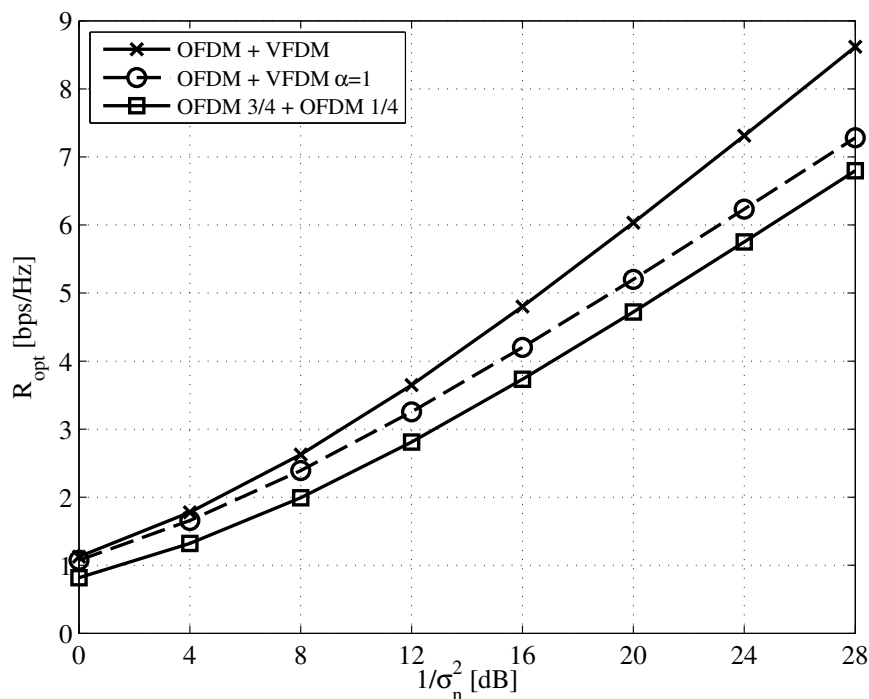


Figure 2.8: VFDM's sum (primary + secondary) spectral efficiency for  $N = 64$ ,  $L = 16$  and  $\alpha \in \{0, 1\}$ , compared to OFDM with (3/4 — 1/4) shared resources.

# Chapter 3

## Towards Multiple Users

**W**E HAVE SEEN previously how to create a pre-coder that enables a simultaneous transmission of a secondary system and a primary system over the same band and at the same time. VFDM has been shown to work for a cognitive interference channel, that counts with only a single primary and secondary receiver. The natural question now is: how can VFDM be modified to allow for the operation of a secondary system along with a multi-user primary system? In this chapter, we extend the previous findings by considering a multi-user primary system based on orthogonal frequency division multiple access (OFDMA). We devise a new pre-coder, inspired on the original VFDM one, able to cope with multiple primary receivers and we show that zero-interference at the primary system can still be achieved. The results in this chapter serve as a leading step to the full multi-user scenario, which will be the focus of chapter 4.

### 3.1 Multi-User: Initial Considerations

Before providing a solution to multiple users, let us first try to understand the limitations of VFDM on a multi-user environment. Herein we will explore the candidate multi-user scenarios and discuss their possibilities and drawbacks with respect to our candidate technique.

For what concerns the primary system, the design of a downlink-only<sup>1</sup> VFDM transmitter is only affected by the primary receiver(s). Therefore, in the discussion to be carried in the following, the multiplicity of primary transmitters is disregarded. Of course, the effect of several primary transmitters on the performance of the secondary system cannot be ignored, but the main interest of this discussion is on the design of the pre-coder. Three target scenarios of interest (figure 3.1) are identified (the remaining, omitted for

---

<sup>1</sup>We remind the reader that, as indicated in the introduction of this thesis, only the downlink is considered throughout this work. The uplink is left as an open issue for a future work.

brevity, are especial cases of the ones presented):

1. **Multiple** primary RX — **Single** secondary TX — **Single** secondary RX:

This is the case of a point-to-point secondary system operating on the same band as a broadcast primary system, as seen in figure 3.1(a). An example of this scenario is a VFDM personal area network (PAN) system, and a primary cellular system. In this case, the secondary transmitter must be able to cancel the interference to multiple primary receivers. This could be either done in a time-sharing manner, if the primary system adopts time division multiple access (TDMA) communications, or all at once if the primary system uses a OFDMA style resource sharing. No changes are required to the secondary receiver, that works just as presented in the previous chapter.

2. **Multiple** primary RX — **Single** secondary TX — **Multiple** secondary RX:

This is the case for a broadcast primary and secondary systems, as shown in figure 3.1(b). An example of such a scenario could be competing cellular technologies, one legacy and one opportunistic. In this case, not much is changed with respect to the previous case regarding the secondary transmitter. The secondary receivers, on the other hand would have to share the already scarce resources in between them, degrading the performance. One option to remediate this is to add multiple antennas at the secondary transmitter.

3. **Multiple** primary RX — **Multiple** secondary TX — **Multiple** secondary RX:

This is the case for a broadcast primary system and a multiple point-to-point secondary system, such as seen in figure 3.1(c). A cellular system at the primary and an ad-hoc system at the secondary could be an example of such a scenario. The main difference with what concerns the secondary transmitters is that, this time, each one will need to cancel its own interference to all the primary users. The secondary receivers this time will not only suffer interference from the primary system, but also from other secondary transmitters. To remediate this, the secondary transmitters can coordinate to form a network-MIMO network to deal with multi-user interference.

Scenario #1 is the simplest one to address and will be the focus of the remainder of this chapter. Instead of the TDMA case, which can be reduced to a timed version of the single user case, herein the OFDMA case is addressed. Scenario #2 is interesting, but its challenges are superseded by those of Scenario #3, which will be addressed in chapter 4. Indeed, Scenario #2, can be seen as a simplification of the one in #3, especially if MIMO is considered at its sole secondary transmitter.

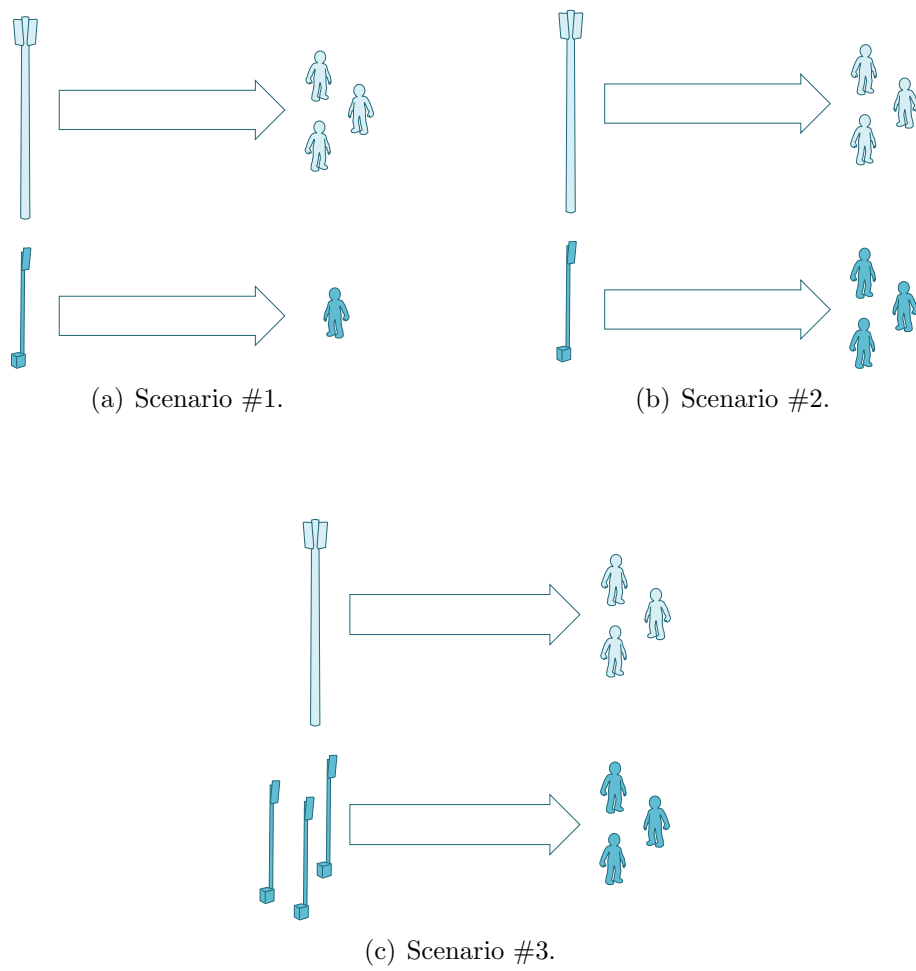


Figure 3.1: Multi-user scenarios.

### 3.2 Multi-Primary — Single-Secondary System Model

Consider the downlink scenario depicted in figure 3.2, where a secondary system composed by a transmitter/receiver pair is added to communicate over the same bandwidth as the primary long term evolution (LTE)-like [60] OFDMA system. The secondary system must not generate interference at the primary one, which is unaware of the existence of the secondary system. Since the primary system has the rights to the spectrum, it does not need to avoid interference to the secondary. We consider only the downlink, with single antenna transmitter/receiver pairs in both systems.

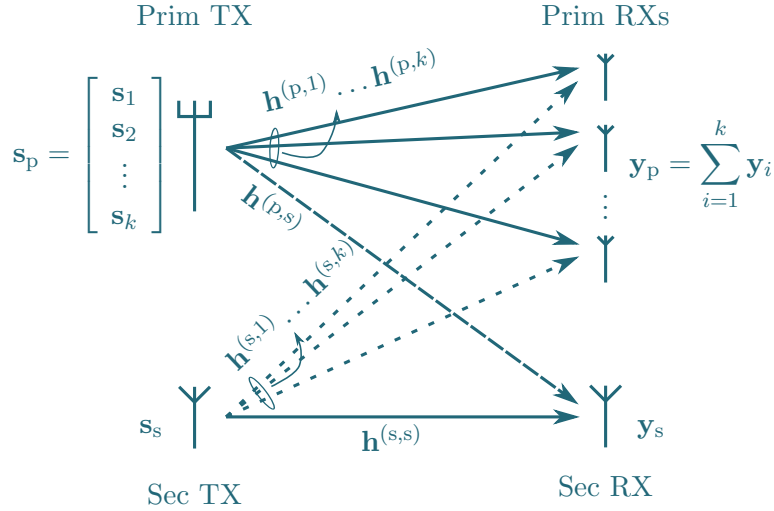


Figure 3.2: OFDMA downlink cognitive interference channel model.

Let  $\mathbf{h}^{(p,i)}$  denote the channel vector between the primary transmitter and receiver  $i$ ,  $\mathbf{h}^{(s,i)}$  the channel between the secondary transmitter and primary receiver  $i$ ,  $\mathbf{h}^{(s,s)}$  the channel between the secondary transmitter and receiver and  $\mathbf{h}^{(p,s)}$  the channel between the primary transmitter and secondary receiver. All channel vectors are composed of  $L + 1$  i.i.d. Gaussian, complex and circularly symmetric taps  $\mathcal{CN}(0, \mathbf{I}_{L+1}/(L + 1))$ . Also indicated in figure 3.2,  $\mathbf{s}_p$  is a zero mean, unit norm aggregate primary transmitted symbol vector composed of all the individual symbol vectors  $\mathbf{s}_i$ , whereas  $\mathbf{y}_p$  is the aggregate primary received symbol vector, defined similarly.  $\mathbf{s}_s$  is a zero mean, unit norm secondary transmitted symbol vector while  $\mathbf{y}_s$  is the received data for the secondary transmission. The primary transmitter employs a  $k$ -user time division duplexing (TDD) OFDMA system of block size  $N + L$ , of which  $N$  is the number of carriers and  $L$  the size of the cyclic prefix. For simplicity, an equal resource sharing is adopted, i.e.  $N/k$  subcarriers per primary receiver,  $\mathcal{S}_i$  being the set of subcarriers indices assigned for user  $i$  with  $\bigcup_{i=1}^k \mathcal{S}_i = \{1, \dots, N\}$ . The overall received signal at primary receiver  $i$  is

$$\mathbf{y}_i = \mathbf{B}_i \mathbf{F} (\mathcal{T}(\mathbf{h}^{(p,i)}) \mathbf{A} \mathbf{F}^{-1} \mathbf{s}_p + \mathcal{T}(\mathbf{h}^{(s,i)}) \mathbf{E} \mathbf{s}_s + \mathbf{n}_p), \quad (3.1)$$

where  $\mathbf{F} \in \mathcal{C}^{N \times N}$  is a unitary DFT matrix,  $\mathbf{n}_p$  is a  $N$ -sized AWGN noise vector  $\mathbf{n}_p \sim \mathcal{CN}(0, \sigma^2 \mathbf{I}_N)$ ,  $\mathbf{A}$  is a  $(N + L) \times N$  cyclic prefix precoding matrix and  $\mathbf{E} \in \mathcal{C}^{(N+L) \times L}$  is

a linear precoder.  $\mathcal{T}(\mathbf{h}^{(\cdot,\cdot)}) \in \mathbb{C}^{N \times (N+L)}$  is a Toeplitz matrix constructed from the  $\mathbf{h}^{(\cdot,\cdot)}$  channel coefficients and  $\mathbf{B}_i$  is a partial identity matrix that models the receiver filter mask for the subcarriers of interest to user  $i$  and is given by  $[\mathbf{B}_i]_{m,m} = 1$ , if  $m \in \mathcal{S}_i$ . Summing up all  $\mathbf{y}_i$  contributions for the primary receivers gives us

$$\mathbf{y}_p = \mathbf{K}_p \mathbf{A} \mathbf{F}^{-1} \mathbf{s}_p + \mathbf{K}_s \mathbf{E} \mathbf{s}_s + \nu_p, \quad (3.2)$$

where  $\mathbf{K}_p = \sum_{i=1}^k \mathbf{B}_i \mathbf{F} \mathcal{T}(\mathbf{h}^{(p,i)})$  and  $\mathbf{K}_s = \sum_{i=1}^k \mathbf{B}_i \mathbf{F} \mathcal{T}(\mathbf{h}^{(s,i)})$  are the overall main channel and overall interfering channel, respectively, and  $\nu_p$  is the Fourier transform of the noise  $\mathbf{n}_p$  and has the same statistics as  $\mathbf{n}_p$ .

Concerning the secondary system, a point-to-point  $(N + L)$ -sized block transmission scheme is adopted with the first  $L$  symbols discarded to avoid block interference. The received signal at the secondary receiver is

$$\mathbf{y}_s = \mathbf{F} (\mathcal{T}(\mathbf{h}^{(s,s)}) \mathbf{E} \mathbf{s}_s + \mathcal{T}(\mathbf{h}^{(p,s)}) \mathbf{A} \mathbf{F}^{-1} \mathbf{s}_p + \mathbf{n}_s). \quad (3.3)$$

Regarding (3.3), as defined for the primary system,  $\mathbf{n}_s$  is a  $N$ -sized AWGN noise vector  $\mathbf{n}_s \sim \mathcal{CN}(0, \sigma^2 \mathbf{I}_N)$ .

Once again, our objective is to find a linear precoder  $\mathbf{E}$  such that for any  $\mathbf{s}_s$ , we effectively satisfy the orthogonal condition

$$\mathbf{K}_s \mathbf{E} = \mathbf{0}. \quad (3.4)$$

### 3.3 Precoder Design

It is clear from (3.4) that such a precoder needs to be on the null-space of the overall interfering channel. We have shown in section 2.3 that we can easily design such a precoder using a specially built Vandermonde matrix whose entries are built upon the roots of the interfering channel  $h_i$  polynomial in  $z$ . Unfortunately, due to the different nature of the overall channel matrix in the OFDMA case, this result is not applicable. Indeed, for the OFDMA case, there is not only one interference channel as for the original cognitive interference channel case, but  $k$ :  $\{\mathbf{h}^{(s,1)}, \dots, \mathbf{h}^{(s,k)}\}$ . Obviously, constructing a Vandermonde matrix based on the roots of the channel is not possible anymore. Fortunately, other means of finding the null-space of  $\mathbf{K}_s$  exist, as shown in section 2.3. Herein, the pre-coder is designed by means of the SVD of the overall interference channel matrix  $\mathbf{K}_s$ . Note that, similar to what has been seen in the previous chapter, the dimensionality of the problem remains the same, meaning  $L$  is the maximum number of symbols that can be transmitted by the secondary system. This restriction is still due to the size of the null-space of  $\mathbf{K}_s$ .

As seen previously, the construction of  $\mathbf{E}$  requires perfect knowledge of the  $\mathbf{h}^{(s,i)}$  CSIs at the secondary transmitter. In chapter 5, a more detailed description of ways of acquiring

CSI are presented. At this point it suffices to say that TDD communications are employed and that channel reciprocity is exploited.

By plugging the pre-coder  $\mathbf{E}$  into (3.2) the received signal at the primary system becomes

$$\mathbf{y}_p = \mathbf{K}_p \mathbf{A} \mathbf{F}^{-1} \mathbf{s}_p + \nu_p, \quad (3.5)$$

from which the interference term has disappeared. Note that this holds true only for the perfectly known CSI case. Imperfect CSI effectively misaligns the pre-coder with respect to the interference channel, causing a certain level of interference to affect the primary receivers. More on imperfect CSI and its effects are discussed in chapter 5.

As for the secondary system,  $\mathbf{y}_s$  can be effectively rewritten as

$$\mathbf{y}_s = \mathbf{H}_s \mathbf{E} \mathbf{s}_s + \mathbf{H}_p \mathbf{s}_p + \nu_s, \quad (3.6)$$

where  $\mathbf{H}_s = \mathcal{T}(\mathbf{h}^{(s,s)}) \in \mathcal{C}^{N \times (N+L)}$  is the overall channel matrix for the secondary system,  $\mathbf{H}_p = \mathbf{F} \mathcal{T}(\mathbf{h}^{(p,s)}) \mathbf{A} \mathbf{F}^{-1} \in \mathcal{C}^{N \times N}$  is the diagonal overall channel matrix for the primary system (interference to the secondary receiver) and  $\nu_s$ , the Fourier transform of the noise  $\mathbf{n}_s$ , has the same statistics as  $\mathbf{n}_s$ .

In the following the performance of the secondary system in this scenario is derived.

### 3.4 Achievable Rates

In order to find the maximum achievable rate for the secondary system the optimization of input covariance needs to be performed. Since the use of the pre-coder  $\mathbf{E}$  allows the primary system to be considered as  $N$  parallel channels, its capacity is given by the classical water-filling solution [55]. The secondary receiver, however, with no knowledge of the primary system's message, performs single-user decoding. Similar to the consideration done in the section 2.2, let  $\boldsymbol{\eta} = \mathbf{H}_p \mathbf{s}_p + \nu_s$  indicate the interference plus noise component of the message at the secondary receiver. Then, (3.6) becomes

$$\mathbf{y}_s = \mathbf{H}_s \mathbf{E} \mathbf{s}_s + \boldsymbol{\eta}.$$

To simplify the mathematical development, consider that a Gaussian constellation is adopted for  $\mathbf{s}_p$ , with covariance  $\mathbf{S}_p$ . Since the effective channel from the primary transmitter to the secondary receiver is diagonal, the overall noise plus interference can be considered Gaussian. Therefore,  $\boldsymbol{\eta}$  can be approximated to a zero-mean Gaussian random vector with covariance given by

$$\mathbf{S}_\eta = \mathbf{H}_p \mathbf{S}_p \mathbf{H}_p^H + \sigma_n^2 \mathbf{I}_N.$$

Finally, for the sake of simplicity, let us suppose that a Gaussian constellation is also used for the signal of interest  $\mathbf{s}_s$ , with covariance is  $\mathbf{S}_s$ , and assume perfect knowledge of  $\mathbf{S}_\eta$  at the secondary transmitter.

To start, a general  $\tilde{\mathbf{E}}$  pre-coder is considered. Let  $P_s$  be the transmit power per precoded symbol. The maximum achievable rate for the secondary system is the solution of the following maximization problem

$$\begin{aligned} \max_{\mathbf{S}_s} \quad & \frac{1}{N+L} \log_2 \left| \mathbf{I}_N + \mathbf{S}_\eta^{-1/2} \mathbf{H}_s \tilde{\mathbf{E}} \mathbf{S}_s \tilde{\mathbf{E}}^H \mathbf{H}_s^H \mathbf{S}_\eta^{-H/2} \right| \\ \text{s.t.} \quad & \text{tr}(\tilde{\mathbf{E}}^H \tilde{\mathbf{E}} \mathbf{S}_s) \leq (N+L)P_s. \end{aligned}$$

Although the optimization problem is convex, the presence of the term  $\tilde{\mathbf{E}}^H \tilde{\mathbf{E}}$  in the constraint restrains the direct application of a water-filling solution. Luckily, this problem is similar to the one solved in section 2.4 and the same manipulation steps therein can be briefly repeated to this case for the sake of completeness.

Let  $\mathbf{G} = \mathbf{S}_\eta^{-1/2} \mathbf{H}_s \tilde{\mathbf{E}}$  and  $\mathbf{G} = \mathbf{U}_g \mathbf{\Lambda}_g \mathbf{V}_g^H$  be its SVD, with  $\mathbf{U}_g \in \mathcal{C}^{N \times N}$  and  $\mathbf{V}_g \in \mathcal{C}^{L \times L}$  unitary matrices.  $\mathbf{\Lambda}_g = [\mathbf{\Lambda}_g^\lambda, \mathbf{\Lambda}_g^0]^T$ , where  $\mathbf{\Lambda}_g^\lambda$  is a diagonal matrix carrying the square roots of the  $L$  eigenvalues of  $\mathbf{G}\mathbf{G}^H$  and  $\mathbf{\Lambda}_g^0$  is an  $L \times (N-L)$  zero matrix. Then, let  $\mathbf{S}_s = \mathbf{V}_g \mathbf{P} \mathbf{V}_g^H$ , where  $\mathbf{P} \in \mathcal{R}^{L \times L}$  is  $\text{diag}[p_1, \dots, p_L]$ . By plugging this new definition of  $\mathbf{S}_s$  and  $\mathbf{G}$  into the original optimization problem and constraint we get

$$\begin{aligned} \max_{\mathbf{P}} \quad & \frac{1}{N+L} \log_2 \left| \mathbf{I}_N + \mathbf{U}_g \mathbf{\Lambda}_g \mathbf{P} \mathbf{\Lambda}_g^H \mathbf{U}_g^H \right| \\ \text{s.t.} \quad & \text{tr}(\mathbf{Q}\mathbf{P}) \leq (N+L)P_s, \end{aligned}$$

where the simplification  $\mathbf{Q} = \mathbf{V}_g^H \tilde{\mathbf{E}}^H \tilde{\mathbf{E}} \mathbf{V}_g$  is introduced. Finally, the initial optimization problem can be cast into a new one given by

$$\begin{aligned} \max_{p_i} \quad & \sum_{i=1}^L \log_2(1 + p_i [\mathbf{\Lambda}_g^\lambda]_{i,i}) \\ \text{s.t.} \quad & \sum_{i=1}^L p_i [\mathbf{Q}]_{i,i} \leq (N+L)P_s. \end{aligned} \tag{3.7}$$

Now, the classical water-filling solution can be applied. The solution to (3.7) is given by  $\mathbf{S}_s = \mathbf{V}_g \mathbf{P} \mathbf{V}_g^H$ , where the  $i$ -th component of the matrix  $\mathbf{P}$  is the weighted water-filling solution

$$p_i = \left[ \frac{\mu}{[\mathbf{Q}]_{i,i}} - \frac{1}{[\mathbf{\Lambda}_g^\lambda]_{i,i}} \right]_+, \tag{3.8}$$

where  $\mu$  is the ‘‘water level’’, determined as to fulfill the total power constraint  $(N+L)P_s$ . We remark that the the solution in (3.8) is the general one and now we need to conform it to the actual employed precoder  $\mathbf{E}$ , whose column are orthonormal. Hence, from (3.8) we get that  $\forall i, [\mathbf{Q}]_{i,i} = 1$  and so the maximum achievable rate for the secondary system is given by

$$R_2 = \frac{1}{N+L} \sum_{i=1}^L \log_2(1 + p_i [\mathbf{\Lambda}_g^\lambda]_{i,i}). \tag{3.9}$$

### 3.4.1 Numerical Results

To illustrate the performance of the new pre-coder design some numerical results are provided herein. Monte Carlo simulations of an OFDMA primary system and a VFDM secondary system are executed. The considered primary system is inspired on LTE [60] with a varying number of users  $k \in \{1, 2, 4, 8, 16, 32, 64\}$ , based on the transmission mode with a bandwidth of 1.92 MHz, characterized by  $N = 128$  active subcarriers and a cyclic prefix of length  $L = 32$  (extended mode). For the simulations, channels and noise are generated according to the definitions made in section 3.2, controlling the SNR by changing the value of  $\sigma$ . Monte Carlo based simulations are executed until 10000 iterations yielding a statistically sufficient amount of samples. Moreover, perfect knowledge of all channels involved at the secondary transmitter is assumed.

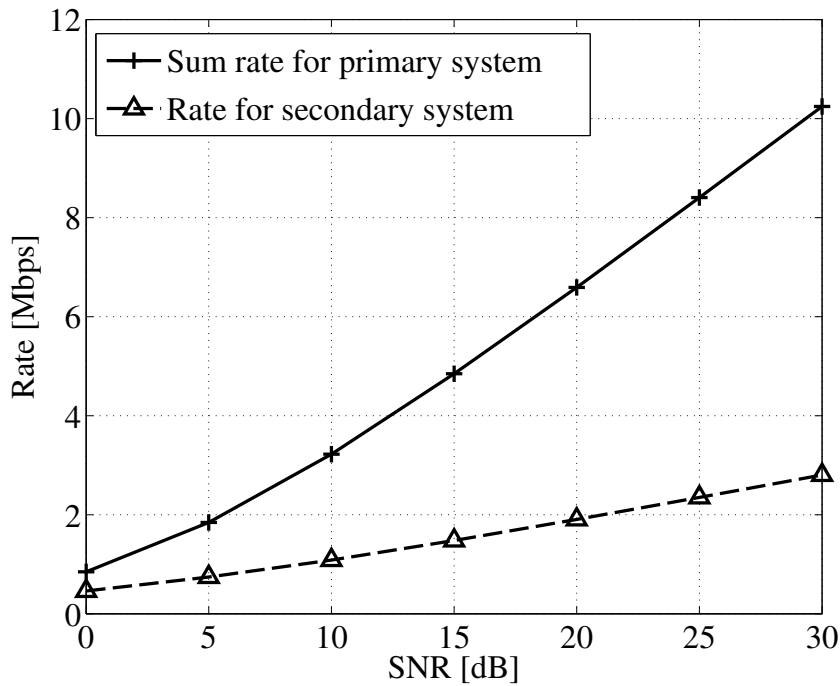


Figure 3.3: Sum rate of the primary system in a 8-user OFDMA configuration compared to the secondary receiver's rate ( $N = 128$ ,  $L = 32$  and bandwidth of 1.92 MHz).

In figure 3.3 the sum rate of the primary and secondary systems are presented for a total of  $k = 8$  primary users for different values of the SNR. Note that the choice of  $k = 8$  does not affect the result since the sum rate at the primary system is independent from  $k$ . While at low SNRs, the ratio between the rate of the primary and secondary systems is of about  $1/2$ , as the SNR grows it tends to  $1/4$ . This behavior can be explained by the proportion in the number of available resources for each system, due to the chosen LTE mode  $N = 128$  and  $L = 32$ , giving  $\frac{L}{N} = 1/4$ .

In figure 3.4, the secondary receiver's rate with respect to the number of primary

users is shown for different values of the SNR  $\in \{0, 10, 20, 30\}$ . Independent of the chosen SNR point, for a large number of users ( $k \geq 8$ ) the rate is seen to be almost constant with the increase in the number of users. This corroborates our expectations that the number of users does not have a considerable effect on the rate at the secondary system. The only exception to this effect comes for lower numbers of primary users (i.e.  $k < 8$ ), where the secondary receiver experiences a slight drop in performance. This behavior is due to the greater channel diversity seen in the  $k \geq 8$  case, and it implies that for a big number of primary receivers the designed pre-coder performs slightly better in terms of rate. Furthermore, the slope of the drop is very low and the difference is negligible if compared to the rate achievable by the secondary receiver. Clearly, the drop is more pronounced in the high SNR regime, since the higher the SNR, the easier it is to exploit diversity.

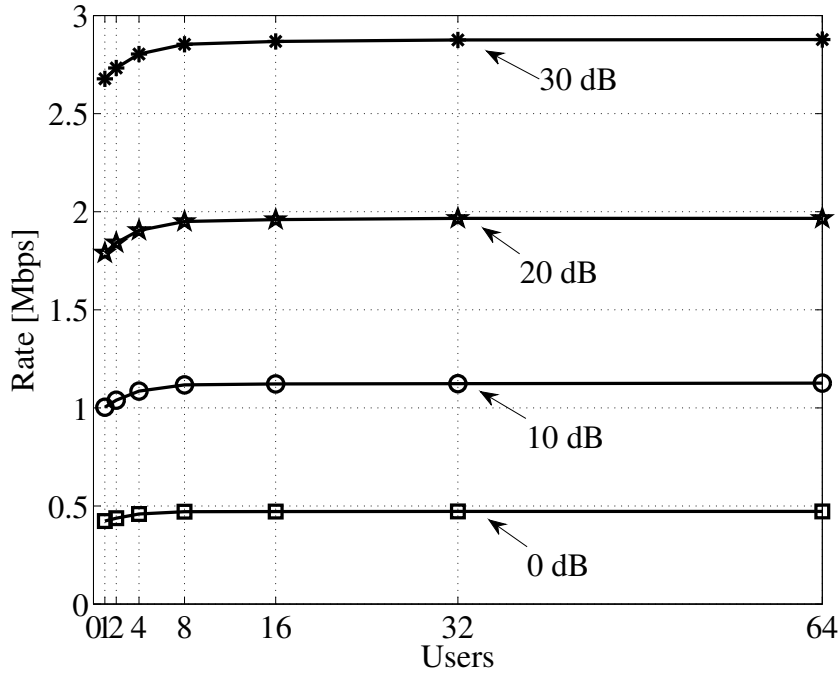


Figure 3.4: Rate of the secondary system for increasing number of primary receivers and several SNR values ( $N = 128, L = 32$  and bandwidth of 1.92 Mhz).

To have a better grasp of the performance of the secondary system, let us see how it compares to a single primary user in a multi-user OFDMA case, as seen in figure 3.5. Clearly, the greater the amount of users in the primary system, the better the performance of the secondary system with respect to a single user. The number of users in which VFDM starts becoming attractive in terms of rate is  $k = 4$ . It must be noted that this result is dependent on the simulated scenario, and is directly related to the pre-coding dimension,  $L$ . Clearly, such a result can only be observed due to the fact that the primary system equally shares resources among users, effectively dividing the rate they experience.

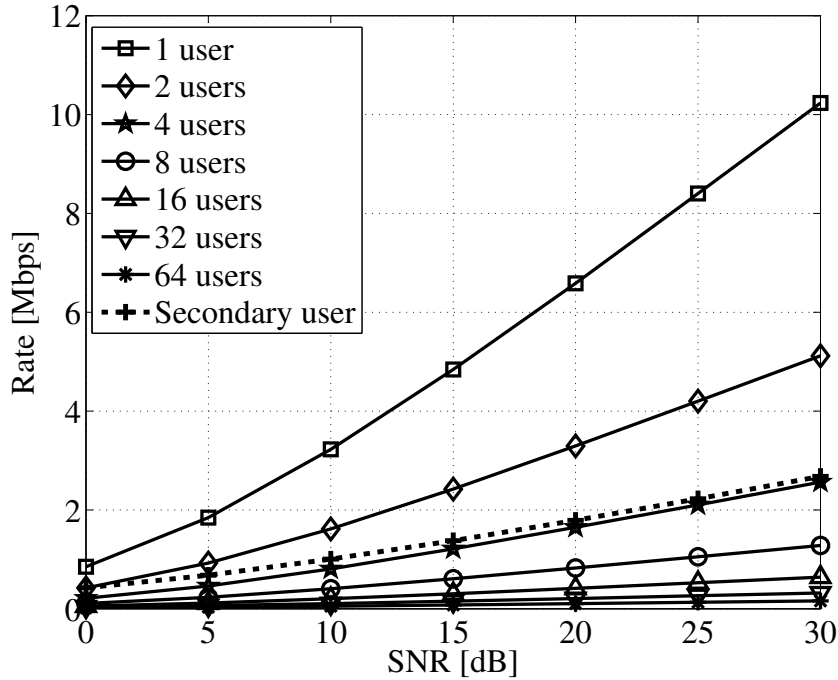


Figure 3.5: Rate of the primary system for different number of users compared to the secondary receiver's rate ( $N = 128$ ,  $L = 32$  and bandwidth of 1.92 MHz).

### 3.5 Closing Remarks

As we have shown in this chapter, by taking into consideration multiple OFDMA primary users in the system model, a new VFDM pre-coder can be designed to deal with the interference towards the primary system. The question that remains is: how can VFDM be extended to multiple *secondary* users? In the next chapter, we provide one possible answer to this question.

# Chapter 4

## Network MIMO VFDM

**F**OLLOWING THE SEQUENCE of the development of VFDM, we now move on to introducing the full multi-user setting, denoted hereafter as multi-user Vandermonde-subspace frequency division multiplexing (MU-VFDM). MU-VFDM is an extension of the case presented in the previous chapter, where we have seen how VFDM can be applied to a multi-user primary and point-to-point secondary systems. As with conventional VFDM, MU-VFDM makes use of frequency selectivity and the redundancy introduced to combat inter-block interference and to cancel the interference from the secondary to primary system. Our simulation results show that, a sum-rate comparable to that of state-of-the art techniques, such as DPC, is obtained in the multiuser small-cell case.

### 4.1 Multi-Primary — Multi-Secondary System Model

Let us start from the primary and secondary system scenario depicted in figure 1.4. In such a scenario, a macro-cell (primary) and several small-cells (secondary) serve their own set of users in such a way as not to interfere with each other. Now, consider that the figure is de-cluttered to the minimum elements necessary for its analysis, the downlink scenario in figure 4.1. Therein, a macro-cell and two of the  $\mathcal{K}$  small-cells transmit over the same frequency band in a given area.

The primary system is composed by a macro-cell that serves  $k$  users. For simplicity and without loss of generality, consider that the secondary system is composed by several small-cells connected point-to-point to their respective user, in a one-to-one relation. Considering that there's little difference between the user equipment (UE) connected to either systems, let us differentiate them according to their association point as macro-cell user equipments (MUEs) and small-cell user equipments (SUEs). Inside the secondary system, cooperation between the small-cells is considered, yielding a full network MIMO transmission system model [61]. A brief explanation of the notation difference follows:

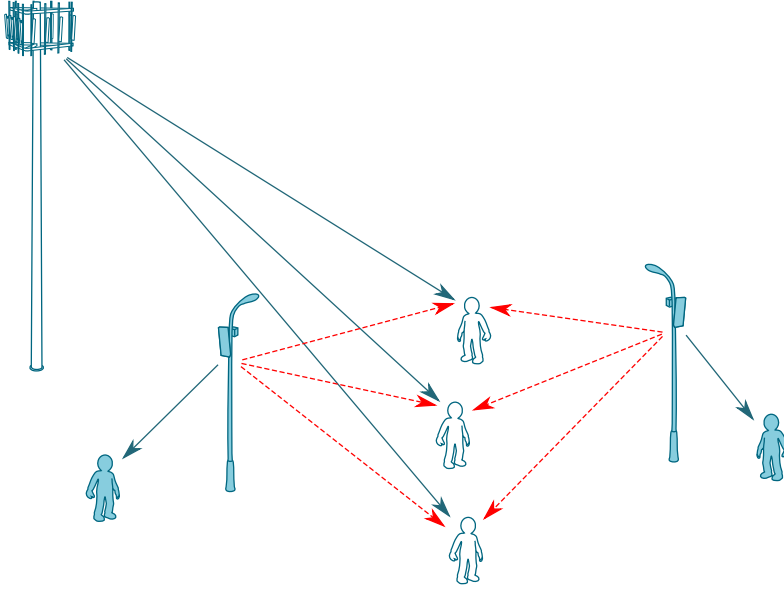


Figure 4.1: OFDMA downlink cognitive interference channel model.

- Subscript “m” refers to the macro-cell, while “s” refers to the small-cells (i.e.,  $h_{sm}^{(i,j)}$  and  $\mathbf{H}_{sm}^{(i,j)}$  represent a link from small-cell  $i$  to MUE  $j$ );
- Square brackets in the superscript  $\mathbf{s}^{[i]}$  (or  $\mathbf{H}_{sm}^{([i],j)}$ ) denote a vector (or matrix) related to the transmission from any small-cell *except*  $i$ .

As with the previous chapters, all channel vectors  $\mathbf{h}_{ab}^{(\cdot,\cdot)} \in \mathcal{CN}(0, \mathbf{I}_{L+1}/(L+1))$  represent the impulse response of i.i.d. frequency-selective Rayleigh fading channels composed of  $L + 1$  paths. In section 3.2, the primary system is a  $k$ -user OFDMA based system transmission of block size  $N + L$  and a cyclic prefix of size  $L$ . For simplicity, a uniform resource allocation as described in section 3.2 is adopted. The secondary system adopts a VFDM inspired block-transmission scheme that will be detailed in section 4.2. Like the MUEs, the SUEs discard the leading  $L$  symbols and perform DFT at the reception.

Let  $\mathbf{y}_m^{(j)}$ ,  $\mathbf{y}_s^{(j)}$  be the received  $N$ -sized vector at the  $j^{\text{th}}$  MUE and SUE, respectively. The overall received vector for all MUEs  $\mathbf{y}_m$ , also of size  $N$ , is given by

$$\mathbf{y}_m = \sum_{j=1}^k \mathbf{y}_m^{(j)}.$$

The secondary system’s overall received vector at the SUEs is obtained by aggregating each SUE’s received component,

$$\mathbf{y}_s \triangleq [\mathbf{y}_s^{(1)\text{T}}, \dots, \mathbf{y}_s^{(k)\text{T}}]^{\text{T}}.$$

Both  $\mathbf{y}_m$  and  $\mathbf{y}_s$  are given by

$$\begin{aligned} \mathbf{y}_m &= \mathbf{H}_{mm}\mathbf{s}_m + \mathbf{H}_{sm}\mathbf{x}_s + \mathbf{F}\mathbf{n}_m \\ \mathbf{y}_s &= \mathbf{H}_{ss}\mathbf{x}_s + \mathbf{H}_{ms}\mathbf{s}_m + (\mathbf{I}_K \otimes \mathbf{F})\mathbf{n}_s, \end{aligned} \quad (4.1)$$

where  $\mathbf{s}_m$  is the macro-cell input vector of size  $N$ , composed of  $k$  individual zero mean, unit norm symbol vectors  $\mathbf{s}_m^{(j)}$ ,  $j \in [1, k]$ , and  $\mathbf{x}_s \triangleq [\mathbf{x}_s^{(1)\top}, \dots, \mathbf{x}_s^{(k)\top}]^\top$  is the overall small-cell transmit vector, detailed in the following section.  $\mathbf{F} \in \mathbb{C}^{N \times N}$  is a unitary DFT matrix.  $\mathbf{n}_m$  and  $\mathbf{n}_s$  are i.i.d. complex Gaussian circularly symmetric thermal noise vectors. The specific sizes of the transmit and receive vectors, as well as the thermal noise vectors  $\mathbf{n}_m$  and  $\mathbf{n}_s$ , will be introduced later for clarity.

Considering the adopted resource allocation, each MUE selects its own set of subcarriers using a mask receiver filter  $\mathbf{B}_j$ , such that

$$\begin{cases} \text{tr}(\mathbf{B}_j) = N/k \\ \sum_{j=0}^k \mathbf{B}_j = \mathbf{I}_N \end{cases} \quad (4.2)$$

with  $[\mathbf{B}_j]_{(n,n)} = 1$  when the subcarrier  $n$  is allocated to MUE  $j$  and zero otherwise. Then, by summing up all the contributions of the MUEs, the equivalent channel matrix of the macro-cell is

$$\mathbf{H}_{mm} = \sum_{j=1}^M \mathbf{B}_j \mathbf{F} \mathcal{T}(\mathbf{h}_{mm}^{(1,j)}) \mathbf{A} \mathbf{F}^{-1}, \quad (4.3)$$

where  $\mathbf{F}^{-1}$  is the inverse discrete Fourier transform (IDFT) matrix at the macro-cell,  $\mathbf{A}$  is a  $(N+L) \times N$  cyclic prefix insertion and  $\mathcal{T}(\mathbf{h}_{mm}^{(\cdot,\cdot)}) \in \mathbb{C}^{N \times (N+L)}$  is a Toeplitz matrix constructed from the  $\mathbf{h}_{mm}^{(\cdot,\cdot)}$  channel coefficients. The overall interference channel from the small-cells to the MUEs is defined similarly to  $\mathbf{H}_{mm}$ . First, the equivalent channel for each one of the small-cells is constructed, such that

$$\mathbf{H}_{sm}^{(i,\cdot)} = \sum_{j=1}^k \mathbf{B}_j \mathbf{F} \mathcal{T}(\mathbf{h}_{sm}^{(i,j)}). \quad (4.4)$$

Then, the overall equivalent representation is obtained by aggregation, giving

$$\mathbf{H}_{sm} = \begin{bmatrix} \mathbf{H}_{sm}^{(1,\cdot)} & \dots & \mathbf{H}_{sm}^{(\mathcal{K},\cdot)} \end{bmatrix}. \quad (4.5)$$

$\mathbf{H}_{sm}^{(i,\cdot)} \mathbf{x}_s^{(i)}$  is the interference term from the small-cell  $i$  to the MUEs.

Now, let  $\mathbf{H}_{ss}^{(i,j)} = \mathcal{T}(\mathbf{h}_{ss}^{(i,j)}) \in \mathbb{C}^{N \times (N+L)}$  be the Toeplitz matrix representing the channel from the small-cell  $i$  to the SUE  $j$ . Then, by defining

$$\tilde{\mathbf{H}}_{ss} = \begin{bmatrix} \mathbf{H}_{ss}^{(1,1)} & \dots & \mathbf{H}_{ss}^{(1,\mathcal{K})} \\ \mathbf{H}_{ss}^{(2,1)} & \dots & \mathbf{H}_{ss}^{(2,\mathcal{K})} \\ \vdots & \ddots & \vdots \\ \mathbf{H}_{ss}^{(\mathcal{K},1)} & \dots & \mathbf{H}_{ss}^{(\mathcal{K},\mathcal{K})} \end{bmatrix}, \quad (4.6)$$

the overall equivalent channel is given by

$$\mathbf{H}_{ss} = (\mathbf{I}_{\mathcal{K}} \otimes \mathbf{F}) \tilde{\mathbf{H}}_{ss}. \quad (4.7)$$

The same approach can be used to model the interfering link from the macro-cell to the SUEs. By defining

$$\tilde{\mathbf{H}}_{\text{ms}} = \begin{bmatrix} \mathbf{H}_{\text{ms}}^{(1,1)} \\ \mathbf{H}_{\text{ms}}^{(1,2)} \\ \vdots \\ \mathbf{H}_{\text{ms}}^{(1,\mathcal{K})} \end{bmatrix}, \quad (4.8)$$

where  $\mathbf{H}_{\text{ms}}^{(1,j)} = \mathcal{T}(\mathbf{h}_{\text{ms}}^{(1,j)})\mathbf{A}\mathbf{F}^{-1} \in \mathbb{C}^{N \times N}$ ,  $j \in [1, \mathcal{K}]$ , we can write the overall equivalent channel as

$$\mathbf{H}_{\text{ms}} = (\mathbf{I}_{\mathcal{K}} \otimes \mathbf{F})\tilde{\mathbf{H}}_{\text{ms}}. \quad (4.9)$$

## 4.2 Pre-coder Design

Even though the model considered in the chapter is slightly different from that of the two previous chapters, we can adopt some of the same principles to derive the overall pre-coder, with our null condition being

$$\mathbf{H}_{\text{sm}}\mathbf{E} = \mathbf{0}, \quad (4.10)$$

obtained by making  $\mathbf{x}_s = \mathbf{E}\mathbf{s}_s$  in (4.1) for any  $\mathbf{s}_s$ . The overall pre-coder, defined as

$$\mathbf{E} = \bigoplus_{i=1}^{\mathcal{K}} \mathbf{E}_i, \quad (4.11)$$

is the direct sum [62] of the  $\mathcal{K}$  pre-coders used at each small-cell. Then, by substituting (4.5) into (4.10), we see that the orthogonality condition is satisfied if the following holds

$$\mathbf{H}_{\text{sm}}^{(i,\cdot)}\mathbf{E}_i = \mathbf{0}, \quad \forall i \in [1, \mathcal{K}]. \quad (4.12)$$

What equation 4.12 tells us is that, to design the overall pre-coder  $\mathbf{E}$ , it suffices to separately design each small-cell pre-coder  $\mathbf{E}_i$ , as done in the previous chapter. This interesting finding indicates that, at least at this step, no cooperation between the small-cells is needed. We remark that, this disjoint pre-coder computation done by the small-cells, results both in a simpler architecture and in a lower backhaul signaling.

As indicated by (4.12), perfect CSI is required to build the null-space pre-coder. As in the previous chapters, all communications are considered to be TDD and perfect CSI related to the interfering links from the small-cells towards the MUEs are assumed available. In section 5.3 we look at how the imperfect CSI affects the performance of MU-VFDM.

Substituting the  $\mathbf{x}_s = \mathbf{E}\mathbf{s}_s$ , with  $\mathbf{E}$  satisfying (4.10), in (4.1), the signal model can be rewritten as

$$\begin{aligned} \mathbf{y}_m &= \mathbf{H}_{\text{mm}}\mathbf{s}_m + \mathbf{F}\mathbf{n}_m \\ \mathbf{y}_s &= \mathbf{H}_{\text{ss}}\mathbf{E}\mathbf{s}_s + \mathbf{H}_{\text{ms}}\mathbf{s}_m + \nu_s. \end{aligned} \quad (4.13)$$

In (4.13),  $\mathbf{E} \in \mathcal{C}^{K(N+L) \times KL}$  and  $\mathbf{s}_s$ , of dimension  $KL$ , is the aggregate small-cell transmitted symbol vector. The aggregate SUE received vector  $\mathbf{y}_s$ , of dimension  $KN$ , is defined similarly and  $\nu_s \in \mathcal{CN}(0, \sigma_n^2 \mathbf{I}_{KN})$  is the DFT of  $\mathbf{n}_s$ .

To simplify the notation, let us introduce

$$\overline{\mathbf{H}}_{ss} = \mathbf{H}_{ss} \mathbf{E}. \quad (4.14)$$

The structure of the received signal is the same for any SUE, so their individual received signal is given by

$$\mathbf{y}_s^{(j)} = \overline{\mathbf{H}}_{ss}^{(i,j)} \mathbf{s}_s^{(i)} + \overline{\mathbf{H}}_{ss}^{([i],j)} \mathbf{s}_s^{[i]} + \mathbf{H}_{ms}^{(1,j)} \mathbf{s}_m + \nu_s^{(j)}, \quad (4.15)$$

in which, a useful component and two interfering terms can be identified. Due to the term  $\overline{\mathbf{H}}_{ss}^{([i],j)} \mathbf{s}_s^{[i]}$ , each SUE deals with one more interference component compared to the single small-cell case of section 3.3. Now, aside from the macro-cell's interference on the small-cells, which is assumed to be always present, a inter-small-cell component can be seen. The performance of the small-cells now critically depends on their number in the system, raising the level of multi-user interference experienced by each SUE. To address this issue, techniques from coordinated network MIMO were analyzed, allowing the small-cells to cooperate aiming at an overall higher performance. The small-cells can be modeled as a MIMO-broadcast channel (BC), whose optimal capacity is achieved with DPC [48]. This nonlinear technique is based on "genie aided" knowledge of each user's interfering signal at each transmitter, and thus, it is not implementable in practice. Many linear suboptimal techniques, aimed at solving the multi-user interference, have been introduced lately [63, 64, 65, 66, 67, 68, 69, 70]. In the following section, a discussion of the suitability of several practical transmit schemes to our scenario is made. The goal is to identify a suitable linear technique that is able to exploit the cooperation among small-cells, achieving the best performance amidst other non-optimal techniques.

### 4.2.1 Practical Transmit Schemes

Let us focus our attention on the small-cells' transmission in (4.15), isolating the term  $\overline{\mathbf{H}}_{ss}$  of dimension  $KN \times KL$ . Note that, in any block transmission system, the added redundancy implies that  $\frac{L}{N} < 1$ , for matters of efficiency. Therefore, in a MU-VFDM system each transmitter faces a dimensionality constraint in order to cancel the interference towards the macro-cell. This implies that a direct use of techniques such as zero force beamforming (ZFBF) [63] or block diagonalization (BD) [64] is not possible in this framework, since both require transmit dimensions to be equal or larger than the receive dimensions. On the other hand, regularized inverse beamforming (RIBF) [65] MF is applicable, in spite of its poor performance at high SNR, also a result of dimensionality issue ( $N > L$  received symbols) since it limits the use of all of the degrees of freedom provided by the channel. It is known from [66], and for the multiple beams case from [67], that opportunistic random beamforming (ORBF) based techniques are able to yield the optimal capacity scaling of  $M \log \log K$  in dense networks with a large number of receivers. Once again the ratio  $\frac{N}{L}$  limits the performance using these techniques. Most of the results

in the literature regarding linear pre-coding techniques under given optimization criteria assume only one antenna per symbol at the receiver. For this reason, a direct extension of these techniques is not possible.

Algorithms like successive minimum mean square error (SMMSE) [68] and iterative regularized block diagonalization (IRBD) [69] deal in general with multiple symbols per antennas per receiver, suppressing the interference only between symbols received by two different receivers, which provides a higher diversity gain. These algorithms perform better than other techniques that rely on the single antenna per symbol assumption, but on the other hand require a joint receiver decoding increasing the complexity of the receivers' architecture.

Simpler solutions, implemented to deal with an arbitrary number of antennas per symbols at each receiver, are user or antenna selection based algorithms. It is known that, by scheduling only a subset of antennas or eigenmodes [64] to be served using a classical ZFBF, the achievable sum rate is asymptotically optimal [71]. However, the condition for the asymptotic optimality is never met in MU-VFDM and neither an exhaustive search of the optimal subset nor a faster and suboptimal greedy selection algorithm [70] can achieve good results.

Looking at the alternatives presented so far, the dimensionality constraint always somehow limits the performance of the secondary system. Moreover, the higher complexity of some of the presented techniques do not bring significant performance increase. With these considerations in mind, a solution for the dimensionality constraint is given in the next section based on an adaptation of the simple RIBF to manage multi-user interference, improving the performance of the considered setup.

## 4.2.2 RIBF Flexible Network Solution

As stated previously, a strategy to overcome the dimensionality constraint, inherent to  $\mathbf{E}$ , needs to be found. This has to be done without reducing the number of considered antennas per symbol at the receivers. To do so, let us introduce the *load rate*  $\beta$  as the ratio between the number of dimensions at the transmitter and the ones at the receiver

$$\beta = \frac{\psi_{tx}}{\psi_{rx}}. \quad (4.16)$$

For VFDM,  $\psi_{tx} = \gamma_{tx}L$  and  $\psi_{rx} = \gamma_{rx}N$ , where  $L$  and  $N$  are constrained to the OFDMA block structure.  $\gamma_{tx}$  and  $\gamma_{rx}$  are two parameters related respectively to the transmitter and receiver, depending on the chosen small-cell layout or secondary system architecture, hence, to the dimensionality of the system. In particular, by changing the number of dimensions at the secondary system, we change the number of available channels for the transmission, experiencing several levels of diversity. For instance, when  $\gamma_{tx} = 1$  and  $\gamma_{rx} \rightarrow \infty$ , a larger number of SUEs (or SUE antennas) from which the best ones to serve are selected, and this represents the condition under which ORBF is optimal. Conversely, if  $\gamma_{rx}$  is kept constant ( $\gamma_{rx} = 1$  for simplicity) while  $\gamma_{tx}$  increases, the small-cells can exploit the available dimensions per SUE to achieve a higher diversity, thanks

to the greater number of available channels. Another interesting configuration is given by  $\gamma_{tx} = N$  and  $\gamma_{rx} = L$ , that is a network where the number of dimensions at the small-cells coincides with those of the SUEs and RIBF becomes efficient in terms of available degrees of freedom.

To put simply, with  $L$  and  $N$  fixed, the system designer can tune  $\gamma_{tx}$  and  $\gamma_{rx}$  to exploit on the flexibility of the model through the addition of more antennas at each small-cell and SUE, or alternatively by increasing the small-cell density. To overcome the dimensionality constraint in the considered scenario, and to implement RIBF efficiently, more dimensions need to be added at the transmitter until the following holds

$$\gamma_{tx}L \geq \gamma_{rx}N. \quad (4.17)$$

Without loss of generality, let  $\gamma_{rx} = 1$  and allow  $\gamma_{tx}$  to increase. Due to the large number of small-cells (or antennas per small-cell), a uniform power allocation strategy is assumed to reduce the computational burden for the small-cells. Note that, since no consideration is made regarding a greater number of channels, thanks to the  $\gamma_{rx}$  and  $\gamma_{tx}$  tuning,  $\mathbf{E}$  and  $\mathbf{s}_s$  have no longer the same sizes as in the previous chapters. This time  $\mathbf{s}_s$  has dimension  $\gamma_{tx}KL$ ,  $\mathbf{E} \in \mathcal{C}^{\gamma_{tx}K(N+L) \times \gamma_{tx}KL}$  and, consequently,  $\overline{\mathbf{H}}_{ss} \in \mathcal{C}^{KN \times \gamma_{tx}KL}$ . Then, by letting  $\mathbf{u}_s \in \mathcal{C}^{KN \times 1}$  be a new aggregate small-cell transmit vector, such that

$$\mathbf{s}_s = \mathbf{\Phi} \mathbf{u}_s,$$

a joint RIBF can be implemented at the small-cells, from which  $\mathbf{\Phi} \in \mathcal{C}^{\gamma_{tx}KL \times KN}$ ,

$$\mathbf{\Phi} = \overline{\mathbf{H}}_{ss}^H \left( \frac{\sigma_n^2}{P_s} \mathbf{I}_{KN} + \overline{\mathbf{H}}_{ss} \overline{\mathbf{H}}_{ss}^H \right), \quad (4.18)$$

is the RIBF pre-coder. The pre-coder is normalized by  $\sqrt{E_{\mathbf{\Phi}}} = \sqrt{\text{tr}(\mathbf{\Phi} \mathbf{\Phi}^H)}$ , given that  $\text{tr}(\mathbf{\Phi} \mathbf{\Phi}^H) = 1$ . The signal model (4.13) can be finally rewritten as

$$\begin{aligned} \mathbf{y}_m &= \mathbf{H}_{mm} \mathbf{s}_m + \mathbf{F} \mathbf{n}_m \\ \mathbf{y}_s &= \mathbf{H}_{ss} \mathbf{W} \mathbf{u}_s + \mathbf{H}_{ms} \mathbf{x}_m + \nu_s, \end{aligned} \quad (4.19)$$

where  $\mathbf{W} = \mathbf{E} \mathbf{\Phi} \in \mathcal{C}^{\gamma_{tx}K(N+L) \times KN}$  is the overall pre-coder. Now, the inner-outer nature of the precoding at each small-cell becomes evident. Once the condition in (4.17) is fulfilled, a two-stage signal processing at the small-cells is implemented with a cascade of two pre-coders: the small-cells cooperate to perform an inner precoding  $\mathbf{\Phi}$  to implement RIBF towards the SUEs. Conversely, to cancel the interference, the outer pre-coder  $\mathbf{E}$  is established without any need for cooperation, as seen previously. This is in contrast with what is typically done in a two stage signal processing at the transmitter (e.g. [72]), where the inner stage has solely power optimization/allocation purposes. Furthermore, we emphasize that, the cascaded pre-coder structure is intrinsically different from that of the previous chapters, even for the  $K, M = 1$  case. In fact, the use of an inner linear precoding scheme, while preserving the interference cancelation condition towards the macro-cell system, substantially changes the dimensionality of the system.

### 4.2.3 Numerical Analysis

In this section, some numerical results are presented to illustrate the performance of the aforementioned techniques applied to the considered scenario. All of the result presented in the following are obtained by means of Monte Carlo based simulations. In accordance with section 4.1 and 4.2, an OFDMA/LTE macro-cell with  $k = 4$  MUEs, and an MU-VFDM based small-cell system are considered. For the sake of simplicity, the least resource-demanding extended mode prescribed by the standard [60] is adopted. It is characterized by  $N = 128$  active subcarriers, a cyclic prefix of length  $L = 32$ , for a total bandwidth of 1.92 MHz. Noise and channel vectors are generated as described in section 2.2.

Consider a scenario composed by  $\mathcal{K} = 3$  small-cells/SUEs. It is well known from [48] that  $C^{\text{SUM}}$ , the maximum ergodic sum rate of a MIMO-BC, is achieved by DPC.  $C_{\text{DPC}}^{\text{SUM}}$  can be computed using the well known formula [55]:

$$C_{\text{DPC}}^{\text{SUM}} = \frac{\mathcal{B}}{N + L} \mathbb{E} \left[ \log_2 \left| \mathbf{I}_{KN} + \left( \frac{N + L}{L\gamma_{tx}} \right) P_s (\sigma_n^2 \mathbf{I}_{KN} + P_m \mathbf{H}_{\text{ms}} \mathbf{H}_{\text{ms}}^H)^{-1} \bar{\mathbf{H}}_{\text{ss}} \bar{\mathbf{H}}_{\text{ss}}^H \right| \right]. \quad (4.20)$$

In figure 4.2, the ergodic achievable sum rate  $C^{\text{SUM}}$  is shown for different values of SNR. Note that, in (4.20),  $\mathcal{B}$  is the considered bandwidth and  $P_m$  is the macro-cell transmit power. In addition to the linear precoding techniques described in section 4.2.1, other solutions were tested, such as, the SVH algorithm [73] with 20 iterations, the ISSMSE (an iterative version of the SMMSE algorithm inspired by [69]) with 40 iterations and, finally, semi-orthogonal user selection ZFBF (SUS-ZFBF) algorithm proposed in [71]. The behavior of the considered linear precoding schemes shows a big rate offset if compared to the optimal value obtained by DPC, and this confirms the dimensionality issue, discussed in section 4.2.1.

To compute the achievable sum rate,  $C_{\text{RIBF}}^{\text{SUM}}$ , of the solution proposed in section 4.2.2, consider  $\mathcal{K} = 3$  SBSs and a load rate of  $\beta = 3$ . Figure 4.3 shows a comparison between  $C_{\text{RIBF}}^{\text{SUM}}$  and  $C_{\text{DPC}}^{\text{SUM}}$ , confirming that the proposed technique has close performance to that of state-of-the-art solutions.

We recall that in order to compute the sum-rate of the secondary system implementing RIBF,  $C_{\text{RIBF}}^{\text{SUM}}$ , we need to evaluate the SINR for any of the  $\mathcal{K}N$  received symbols. Let  $\Phi = [\phi^{(1)}, \dots, \phi^{(\mathcal{K}N)}]$ . We denote the  $j^{\text{th}}$  row of  $\bar{\mathbf{H}}_{\text{ss}}$  as  $\bar{\mathbf{h}}_{\text{ss}}^{(j)} = [[\bar{\mathbf{H}}_{\text{ss}}]_{j1}, \dots, [\bar{\mathbf{H}}_{\text{ss}}]_{j\gamma_{tx}\mathcal{K}L}]^T$ , then we can write

$$\text{SINR}_j = \frac{|\bar{\mathbf{h}}_{\text{ss}}^{(j)} \phi^{(j)}|^2}{\sum_{i \neq j}^{\mathcal{K}N} |\bar{\mathbf{h}}_{\text{ss}}^{(j)} \phi^{(i)}|^2 + \frac{\text{tr}(\mathbf{w}\mathbf{w}^H)\sigma_n^2}{P_s \mathcal{K}(N+L)}},$$

where we recall that the dimension of  $\bar{\mathbf{H}}_{\text{ss}}$  depends strictly on the value assumed by  $\beta$ . Then, it is straightforward to see that for a  $\mathcal{K}$ -secondary system the achievable sum rate is given by

$$C_{\text{RIBF}}^{\text{SUM}} = \frac{\mathcal{B}}{N + L} \sum_{j=1}^{\mathcal{K}N} \log_2(1 + \text{SINR}_j). \quad (4.21)$$

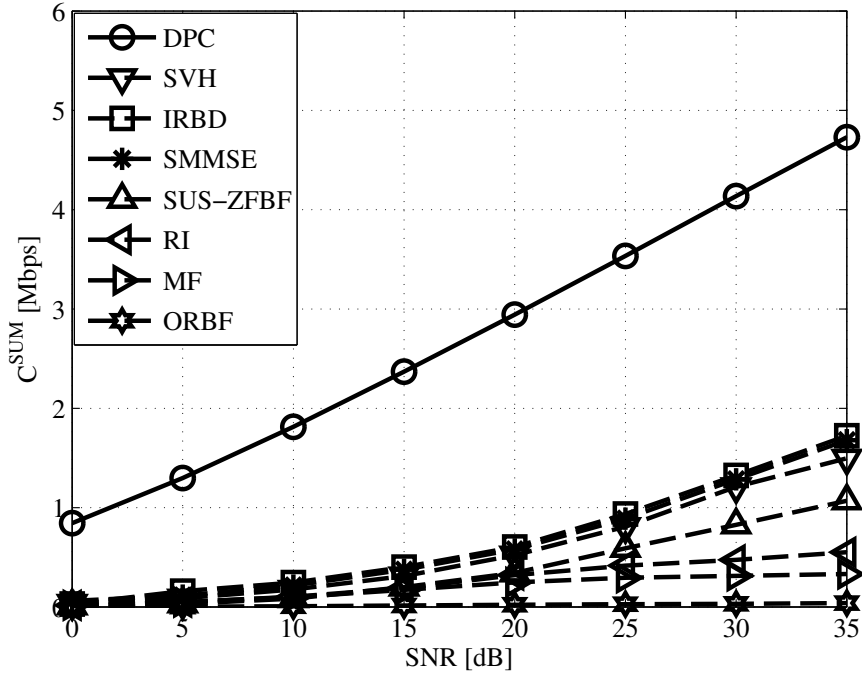


Figure 4.2: Rate of the small-cells for different techniques,  $\mathcal{K} = 3$  ( $N = 128$ ,  $L = 32$  and bandwidth of 1.92 Mhz).

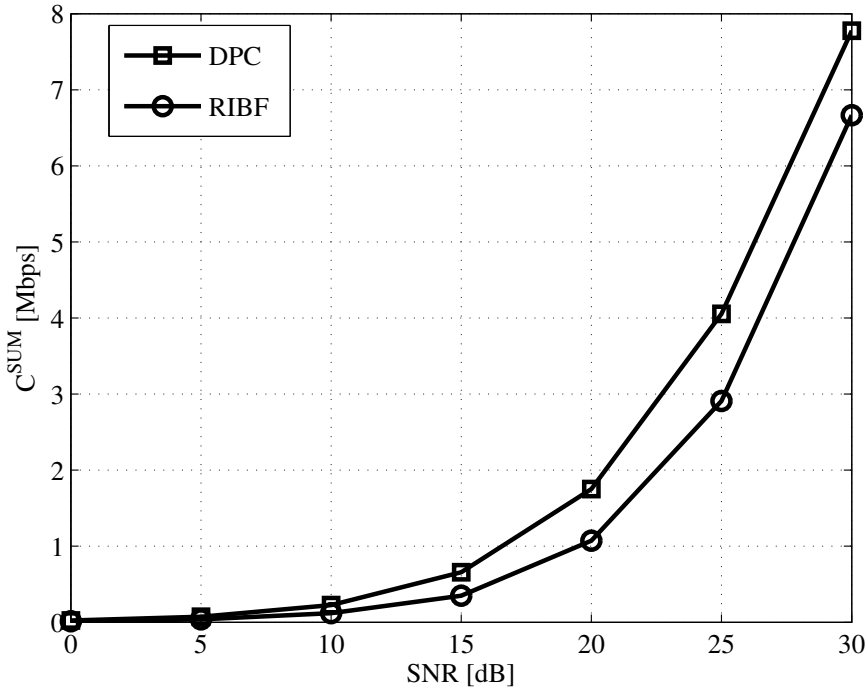


Figure 4.3: Achievable Rate of the SBSs with the RIBF flexible network solution,  $K = 3$ ,  $\beta = 3$  ( $N = 128$ ,  $L = 32$  and bandwidth of 1.92 Mhz).

We remark that, the smaller complexity of the RIBF based solution allow us to consider values of  $\beta$  unfeasible for any linear precoded scheme analyzed in figure 4.2, due to their higher complexity. This consideration validates the proposed solution for the MU-VFDM dense network deployment. By increasing the number of dimensions at the transmitter, we can improve the small-cells' performance without being limited by the simplicity inherent to the RIBF based scheme.

Finally, in figure 4.4 we show how the sum rate increases with the number of small-cells. Thanks to the pre-coder  $\mathbf{E}$  the small-cells protect the MUEs from interference, effectively increasing the spectral efficiency and the capacity per area. This result corroborates with our expectations for highly dense small-cells networks.

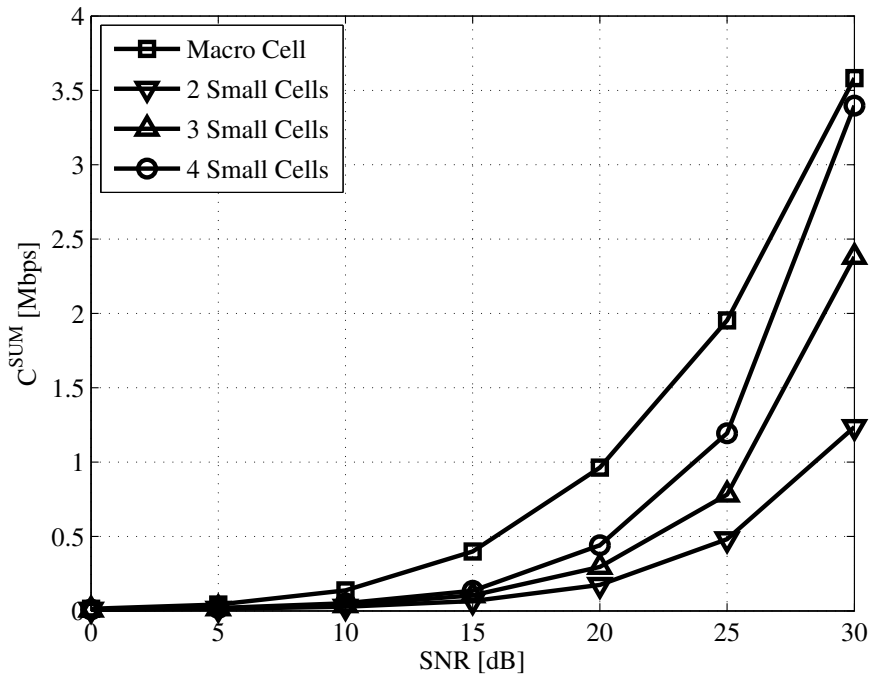


Figure 4.4: Rate of the SBSs with the RIBF flexible network solution for different numbers of Small Cells,  $\beta = 2$ , ( $N = 128$ ,  $L = 32$  and bandwidth of 1.92 Mhz).

### 4.3 Comparison with existing solutions

As shown in this chapter so far, MU-VFDM allows the coexistence of small- and macro-cells inside the same coverage area, nulling the interference from the former to the latter. If compared to other state-of-the-art techniques that allow the deployment of a two-tiered LTE and small-cells network [74], MU-VFDM can be seen as a *complete sharing* approach<sup>1</sup>, since it guarantees zero interference from the small-cells to the macro-cells

<sup>1</sup>State-of-the-art techniques that allow the deployment of a two-tiered network can be classified according to [74]: 1) *Complete sharing*, 2) *partial sharing*, 3) *complete separation*.

while sharing the same bandwidth.

In this section, the performance of MU-VFDM is put to the test against a *complete separation* technique based on bandwidth division. This technique is described as follows

- The total available bandwidth is divided in two, to assure zero interference:
  1.  $\mathcal{B}_m = \mathcal{B} - \mathcal{B}_s$ , assigned to the primary system and;
  2.  $\mathcal{B}_s = \frac{\mathcal{B}L}{N}$ , assigned to the secondary system;
- Each small-cell antenna transmits the same number of symbols as in MU-VFDM;
- To guarantee fairness in the comparison, small-cells adopt a network MIMO-OFDMA transmission towards the SUEs;
- ZF is adopted such that the received symbols have the same structure as in MU-VFDM
- The primary system performs legacy OFDMA transmission, as done in the MU-VFDM case.

For the results herein, the same configuration introduced previously is used:  $N = 24$  and  $L = 6$ . This time, MU-VFDM is considered to suffer from full interference from the macro-cell. For the selected  $N$  and  $L$ , in the bandwidth splitting scheme (complete

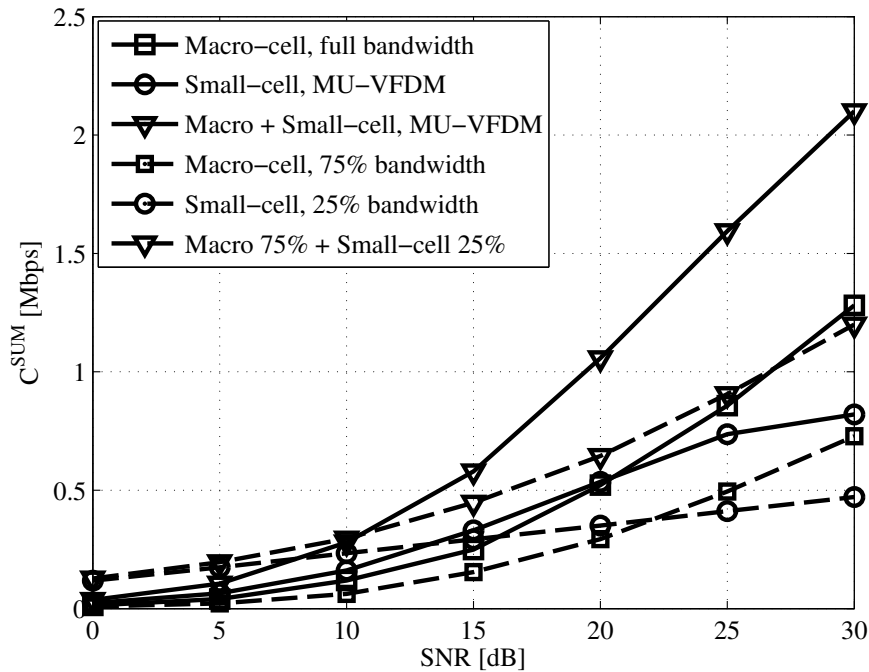


Figure 4.5: Capacity of MU-VFDM vs. complete separation scheme,  $\mathcal{K} = 2$ ,  $\beta = 4$ , ( $N = 24$ ,  $L = 6$  and bandwidth of 0.48 Mhz).

separation), the primary system disposes of 75% of the total available bandwidth while the secondary disposes of the remaining 25%.

In figure 4.5, the capacity of MU-VFDM (continuous curves) and bandwidth splitting (dashed curves) are presented under perfect CSI and  $\beta = 4$ . By following both sum capacity curves (curves with triangles), we see that MU-VFDM presents a clear advantage in the high SNR regime, from about 10 dB on. Indeed, MU-VFDM is capable of offering better overall spectral efficiencies since, not only it provides a higher capacity than the small-cell based splitting mechanism (comparing the curves with circles) but it also does not borrow bandwidth from the primary system (macro-cell), not cannibalizing on its performance (comparing the curves with squares), as it happens with the bandwidth splitting technique.

## 4.4 Closing Remarks

As shown in this chapter, we have extended VFDM to a full multi-user setting, by proposing a new cascaded pre-coder based on network MIMO. Such a pre-coder is able to, at the same time, cancel the interference to the primary system and the interference between secondary users. We have shown that MU-VFDM is somehow even more flexible than the single user single antenna case, shown in the previous chapters, since by changing the dimensions  $\beta$  better performances can be reached. Finally we have shown that, for the conditions simulated, MU-VFDM can outperform a commonly adopted spectrum splitting scheme. In the next part, we shift the approach to developing VFDM, by looking at it from a implementation point of view.

## **Part II**

# **Practical Aspects and Implementation**



# Chapter 5

## Practical Aspects

**I**N THE PREVIOUS part of this thesis we have introduced Vandermonde-subspace frequency division multiplexing (VFDM), showing how it works and its performance in terms of achievable spectrum efficiency. In order to develop the main concepts behind VFDM, some very stringent assumptions had to be made. Now, the natural question to be answered is: *can VFDM be implemented in a real-life scenario?* In this chapter, a discussion on the real necessity of some previously made assumptions is made under the light of a practical implementation. Then, the performance of VFDM when some of these assumptions are relaxed is presented along with a discussion of the cost they incur on performance. Finally, we present some topics on implementation issues.

### 5.1 Channel State Awareness and Estimation

As seen throughout this thesis so far, awareness of some of the related secondary channel state information (CSI) is needed by VFDM. This is necessary both to allow the creation and adaptation of the pre-coder as well as for decoding at the receiver. The actual channels to be known depend on the receiver strategy employed. Looking back at section 2.3, due to the structure of VFDM, it is imperative that the CSI for  $\mathbf{h}^{(21)}$  be present at the transmitter for the construction of the pre-coder  $\mathbf{E}$ . Also,  $\mathbf{h}^{(22)}$  is needed for input covariance optimization. At the secondary receiver, both the CSI for  $\mathbf{h}^{(22)}$  and  $\mathbf{h}^{(12)}$  are needed in order to perform the reception and feedback the covariance of the interference plus noise from the primary transmitter  $\mathbf{S}_\eta$  to the secondary one. To gather knowledge about these channels while adapting to the primary system's transmission protocol, an elaborate channel estimation procedure must be designed to dictate when and with what technique the channels will be estimated at the secondary transmitter and receiver. The actual channel estimation technique involved is also of importance since it will directly influence the estimation quality and time.

One common way CSI is acquired is through pilot estimation and tracking. Several radio communications standards (e.g., [9, 13]) mandate the use of pilot signals to be sent, allowing for base stations and/or user terminals to estimate the channel state and adapt its transmission/reception accordingly. For the specific case of orthogonal frequency division multiplexing (OFDM), since it requires constant tracking of the channel in order to perform equalization, pilot tones are usually inserted into specific subcarriers of each OFDM symbol [13]. These estimations are valid in only one way (uplink or downlink), in case of frequency division duplexing (FDD) or for both the uplink and downlink, for the case of time division duplexing (TDD) communications. For now, as stated before, let us consider that all communications are carried out in TDD mode and that channel reciprocity can be exploited.

Being a cognitive radio (CR) based system, the secondary must understand the primary system's technology in order to know the pilot signal structure and their allocation inside of the OFDM symbol. It is important to note that VFDM has to be fast enough to perform the channel estimation, pre-coder construction and transmission inside of the coherence time of the channel. This fact, of course, restricts VFDM to operate alongside an OFDM system whose frequency band size is compatible with VFDM's processing capabilities, under a low mobility scenario. A successful outcome, with respect to coherence time, would look like the one in figure 5.2.

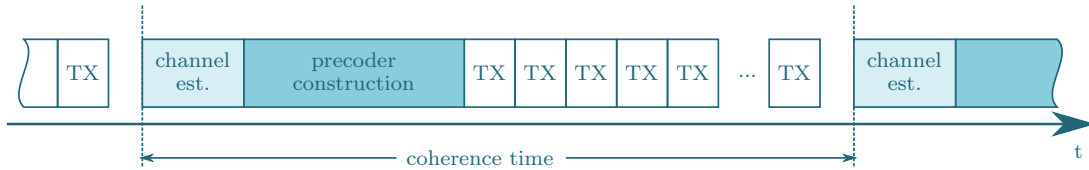


Figure 5.1: VFDM's relation to the coherence time.

Of course, channel estimation procedures using pilot signals are prone to errors, especially in noisy environments. In addition to degrading the secondary communication, imperfect channel state information becomes critical in the case of VFDM. It turns out that VFDM's pre-coder structure is very sensitive to imperfect CSI, as one can easily guess from equation (2.7), where the presence of erroneous estimations jeopardizes the zero interference claim. VFDM's relationship to imperfect CSI is detailed in the following.

## 5.2 Single User Channel Estimation Protocol

To devise a practical secondary VFDM system, a channel estimation protocol needs to be designed, taking into consideration prior knowledge of the primary system and its own channel estimation procedure. Herein we propose a channel estimation procedure and evaluate the impact of training versus transmit symbols on the performance of VFDM. Before we start, let us assume that perfect synchronization is achieved in all transmissions, that TDD communications are used and that channel reciprocity can be exploited.



for equalization purposes. During the same time, the secondary transmitter sends a set of pilots  $\Psi_2$  which is orthogonal to  $\Psi_1$ . These pilots symbols are used to estimate  $\mathbf{H}_{22}$ , the overall channel matrix, used later for equalization. Equal power allocation is considered at the secondary transmitter to simplify the channel estimation procedure. Since  $\Psi_1 \perp \Psi_2$ , and considering that both transmissions are synchronized<sup>2</sup>, no interference will be seen at the both the primary and secondary systems during the downlink phase.

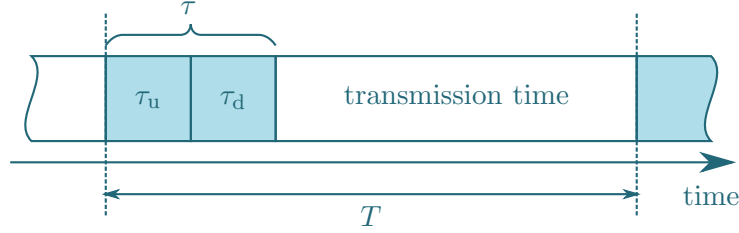


Figure 5.3: Channel estimation and transmission time for the primary system.

All of this happens during the complete channel estimation time for the primary system  $\tau = \tau_u + \tau_d$  as presented in figure 5.3.

## 5.2.2 Primary System

As stated before, the primary receiver transmits training symbols on the uplink back to the primary transmitter. In the uplink,  $\Psi_1 \in \mathbb{C}^{N \times \tau_u}$  are orthogonal Fourier-based training symbols sent during a time  $\tau_u \geq N + L$ , such that

$$\begin{cases} [\Psi_1]_{k+1, l+1} e^{-i2\pi \frac{kl}{\tau_u}} \\ k = 0, \dots, N-1 \\ l = 0, \dots, \tau_u, \end{cases}$$

which depends on the amount of symbols required for the channel estimation. After that, the primary transmitter sends back the same training symbols  $\Psi_1$  during a time  $\tau_d \geq N + L$ , used by the primary receiver to estimate  $\mathbf{h}^{(11)}$ , this time for equalization purposes.

## 5.2.3 Secondary System

During  $\tau_u$ , the secondary transmitter taps into the primary system's uplink training transmission, receiving

$$\mathbf{Y}_{2u} = \mathbf{H}'_{21} \Psi_1 + \Upsilon_{2u},$$

<sup>2</sup>We consider that both transmissions are synchronized at reception time at both receivers. Note that this is a strong assumption since it requires that both receivers be equally spaced to their respective *and* interferer transmitters.

where  $\mathbf{Y}_{2u} \in \mathbb{C}^{N \times \tau_u}$  is a matrix of received OFDM symbols during a time  $\tau_u$ ,  $\mathbf{H}'_{21} = \mathbf{F}\mathcal{T}(\mathbf{h}^{(21)})\mathbf{A}\mathbf{F}^{-1}$  is a diagonal overall channel matrix from the primary receiver to the secondary transmitter and  $\mathbf{\Upsilon}_{2u} \in \mathbb{C}^{N \times \tau_u}$  is the overall received noise matrix over time  $\tau_u$ . We remark that  $\mathbf{H}'_{21}$  is essentially different from  $\mathbf{H}_{21} = \mathbf{F}\mathcal{T}(\mathbf{h}^{(21)})\mathbf{E}$ , since the latter is the (not diagonal) overall channel including the pre-coder  $\mathbf{E}$ . The estimate  $\hat{\mathbf{H}}'_{21}$  is then obtained by

$$\begin{aligned}\hat{\mathbf{H}}'_{21} &= \frac{\sqrt{N}}{\tau_u} \mathbf{Y}_{2u} \mathbf{\Psi}_1^H \\ &= \mathbf{H}'_{21} + \frac{\sqrt{N}}{\tau_u} \mathbf{\Upsilon}_{2u} \mathbf{\Psi}_1^H.\end{aligned}\quad (5.1)$$

The uplink channel estimation in (5.1) is made possible since the secondary system possesses prior knowledge of the channel estimation procedure and training symbol structure of the primary system.

To construct  $\mathbf{E}$ , the secondary transmitter must first convert the overall channel estimation  $\hat{\mathbf{H}}'_{21}$  to the time domain  $\hat{\mathbf{h}}^{(21)} = [\hat{h}_0^{(21)}, \dots, \hat{h}_L^{(21)}]^T$  where

$$\hat{h}_{k-1}^{(21)} = \left[ \mathbf{F}^{-1} \hat{\mathbf{H}}'_{21} \right]_{k,k} \quad k \in \{1, \dots, L+1\}.$$

$\mathbf{E}$  can be finally constructed as described in section 2.3, finishing the uplink channel estimation cycle.

A new channel estimation procedure is necessary on the downlink during  $\tau_d$ , to enable the secondary receiver to equalize the subsequent transmitted symbols. At this stage, the secondary transmitter also sends precoded Fourier-based pilot symbols  $\mathbf{\Psi}_2$  (another set orthogonal to  $\mathbf{\Psi}_1$ , such that  $\mathbf{\Psi}_1 \mathbf{\Psi}_2^H = \mathbf{0}$ ) to the secondary receiver, so it can estimate the channel  $\hat{\mathbf{h}}^{(22)}$ . It is the orthogonality between  $\mathbf{\Psi}_1$  and  $\mathbf{\Psi}_2$  that allows the secondary transmission to be interfere-free from the primary's channel estimation and vice versa. The received training signal for the secondary user becomes

$$\mathbf{Y}_{2d} = \mathbf{H}_{22} \mathbf{\Psi}_2 + \mathbf{\Upsilon}_{2d}, \quad (5.2)$$

which allows a similar channel estimation procedure as for the primary case, given by

$$\begin{aligned}\hat{\mathbf{H}}_{22} &= \frac{\sqrt{N}}{\tau_d} \mathbf{Y}_{2d} \mathbf{\Psi}_2^H \\ &= \mathbf{H}_{22} + \frac{\sqrt{N}}{\tau_d} \mathbf{\Upsilon}_{2d} \mathbf{\Psi}_2^H.\end{aligned}\quad (5.3)$$

Finally, both systems engage in the transmission phase during  $T - \tau$ . For the secondary system, transmission and reception is carried out as described in the previous sections. Unlike the perfect CSI case, the received signal for the primary user in (2.8) now becomes

$$\mathbf{y}_1 = \mathbf{H}_{11} \mathbf{s}_1 + \mathbf{H}_{21} \mathbf{s}_2 + \boldsymbol{\nu}_1, \quad (5.4)$$

where  $\mathbf{H}_{21} \mathbf{s}_2 \neq \mathbf{0}$ . This is due to the channel estimation error in  $\hat{\mathbf{h}}^{(21)}$  that breaks the orthogonality between  $\mathcal{T}(\mathbf{h}^{(21)})$  and  $\mathbf{E}$ .

### 5.2.4 Performance Under Imperfect CSI

To quantify the performance of VFDM under imperfect CSI, Monte Carlo simulations were executed for the cognitive interference channel scenario presented in section 2.2. The parameters used in this section are inspired by Institute of Electrical and Electronics Engineers (IEEE) 802.11a [9]. A brief listing of the main parameters can be seen in table 5.1. Transmit powers are considered to be unitary for both primary and secondary system, and the signal to noise ratio (SNR) is controlled by varying the noise variance  $\sigma_n^2$ .  $\mathbf{E}$  is generated by a Gram-Schmidt process on the columns of  $\mathbf{V}$ , as described in Sec. 2.3. A zero forcing (ZF) linear equalizer is adopted at the primary and secondary receivers (see section 2.5 for details). As introduced in section 2.4.1, in order to control the secondary system's performance with respect to the interference coming from the primary system, an interference weighting factor  $\alpha$  is adopted. For the simulations, even though the maximum training size is of  $T - \tau$ , we concentrate on the initial region of the curves in order to emphasize the best region of the ratio between training and transmit symbols  $\tau/T$ .

parameter	value
Number of carriers ( $N$ )	64
Cyclic prefix size ( $L$ )	16
Channels	$\mathcal{CN}(0, \mathbf{I}_{L+1}/(L+1))$ (see section 2.1)
Additive noise	$\mathcal{CN}(0, \sigma_n^2 \mathbf{I}_N)$ (see section 2.1)
Coherence time ( $T$ )	$1000 \times N$ symbols
Training symbol size ( $\tau$ )	$N \leq \tau \leq (T - N)$ symbols
Interference factor ( $\alpha$ )	0
Equalizer	ZF at primary and secondary

Table 5.1: Imperfect CSI simulation parameters.

As it will be seen, the performance of channel estimation in terms or spectral efficiency is dependent on two main parts: a) the pre-log factor, a multiplicative linear factor that depends directly on the amount of training symbols  $\tau$  and b) the log factor, varying with respect to the SNR given by the channel estimate, which is also a function of  $\tau$ .

In figure 5.4, the impact of imperfect channel estimation, as a function of  $\tau/T$  for the primary system, is presented. The initial part of the curves, before the maximum point (better seen in the 10 and 20 dB curves), is affected mainly by the log factor of the imperfect channel estimation on the SNR. From the maximum and on, the pre-log factor kicks in and the reduction is predominantly linear, due to the exchange in the amount of data symbols in favor of more training. As expected, the lower the SNR, the more training symbols are needed to provide a better estimation. As the SNR increases, less symbols are needed. The same behavior can be seen for the secondary system, in figure 5.5. Unlike the primary system, the secondary system's performance is not dependent on the SNR and achieves the best spectral efficiency at a very low  $\tau/T$ .

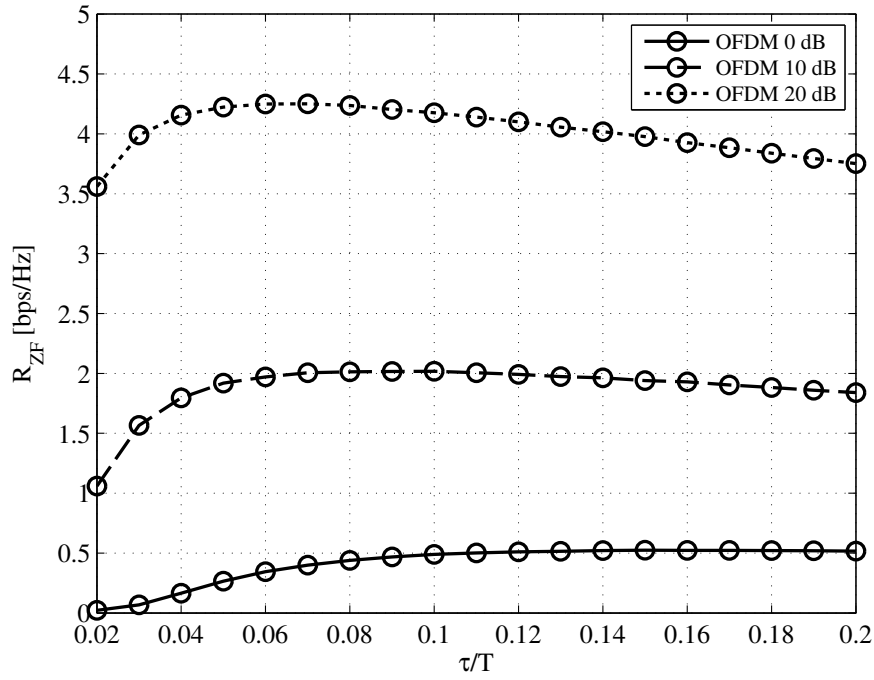


Figure 5.4: Spectral efficiency for the primary (OFDM) system with varying SNR levels  $\{0, 10, 20\}$  dB ( $N = 64, L = 16$ ).

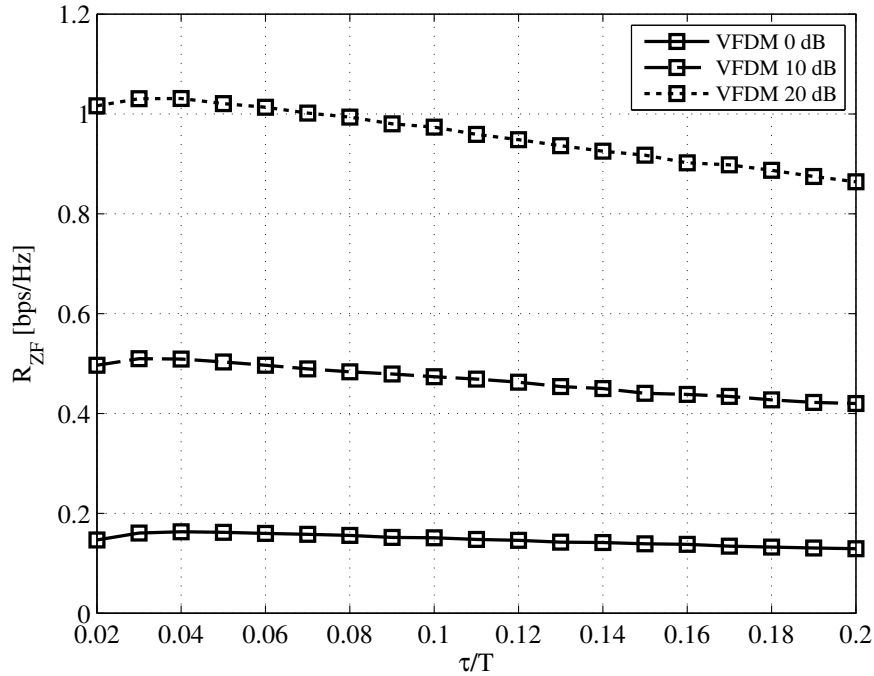


Figure 5.5: Spectral efficiency for the secondary (VFDM) system with varying SNR levels  $\{0, 10, 20\}$  dB ( $N = 64, L = 16$ ).

### 5.3 MU-VFDM's Performance Under Imperfect CSI

In section 4.2, perfect CSI was assumed in order to compute  $\mathbf{E}$ . In a realistic multi-user Vandermonde-subspace frequency division multiplexing (MU-VFDM) implementation this assumption can not hold, and any device in the system will suffer from imperfect CSI. Differently from the single user case of the previous section, herein a different model will allow the abstraction of a complicated channel estimation procedure. Such a model, inspired by [77] is based on a block fading channel in which the channel estimation remains valid throughout the coherence time  $T$ . If the channel estimations are performed during a period  $\tau$ , the available time for transmission is limited by  $T - \tau$ . Then, each channel observation is of the form

$$\mathbf{r} = \sqrt{\rho\tau}\mathbf{h} + \mathbf{n}, \quad (5.5)$$

where  $\mathbf{h}$  is the actual channel vector,  $\rho$  is the SNR at the receiver and  $\mathbf{n} \sim \mathcal{CN}(0, \sigma_n^2 \mathbf{I}_{(L+1)})$  is the noise. Each device computes the minimum mean square error (MMSE) estimate of  $\mathbf{h}$ , by evaluating the observation  $\mathbf{r}$ . Then  $\mathbf{h}$  is decomposed into two components, i.e., an estimate  $\hat{\mathbf{h}}$  and an independent error  $\tilde{\mathbf{h}}$ , that is

$$\mathbf{h} = \hat{\mathbf{h}} + \tilde{\mathbf{h}}. \quad (5.6)$$

This approach yields two independent zero-mean random variables, with covariance matrix respectively [78]

$$\Sigma_{\hat{\mathbf{h}}}(\tau) \triangleq \mathbb{E}[|\hat{\mathbf{h}}|^2] = \frac{\frac{\rho\tau}{L+1}}{\sigma_n^2(L+1) + \rho\tau} \mathbf{I}_{L+1} \quad (5.7)$$

$$\Sigma_{\tilde{\mathbf{h}}}(\tau) \triangleq \mathbb{E}[|\tilde{\mathbf{h}}|^2] = \frac{\sigma_n^2}{\sigma_n^2(L+1) + \rho\tau} \mathbf{I}_{L+1}. \quad (5.8)$$

#### 5.3.1 Performance under imperfect CSI

For the imperfect CSI analysis, in order to reduce Monte Carlo simulation times, an  $N = 24$  active subcarriers and  $L = 6$  of cyclic prefix length, is considered. The system configuration replicates the one seen in section 4.2.3 where  $K = 3$  small-cells with a load rate of  $\beta = 1$  are adopted. An imperfectly built  $\mathbf{W}$  pre-coder will affect the interference cancelation at the primary system as well as the secondary system's performance, due to an increase in the multi-user interference. Moreover, an imperfect channel estimation has an impact on the signal to interference plus noise ratio (SINR) experienced at the receiver. From [77], given the SINR  $\gamma$  for the perfect CSI, an effective SINR can be defined as

$$\gamma_{\text{eff}} = \frac{\gamma^2\tau}{1 + (1 + \tau)\gamma}, \quad (5.9)$$

where the same transmit power is assumed for training and data symbols. Then, the sum-rate of the primary and secondary system are, respectively

$$C_m^{\text{SUM, I}} = \frac{T - \tau}{T(N + L)} \sum_{j=1}^N \log_2(1 + \gamma_{\text{eff},j}) \text{ and}$$

$$C_s^{\text{SUM, I}} = \frac{T - \tau}{T(N + L)} \sum_{j=1}^{KN} \log_2(1 + \gamma_{\text{eff},j}),$$

under imperfect CSI. No interference from the primary system to the small-cell user equipments (SUEs) is considered, such that the effect of the imperfect channel estimation at the small-cells can be isolated for this study.

In figure 5.6, the ratio between the rate obtained with imperfect CSI and the rate obtained with perfect CSI, is computed for the primary system as different  $\tau/T$  proportions are chosen for SNRs  $\in \{0, 10, 20\}$  dB. As seen in the figure, the optimal  $\tau/T$  depends on the SNR. For the low SNR regime, an optimal  $\tau/T$  can be seen at about 0.16. On the other hand, as the SNR increases, the best  $\tau/T$  is identified at the smallest possible training symbol size of  $\tau/T \simeq 0.08$ . In the high SNR regime, the sum-rate decreases almost linearly following the pre-log factor.

In figure 5.7, the ratio between the rate of the imperfect and perfect CSI cases for the secondary system is computed for an SNR range. Unlike the primary system, the

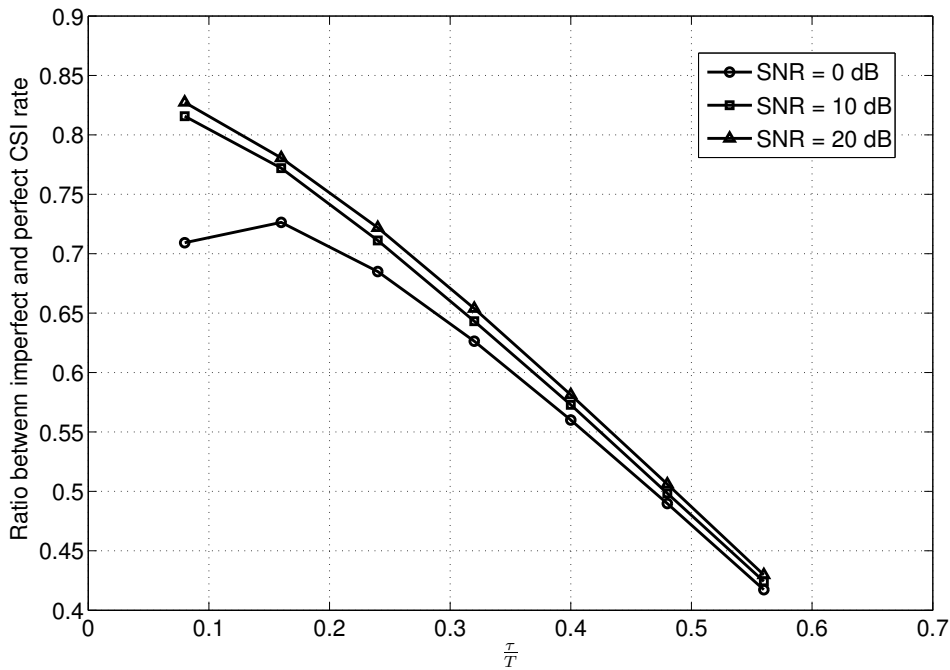


Figure 5.6: Primary system performance under imperfect CSI,  $K = 3$ ,  $\beta = 1$ , ( $N = 24$ ,  $L = 6$ ).

secondary one experiments a different optimal value for  $\tau/T$  for a larger training times for different SNRs. Compared to the loss experienced by the primary system, a poorer CSI largely affects the sum-rate of the secondary system, penalized especially at low SNRs.

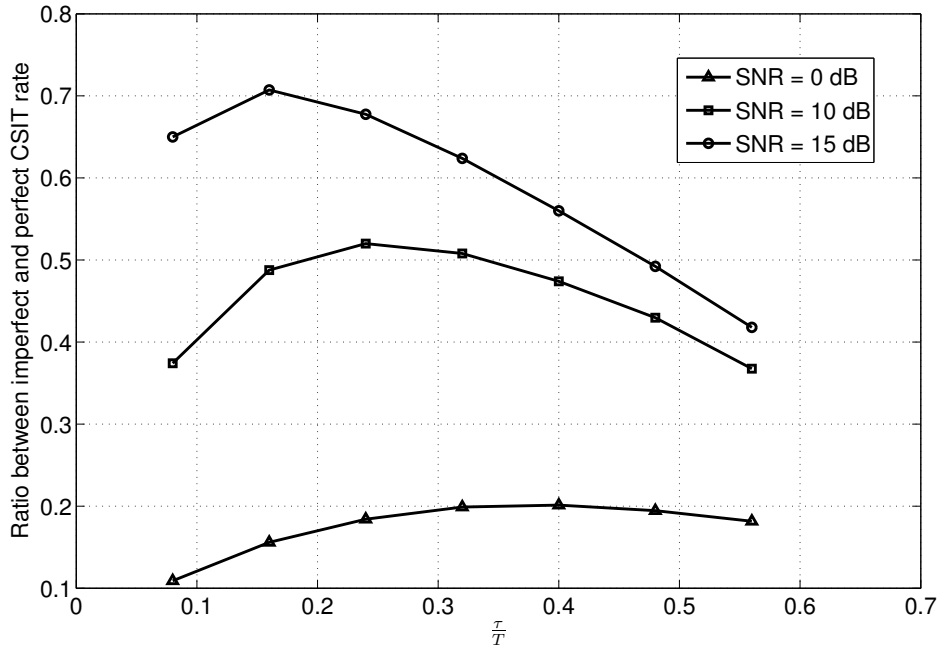


Figure 5.7: Secondary system performance with imperfect CSI,  $K = 3$ ,  $\beta = 1$ , ( $N = 24$ ,  $L = 6$  and bandwidth of 0.48 Mhz).

## 5.4 Synchronization

Another very important aspect of VFDm is synchronization. In fact, this is critical, since it is through the cyclic prefix removal at the primary receiver that the interference cancelation is effectively accomplished. If the signal arrives too early or too late, the cyclic removal procedure will discard the wrong part of the signal, and hence, the primary receiver will be susceptible to interference, as seen in figure 5.8. Furthermore, this synchronization needs to be ensured at symbol level.

To provide an idea of the harmful effect caused by out of sync reception, figure 5.9 provides some numerical results for the “delayed message” case of figure 5.8, but the results would be the same in the “early message” case. The focus is only on the interference at the primary. Note that a negative effect can be also seen at the secondary receiver’s performance, but it is not shown here. For this result, 1000 Monte Carlo iterations were executed for the same setting as in section 5.2.4. To model the effect of the unsynchronized reception, the columns of  $\mathbf{E}$  are rotated by the decided number of off sync samples. As the number of off sync samples were varied from 1 to 20 the interference increases until it

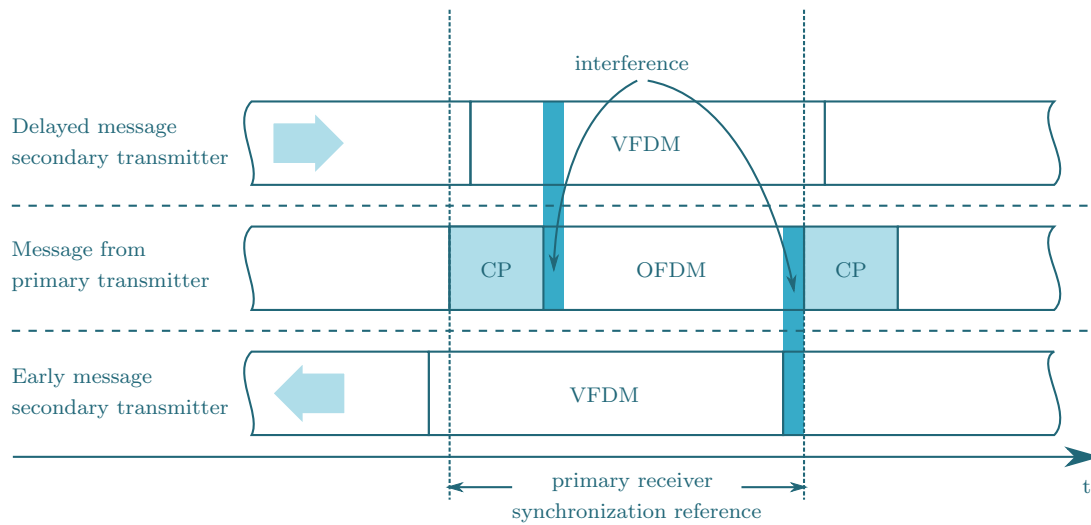


Figure 5.8: VFDM when unsynchronized w.r.t. the primary receiver.

saturates, at 16 samples. Clearly, as stated before, as samples slip through the cyclic prefix removal process, they add extra interference up to the point where all the 16 samples are inside and no more interference is added.

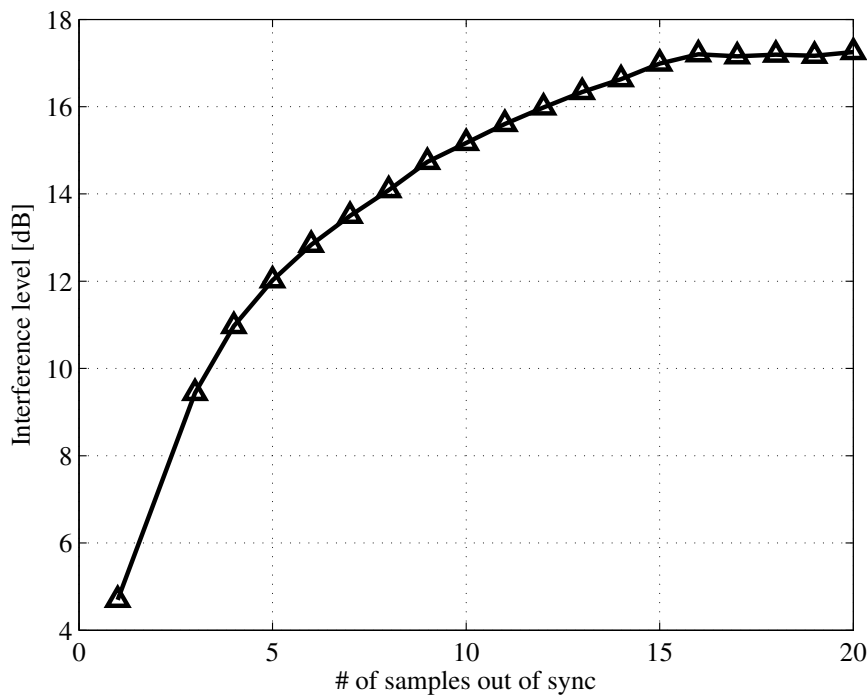


Figure 5.9: Interference caused by off sync reception of the VFDM precoded message at the primary system.

Full synchronization for the scenario depicted in section 2.2 is to be carried in two steps: 1) synchronization of the secondary transmitter with the primary receiver; 2)

synchronization of the secondary receiver with the secondary transmitter.

For the first step, the greatest challenge is synchronizing the secondary transmission with the primary ongoing communication, in a way that both messages arrive simultaneously at the primary receiver. Synchronization of two sources at reception time is not straight forward. One way in which this could be done is by estimating the position of the secondary transmitter with respect to the primary and transmitter and receiver, by measuring the received powers and signal arrival times from both. This requires precise receivers and clocks at the secondary transmitter. Of course, an estimation period needs to take place, in which the secondary transmitter performs measurements to decide the right synchronization instant. Bear in mind that, such an estimation period is different from the one depicted in figure 5.3, and usually precedes other channel estimation procedures. Fortunately, unless for the case of high speed mobility scenarios, synchronization does not change very much in time, and once estimated can simply be periodically updated.

Once the secondary transmitter synchronizes with primary receiver, then the secondary communications can become synchronized. Similar to what's done for OFDM, VFDM can send synchronization pilots over the air so that the secondary can achieve synchronization. A simpler method could be switching the secondary transmitter to OFDM mode to send pilot synchronization symbols during an idle moment of the primary system. It is important to note that by guaranteeing that the secondary receiver is synchronized to the secondary transmitter does not guarantee that the interference coming from the primary system to the secondary receiver will also be synchronized. This will directly affect the diagonalization of the primary interference at the secondary receiver.

Last, but not least, there is the issue of structured communications versus random communications. The synchronization of the secondary system with respect to the primary one becomes much simpler if the latter assumes a structured communications (e.g. long term evolution (LTE)). This happens because the secondary system, once synchronized, can adapt its clock to match that of the primary transmitter and avoid re-synchronization. If the primary system employs a random access communications, at each primary transmission, a new synchronization has to be performed at the secondary transmitter (and later secondary receiver). Depending on the time taken by the synchronization algorithms to align the clocks, the communications from the primary system may already be over, rendering the use of VFDM for this case, impossible.

## 5.5 System-Level Aspects

Aside from the practical aspects related to the physical layer, some system-level practical aspects are also important for the deployment of VFDM on a realistic setting. A detailed discussion of system level aspects depends mainly on what kind of systemic architecture VFDM is to be employed in. Since a thorough discussion on this topic is off the scope of this thesis, the discussion herein will be limited to some of the system-level aspects of the small-cell scenario, targeted by this work.

### 5.5.1 VFDM Cell Border Issue

One of the most obvious issues concerning VFDM is the one pictured in figure 5.10. Let us, for a moment, suppose a MU-VFDM system deployed in a multi-user multi-cell environment, where two nearby macro-cells are serving their own users. A VFDM small-cell in the cell border (colored in light blue) tries to serve a user (also colored in light blue) outside of the macro-cells coverage. The small-cell uses its cognitive capabilities to coordinate with cell 1, canceling the interference to the user connected to macro-cell (dashed red arrow). However, another macro-cell user, connected to cell 2 is close to the cell border where the VFDM equipped small-cell user is located. If unmanaged, the VFDM small-cell cannot, at the same time, synchronize to the cells 1 and 2, generating severe interference one of the macro-cell users (red continuous arrow).

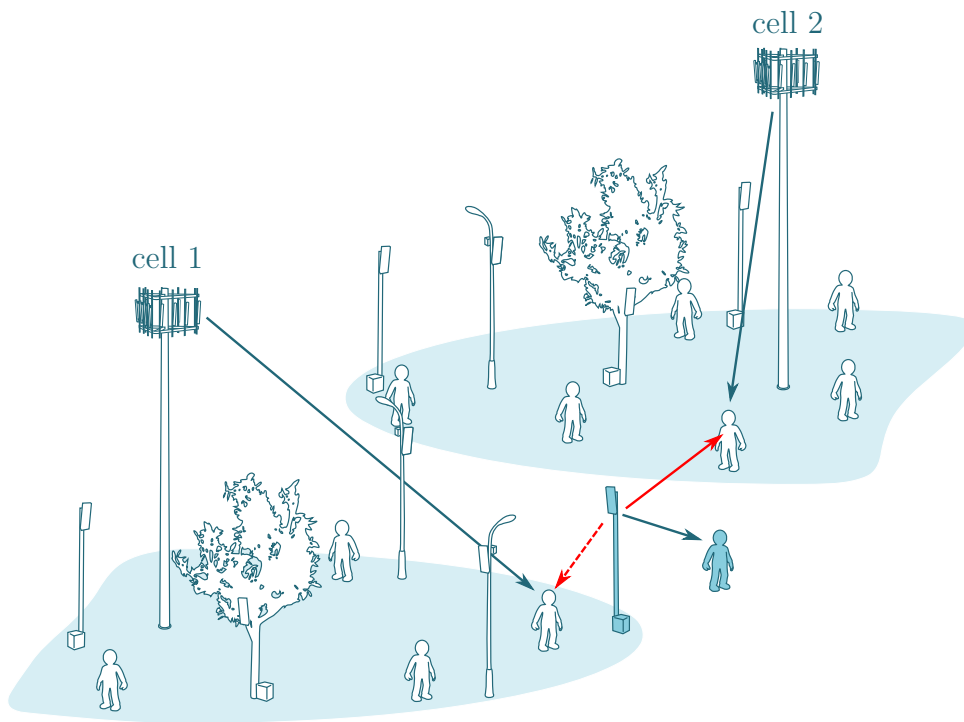


Figure 5.10: Cell border issue with VFDM.

This is a potentially serious problem for VFDM, especially since, it aims at serving as a cell coverage/capacity reinforcement, and small-cells random deployment makes it hard to foresee such situations. Some potential solutions are:

- If macro-cell frequency reuse is less than one, then cell border operation is possible and no problem exists. This effectively means that neighboring cells use a different frequency than the target one, and no interference will be generated. (MU)-VFDM can be employed without any problems in this case. Nevertheless, last-generation cellular systems employ full frequency reuse;

- If full frequency reuse is employed in the macro-cells, then MU-VFDM can be used if the macro-cells are synchronized in time and respect the carrier allocation of the other cells, especially for the users in the cell border.
- If both full frequency reuse and no cooperation between macro-cells are the case, then multiple antennas should be adopted at the small-cells such that beamforming can be used, steering the harmful interference away from the unmanaged primary users. Since interference does not need to be avoided to many directions, a simple antenna array can be used;
- Finally, if none of the assumptions above can be guaranteed, since small-cells are to be deployed in a very dense configuration, they can coordinate among themselves to find another small-cell transmitter who is at the same time near to the small-cell user and out of reach of the macro-cell user at cell 2.

## 5.5.2 Mobility

One of the most important characteristics of cellular systems are their ability to operate in mobility environments. Macro-cells need to be able to serve users in pedestrian mobility profiles as well as those using fast means of transportation, such as vehicles and trains.

One potential issue with mobility is related to channel estimation and the coherence time. In section 5.1 the tight relationship between VFDM and channel knowledge has been presented. It is known that mobility reduces the coherence time, the higher the speed of the user [79]. As seen in figure 5.11, depending on the amount of time required by the pre-coder processing, this could pose a problem, despite of the fact that the primary system is designed to work within the same coherence time.

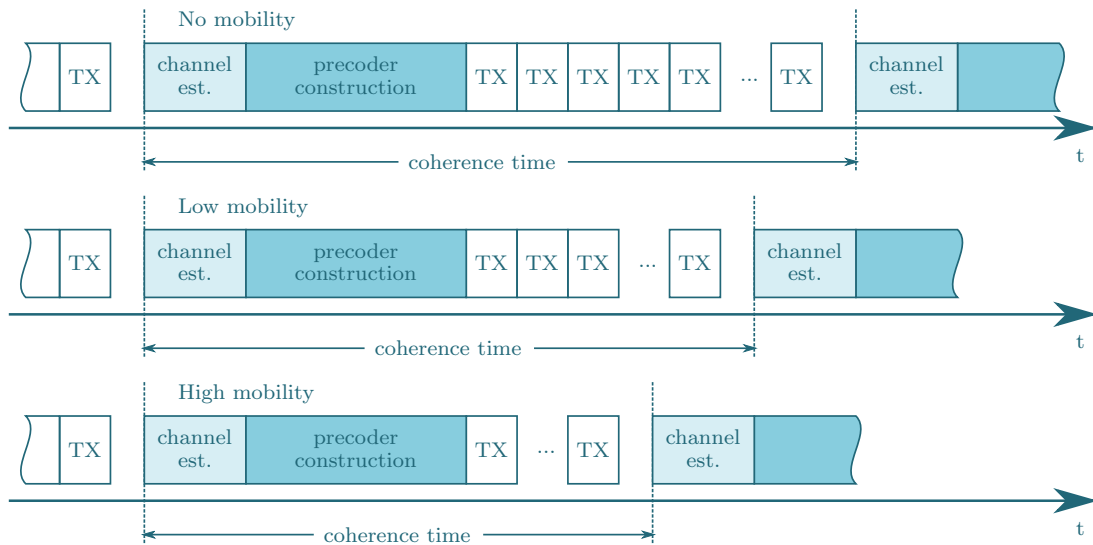


Figure 5.11: Effect of mobility on the coherence time and VFDM's performance.

### 5.5.3 MU-VFDM Subset Selection

MU-VFDM depends on a minimum number of available transmit dimensions in order to serve a set of secondary users, as seen in section 4.2.2. Therefore, for a given set of secondary users, an associated set of MU-VFDM small-cells should be selected. If MU-VFDM small-cells are deployed in a very dense formation, then enough small-cells can be assumed to be in the pool from which such a sub-set of small-cells are to be selected.

As of now, the main open issue with respect to MU-VFDM small-cell subset selection is the adopted criterion. Indeed several criteria can be adopted either alone or combined, for example:

- **Propagation conditions.** MU-VFDM small-cells that offer good propagation conditions can be selected to compose the set. These propagation conditions can be either to the secondary receivers, in the case where rate maximization is sought, or to the primary receivers, in the case where best interference protection is sought.
- **Load.** MU-VFDM small-cells that may be already serving other small-cell users could be left out of the selection. Alternatively, incoming users could be included in an already existing set of MU-VFDM small-cells, as dimensions allow.
- **Interference.** As illustrated in section 5.5.1, MU-VFDM small-cells located near the macro-cell border can interfere with a primary user communication ongoing at a nearby macro-cell. Potentially interfering MU-VFDM small-cells could then be left out of the selection, until nearby primary communications end.

## 5.6 Closing Remarks

In this chapter we presented some of the practical aspects related to the implementation of VFDM. The practical aspects presented herein are by no means exhaustive and serve merely to identify some potential critical points.

Some of the conclusions taken from this chapter serve as a starting point for the initial implementation of VFDM on a transmission platform, presented in the next chapter.



# Chapter 6

## Prototype Implementation

**I**N THIS CHAPTER, the implementation of a prototype VFDM transceiver is described. To implement a VFDM prototype, a hardware/software platform capable of actual radio frequency (RF) transmission/reception is required. This chapter starts with a description of a transmission platform whose development was partly done within this doctoral work. The platform, called SDR4all, is based on Matlab, as a programming language for flexibility, and counts with a commercially available hardware part. Then, the VFDM transceiver prototype is described. This prototype serves as a proof of concept of the data transmission part of VFDM, an essential step to provide a proof of concept of a full VFDM demonstrator.

### 6.1 SDR4all Platform

SDR4all is based on the concept of software defined radio (SDR) to enable the implementation of algorithms that can be tested with real transmissions using actual hardware transceivers. The idea of this platform is to enable the telecommunications academia to test their ideas and algorithms on real transmissions while still keeping the simplicity of a high level programming language environment, such as Matlab. The platform has also gained life outside of the VFDM context, allowing telecommunication theorists to bridge the gap between theory and practice and has also been used for teaching in telecommunication courses.

SDR4all is composed of a hardware part, developed by ETTUS<sup>1</sup> Research LLC [80], initially conceived to be used with GNU Radio [81], and a software part developed partly by CEA-LETTI (hardware drivers) and also by the Alcatel-Lucent Chair in Flexible Radio at Supélec (Matlab toolbox). The hardware part is in charge of the RF and sampling processing while the radio transceiver's base-band is software driven, running in an ordinary computer.

---

<sup>1</sup>As of the writing of this thesis, a SDR4all in-house made transceiver card is under development.

The current version of the hardware of the platform was based on the universal software radio peripheral (USRP) version 1 cards [80]. These cards are divided into two parts: a mother-board and one or two daughter-boards. The mother-board is responsible for the RF control, communication over the universal serial bus (USB) link, analog-to-digital (A/D), digital-to-analog (D/A) conversions and sampling. The daughter-board is responsible for the RF circuitry, including filters, amplifiers and oscillators. A wide variety of daughter-boards, also made by ETTUS, are available to allow testing in multiple bands. As of now, SDR4all only supports the RF circuitry provided by the RFX2400 daughter-board. The 2.4 GHz industrial, scientific and medical (ISM) band was chosen since it shares the same characteristics with the widely popular 802.11(b/g) and Bluetooth. Along with the RFX2400 daughterboard, dual VERT2450 antennas (TX and RX, each) are adopted. These are standard isotropic antennas made for the 2.4 and 5 GHz ISM band. The main parameters for the mother-board and RF circuitry are provided in table 6.1.

parameter	value
operating band	ISM 2.4 ~ 2.49 GHz
base-band filtering	20 MHz
channels	1 to 13 (802.11)
total TX power	20 mW
signal bandwidth	up to 16 MHz

Table 6.1: Parameters for the hardware part.

As previously stated, the PHY layer is implemented in software, part of a Matlab toolbox developed specifically to this end. In order for the toolbox to correctly communicate with the cards, a driver was built. At the moment, the driver enables non real-time communication between one card and a computer<sup>2</sup>. It is able to transmit a given vector of baseband I/Q symbols and to listen for a certain amount of time and provide a vector of the received baseband I/Q samples. The driver also allows to configure the bandwidth and the center frequency for both transmission and reception. The toolbox implements basic communication blocks, such as bit operations, modulation, packet formatting and so on. An OFDM transceiver chain and channel sounder was also implemented. The kernel driver of the toolbox handles the data streams and communicates with the USRP over USB link. Inside the USRP, a Cypress FX2 chipset receives the stream and sends it to Altera Cyclone field-programmable gate array (FPGA) for digital up/down-conversion from baseband to intermediate frequency (IF) and vice versa. Daughterboards perform an analog up/down-conversion from IF to RF and vice-versa.

The overall layout of SDR4all can be seen in figure 6.1. A photograph of an actual setup employing two laptops and two USRPs are presented in figure 6.2.

<sup>2</sup>Multi-card, real-time operation is currently under development.

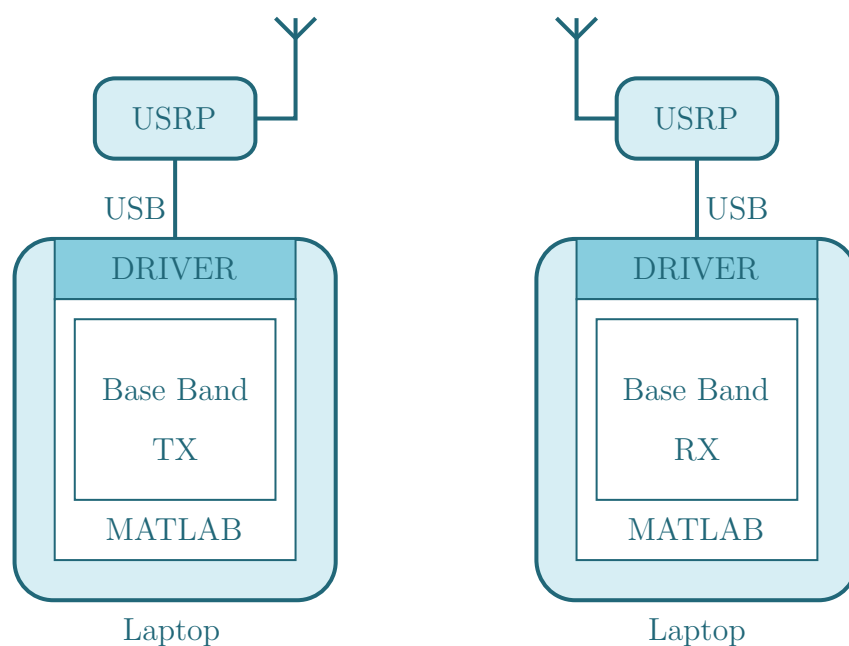


Figure 6.1: SDR4all overall layout.



Figure 6.2: Laptops and USRPs.

## 6.2 Considerations and VFDM Scenario

Let us recall the cognitive interference channel scenario presented previously in sections 2.1 and 2.2, a secondary transmitter sends data to a secondary receiver (over link<sup>3</sup>  $\mathbf{h}^{(22)}$ ), while nulling the interference towards the primary receiver. To show how a VFDM transceiver can be implemented in practice, let us forget initially the unrelated parts concerning the

---

<sup>3</sup>From this point on, we will refer to the term *link* as the logical connection between a transmitter and a receiver over a specific channel. The term *channel* still refers to the propagation environment between a transmitter and a receiver.

primary system, focusing on the ones that directly influence VFDM. The important links, with respect only to the VFDM transceiver, can be isolated as  $\mathbf{h}^{(21)}$  and  $\mathbf{h}^{(22)}$ , seen in figure 6.3.

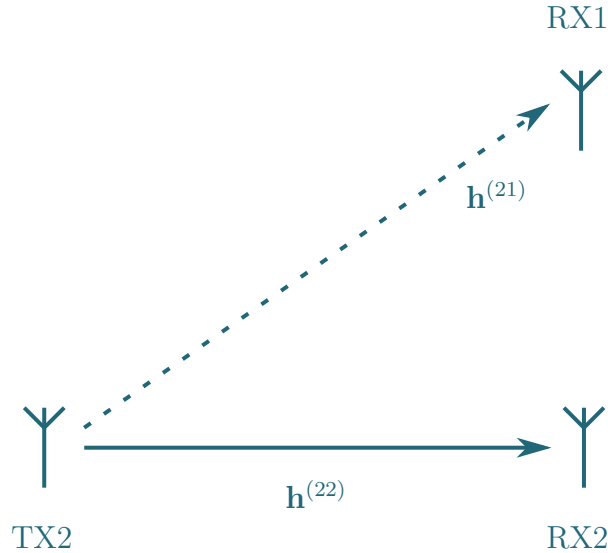


Figure 6.3: Cognitive interference channel scenario, focusing on secondary and its links.

As detailed in section 5.1, the link  $\mathbf{h}^{(22)}$  refers to the actual data transfer link, whose channel must be known at the receiver RX2. The link  $\mathbf{h}^{(21)}$ , on the other hand is required in order to create  $\mathbf{E}$ , the null-space pre-coder.

At this moment, to simplify the work by concentrating only on the VFDM's transceiver, channel estimation is performed only for  $\mathbf{h}^{(22)}$ , since its is required for the equalization of the received signal at the secondary receiver. To emulate the knowledge of the channel  $\mathbf{h}^{(21)}$ , a unit-norm, independent and identically distributed (i.i.d.), complex circularly symmetric and Gaussian  $\mathcal{CN}(0, \mathbf{I}_{L+1}/(L+1))$  channel is generated, according to the same model as described in section 2.2. A future version of this work will contemplate the full channel estimation scenario required, as described in section 5.3.

### 6.3 Base-Band Transceiver Implementation

As a first step towards the implementation of the VFDM transceiver, initially an OFDM transceiver was created in SDR4all. This OFDM implementation served as a starting point as well as to validate the SDR4all platform. An interested reader can refer to appendix A for more details on the OFDM implementation, modes of operation and output metrics.

Resembling the OFDM implementation, the VFDM base-band (BB) signal processing is carried on by the SDR4all toolbox, running in Matlab. The block diagram of the VFDM transmitter is shown in figure 6.4.

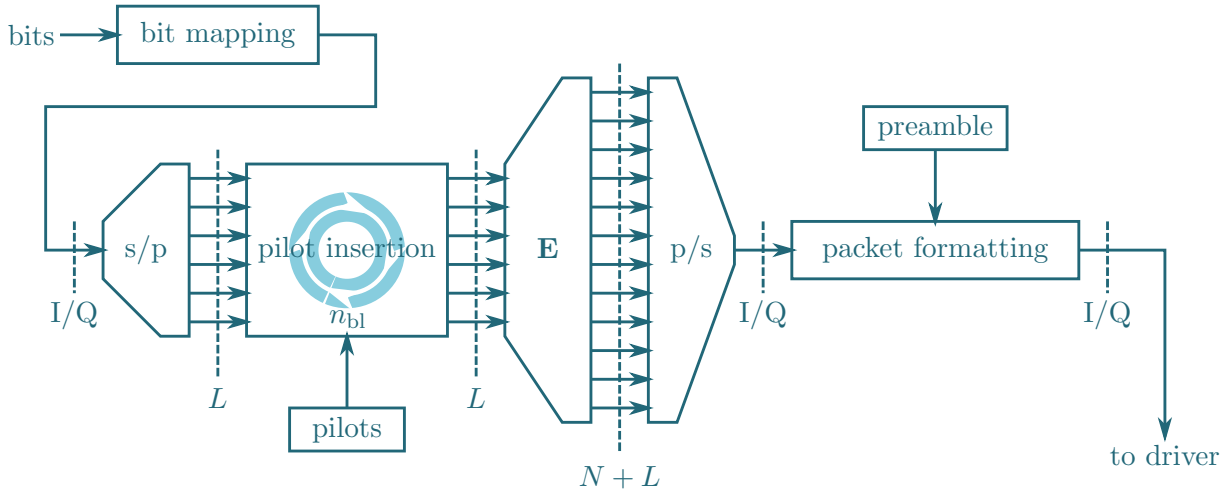


Figure 6.4: VFDM Transmission chain.

The functional behavior of the transmitter chain is as follows (from left to right in figure 6.4):

1. The input bit sequence is fed to the constellation mapper, that can be configured for any constellation type (binary phase shift keying (BPSK), quadrature phase shift keying (QPSK), 16 - quadrature amplitude modulation (16-QAM), and so on);
2. The output complex symbols are converted from serial to parallel in  $L$  by  $L$  chunks as required by the pre-coder;
3. A total of  $n_{bl}$  sequences of  $L$  complex symbols are formatted into a packet by the addition of a pre-computed pilot block  $\Psi_2$  of size  $\tau$ . The pilots are Fourier based as described in section 5.2.2. Both  $n_{bl}$  and  $\tau$  are user configurable;
4. The packets are multiplied by the pre-coder  $\mathbf{E}$  created based on a generated Rayleigh fading channel of  $L + 1$  taps as described previously;
5. The  $N + L$  complex parallel samples are then converted back to serial;
6. Then, a preamble is inserted. The preamble is designed such that it starts with a Golay complementary sequence [82]  $\mathbf{g}$  of length  $n_{gl}$  taking values in  $\{1 + j, -1 - j\}$ , to be used at the receiver for synchronization purposes and a constant sequence of symbols  $1 + j$  of size  $n_{cs}$ , for phase offset detection. Furthermore, a guard time of size  $n_{gt}$ , is added between the preamble and the payload. Also, both the preamble and payload parts are separately normalized to one at this point;
7. Finally, the frame is pushed to the driver, which produces 10 repetitions of the frame spaced with silence slots of the same size of the frame. The whole transmit vector is then fed to the USRP, which pushes it over the air. At the same time, a trigger

signal is sent over the ethernet towards the receiver. The purpose of this trigger is to initiate the reception and will become clearer briefly.

As described before, all of the BB part of the transmission runs on Matlab, in *non real-time* mode, and the processing can take up a couple of seconds depending on the configuration. The finished transmission frame, composed of alternating blocks of pre-coded pilot and data, with the preamble, is shown in figure 6.5. With an optimized set of underlying algorithms, the VFDM transmitter could perfectly run in real-time<sup>4</sup>.

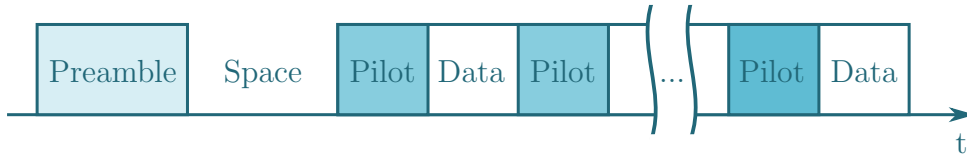


Figure 6.5: VFDM frame structure.

At the secondary receiver, the analogous operations to the ones at the transmitter are performed. The block diagram of the VFDM receiver chain is shown in figure 6.6. Its functional scheme is detailed in the following (again, from left to right in figure 6.6):

1. Initially, the driver is configured with a receive time of  $t_{RX}$  by the Matlab BB code, which waits for a trigger from the transmitter;
2. Once the trigger is received, the driver collects  $\mathcal{N}$  samples from the USRP, such that

$$\mathcal{N} = t_{RX} \times \frac{1}{f_s}.$$

3. The input I/Q vector  $\mathbf{y}$  undergoes a frame detection procedure to detect the start of a usable frame inside the  $\mathcal{N}$  received symbols. The frame detection procedure is based on the autocorrelation of the Golay complementary sequence. By performing the cross-correlation between the received signal  $\mathbf{y}$ , and the known Golay sequence  $\mathbf{g}$ , that is

$$R(t) \triangleq \sum_{i=1}^{\mathcal{N}} \mathbf{y}^*(t) \mathbf{g}(t+i) \quad (6.1)$$

the estimated starting point of the frame can be detected at  $k^*$ , by taking

$$k^* = \operatorname{argmax}_{t \in \{1, \dots, \mathcal{N}\}} (R(t)).$$

Since  $\mathbf{y}$  might contain several (full or partial) frames, some extra simple logic is required to select a, so called, usable frame;

<sup>4</sup>A real-time version of the full VFDM demonstrator is currently under construction.

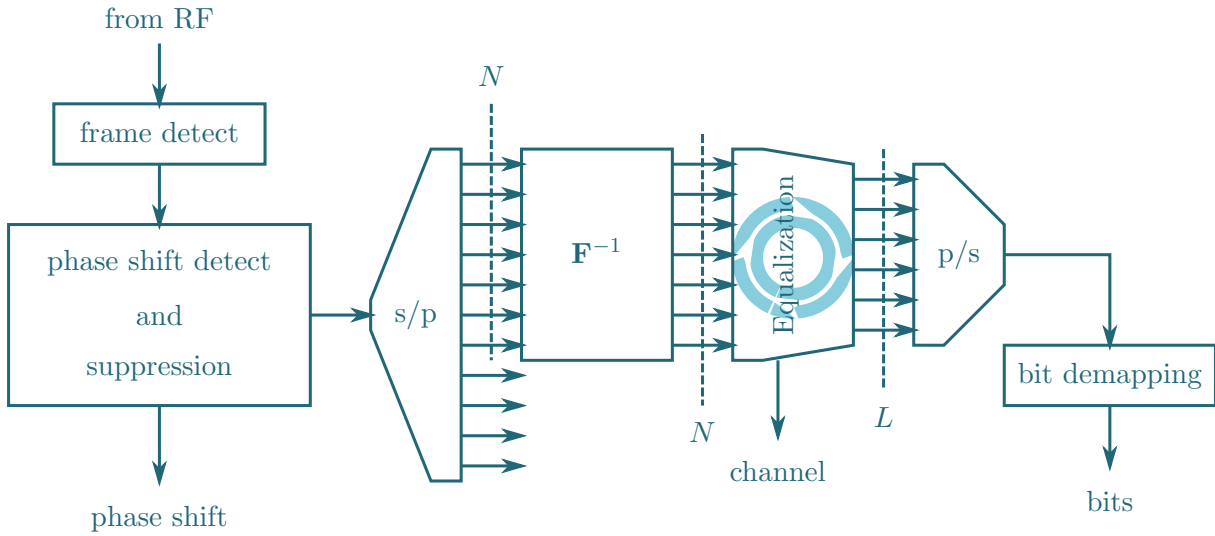


Figure 6.6: VFDM Reception chain.

4. Once the start of a usable frame is detected, the frame is cut off from the rest of the received symbol vector. This is necessary to reduce the processing time of the remainder of the receiver procedure;
5. Then comes phase shift detection and suppression. In fact, with the USRPs (and many other radio cards), a phase-locked loop (PLL) imprecision creates a mismatch between the frequency  $f_c$  of the transmitter and that of the receiver. If unsuppressed, this issue affects severely the accuracy of the decoding. Unlike the OFDM implementation, for VFDM a two-step phase shift estimation is done [9, 83]. The *coarse* phase shift estimation/compensation, makes use of the fact that constant-phase symbols are present inside the preamble. The coarse phase offset is estimated by

$$\hat{\phi}_c = \frac{1}{n_{cs}} \sum_{i=k^*}^{k^*+n_{cs}+N-1} [\angle(r_{i+1}) - \angle(r_i)], \quad (6.2)$$

where  $\angle(\cdot)$  is the angle operator of a given complex value, and each subsequent phase offset computation is averaged out to compensate for phase noise. Once the coarse phase shift of the received VFDM frame is detected, a first compensation takes place. Then operation, the preamble sequence is divided in two equal portions,  $\mathbf{p}_1$  and  $\mathbf{p}_2$ , to estimate the residual *fine* phase shift,  $\hat{\phi}_f$ . The procedure used is described in [9]. The estimate  $\hat{\phi}_f$  is given by

$$\hat{\phi}_f = \frac{4}{(n_{cs})^2} \sum_{m=k^*}^{k^* + \frac{n_{cs}+N-1}{2} - 1} \angle |r_m r_{\frac{n_{cs}+N-1}{2}}^*|. \quad (6.3)$$

Then, the fine phase shift is compensated.

6. The output complex symbols with phase correction are converted from serial to parallel and then has its cyclic prefix discarded, such that  $N$  by  $N$  chunks are passed on to the next step;
7. The  $N$  complex symbols undergo a discrete Fourier transform (DFT), to diagonalize the overall interference channel from the primary transmitter. Even though a primary transmitter is not present, the DFT operation remains for testing purposes;
8. Equalization follows. Initially, the received version of the pilots  $\Psi_2$ ,  $\tilde{\Psi}_2$  are extracted from the frame. Note that, depending on the size of the data to be transmitted, several occurrences of  $\tilde{\Psi}_2$  are present inside the frame, and each will provide a channel estimation. The channel estimations, obtained by

$$\hat{\mathbf{H}}_{22}(t) = \tilde{\Psi}_2(t)\Psi_2^H,$$

are used to equalize the subsequent data symbols, since  $\Psi_2\Psi_2^H = \mathbf{I}_L$ .

9. A simple ZF linear equalizer as the one presented in section 2.5 was implemented to equalize the received data by

$$\mathbf{D}(t) = \hat{\mathbf{H}}_{22}^\dagger(t)\mathbf{Y}(t), \quad (6.4)$$

where  $\mathbf{D}(t)$  is the equalized data matrix at instant  $t$ .

10. Blocks of  $L$  complex parallel samples are then converted back to serial;
11. Finally, the output I/Q symbols undergo a constellation de-mapper, following the constellation type at the transmission to yield a bit sequence;

The proposed VFDM receiver works similarly to an OFDM receiver, which suggests that a configurable shared receiver could be developed where a parameter could switch from OFDM to VFDM and vice-versa.

## 6.4 Experimental Setup

A test bed composed of two laptops, each connected to their own USRP behaving as either the transmitter or the receiver has been set up to validate the VFDM transceiver architecture. The setup resembles that of figure 6.2, but in the actual experiment the laptops and cards were placed about 3 m apart across a computer laboratory environment as depicted in figure 6.7.

Figure 6.7: Laboratory environment used in the VFDM transmission tests.

The secondary transmitter was configured to perform two unassisted sets of 1000 transmissions, such that statistically relevant results can be obtained. In the two sets the

proportion  $N/L = 8$  was kept constant and the number of dimensions was reduced, to see its effect on the performance. Furthermore, the transmission bandwidth  $f_s$  was increased from 2 MHz to 4 MHz to keep the transmission time within the maximum listening time limit. The transmissions were executed in the Supélec building. They were started by remote activation, when the lab and its surroundings were empty during the night, to avoid disturbances to the transmissions. Finally, the bit stream fed into the transmitter is a rescaled grayscale version of the famous Lena picture as seen in figure 6.8. The main parameters used for system configuration are provided in table 6.2.

parameter	value (set 1)	value (set 2)
Number of carriers (N)	64	128
Cyclic prefix size (L)	8	16
Golay sequence size ( $n_{gl}$ )	64	64
Constant sequence size ( $n_{cs}$ )	2048	2048
Guard time size ( $n_{gt}$ )	128	128
Receiver listening time ( $t_{RX}$ )	500 ms	500 ms
Pilot size ( $\tau$ )	30 blocks	30 blocks
Data size ( $n_{bl}$ )	30 blocks	30 blocks
Transmission BW $f_s$	1 MHz	4 MHz
Modulation order	QPSK	QPSK

Table 6.2: Parameters for the VFDM transceiver.



Figure 6.8: Original Lena picture fed into the transmitter.

## 6.5 Illustrative Results

For the sake of simplicity, some of the following presented results focus only on a randomly selected transmission, among the 2000 performed. Some of the transmissions resulted in a synchronization error, and provided no valuable results. Since this implementation of VFDM shares the same ISM band as the wireless fidelity (WIFI) hotspots present in the

campus, some of the transmissions might have been interfered by WIFI beacons, and lost synchronization. Such an event has been observed occasionally during the trial phase even in the absence of normal WIFI usage. The linear normalized power profile of an example received frame can be seen in figure 6.9. It can be seen that the payload exhibits a very

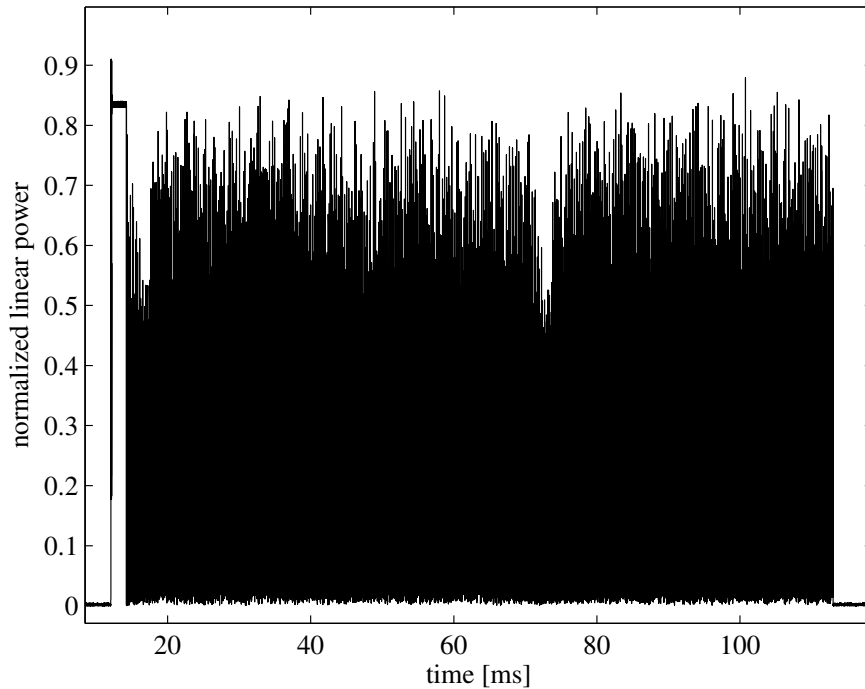


Figure 6.9: Example receive frame.

irregular power profile, especially if compared to that of the preamble. This behavior, present in both sets of runs, suggests that VFDM suffers from a peak to average power ratio (PAPR) problem, similar to OFDM.

Due to its more stable nature, the preamble SNR is computed by comparing the power of the preamble with the power of the subsequent silence. Throughout the experiment, the average preamble SNR was of 26.41 dB for the first set and 25.11 dB for the second one. The empirical cumulative distribution function (CDF) for the first set can be seen in figure 6.10 and second set in figure 6.11. The CDF of the SNR shows that, for this experiment, it was limited to a maximum of about 27 dB for the first set and about 26 dB for the second. The difference between the two has no relation to the VFDM technique itself, but rather to the RF hardware and radio propagation. The majority of the SNRs situate above 24 dB, with a few samples below related to the bad synchronization cases. It is expected, that the payload SNR be substantially different from the preamble SNR. Finally, an average phase shift of  $\hat{\phi} \simeq -0.72^\circ$  for set 1 and  $\hat{\phi} \simeq -0.41^\circ$  for set 2, was estimated throughout each of the respective 1000 transmissions. Again, their difference is not due to VFDM.

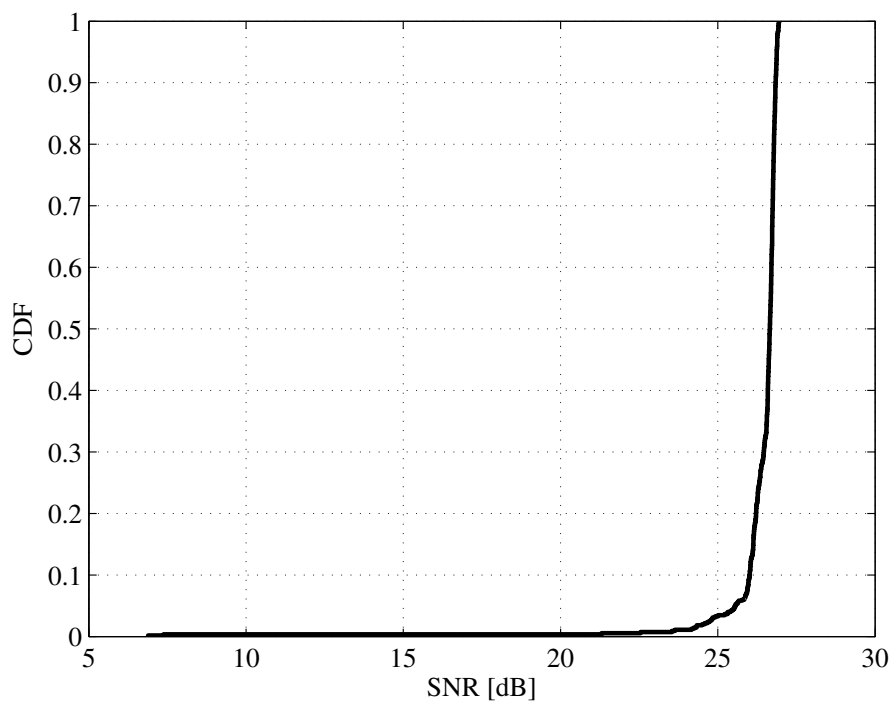


Figure 6.10: Empirical CDF of the preamble SNR ( $N = 128$  and  $L = 16$ ).

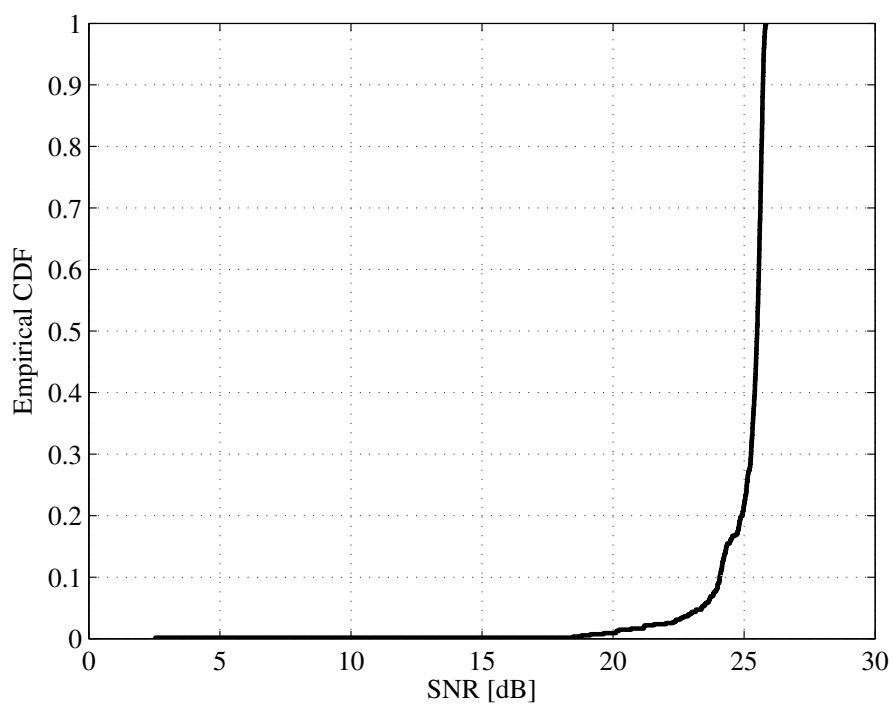


Figure 6.11: Empirical CDF of the preamble SNR ( $N = 64$  and  $L = 8$ ).

### 6.5.1 Decoding

The decoding of the frames do work correctly, as seen by a representative example of decoded image in figure 6.12. At a preamble SNR of around 25 dB, some errors can still be seen when comparing the originally transmitted picture (figure 6.12(a)) with the received one (figure 6.12(b)). This is likely due to the reduction in the payload SNR due to the normalization procedure and the PAPR problem cited before.

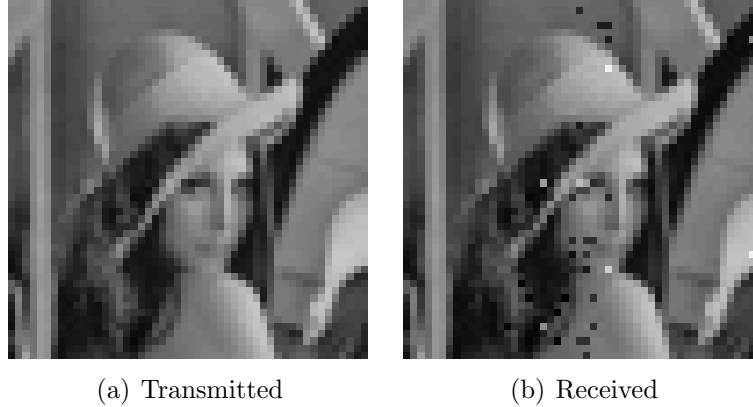


Figure 6.12: Outcome of the selected transmission.

Since the SNR of the payload was not directly captured, the bit error rate (BER) can be used as an indirect indication of its behavior. In figures 6.13 (set 1) and 6.14 (set 2), the CDFs of the BERs experimented throughout all the transmissions are presented. Indeed, for the first run of tests the majority of the BER measurements are lower than about 0.18 (90<sup>th</sup> percentile), indicating that probably the perceived SNR of the payload is too low with respect to the preamble one. In the second run, a similar conclusion can be taken with respect to the payload SNR, but this time the 90<sup>th</sup> percentile indicates a BER of 0.12. This discrepancy is believed to be due to the PAPR and the number of dimensions used for transmission. The more dimensions there are, the higher the PAPR, meaning that normalized transmissions like ours suffer from an even smaller perceived SNR.

When comparing these results to the ones presented before in section 2.5.1, figure 2.5, where we see that, for the first run, a BER value of 0.18 the actual SNR might be even lower than 0 dB. On the other hand, looking at the 10<sup>th</sup> percentile in figure 6.13, the majority of the BER perceived were higher than 0.05, which indicates an SNR of about 12 dB, as seen in figure 2.5. The same kind of conclusion can be taken for the second run, with even better results, due to the afore mentioned PAPR issue.

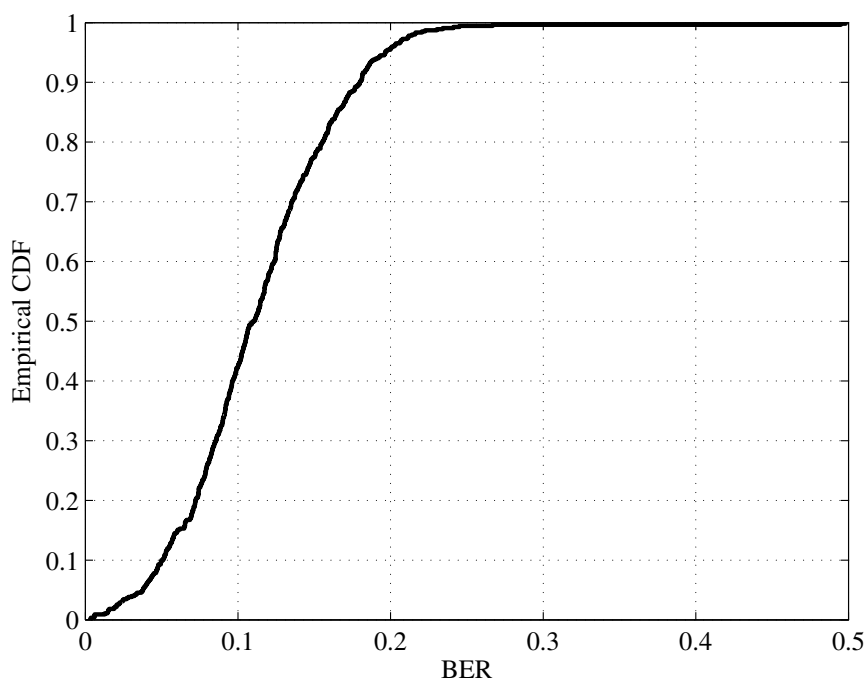


Figure 6.13: Empirical CDF of the payload BER ( $N = 128$  and  $L = 16$ ).

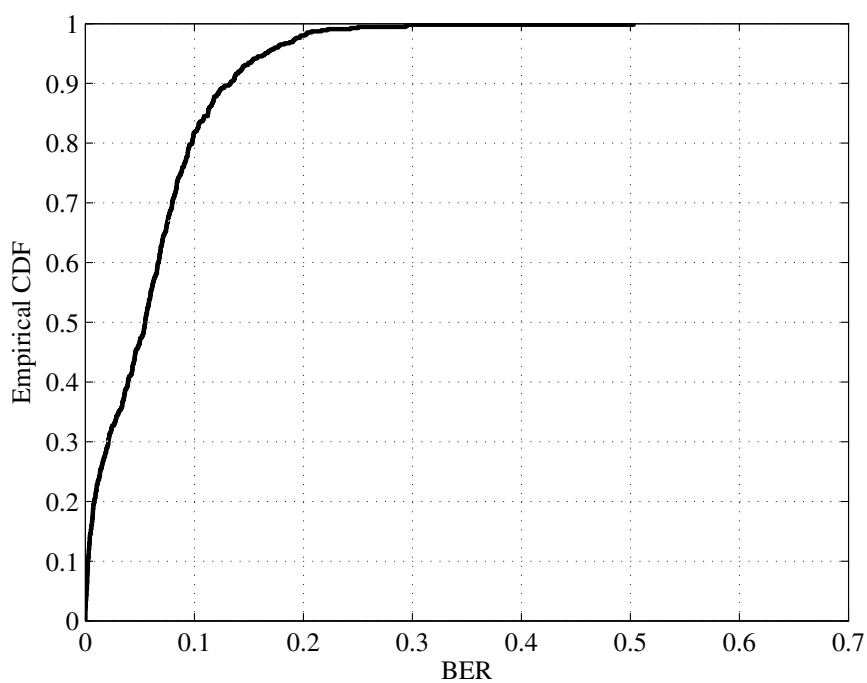


Figure 6.14: Empirical CDF of the payload BER ( $N = 64$  and  $L = 8$ ).

## 6.6 Closing Remarks

In this chapter we have shown a partial implementation of a VFDM transceiver. We have identified several issues, mainly concerning VFDM's PAPR, that need to be further investigated. Also, with a working OFDM and VFDM implementation, the full proof of concept remains to be done. For this, some critical issues need to be studied, such as how to deal with strongly line of sight (LOS) channels which reduce the number of usable dimensions and are expected to deteriorate the performance of VFDM.

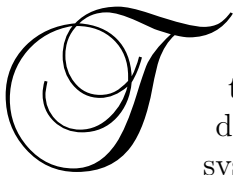
## Part III

# Conclusions, Perspectives and Appendices



# Chapter 7

## Conclusions and Perspectives



THIS PH.D. WORK aimed at introducing a novel technology able to allow two radio access technologies (RATs) to operate side-by-side in a cognitive radio (CR) setting, i.e. while sharing the same band and protecting the legacy system from interference. Named Vandermonde-subspace frequency division multiplexing, this technology exploits the frequency selectivity of channels to achieve spectrum sharing. It creates a pre-coder orthogonal to the interfering channel that achieves interference mitigation.

We have shown how such a pre-coder can be constructed and analyzed its performance considering an optimal and linear receiver structures. Once the single user scenario has been dealt with, we moved on the multi-user scenario, starting with a simple case of a orthogonal frequency division multiple access (OFDMA) cellular-like primary network along with a Vandermonde-subspace frequency division multiplexing (VFDM) single user opportunistic system. We then, moved onto the full multi-user setting, where we made use of techniques from the network MIMO domain to allow the expansion to a multi-user opportunistic small-cell scenario. We have shown that VFDM, under certain constraints can allow a secondary opportunistic network to be installed along with a legacy primary. We have used numerical examples help to show that, even though VFDM's performance is constrained by the size of the Vandermonde-subspace of the interfering channel between the secondary transmitter and primary receiver, non-negligible rates can be achieved.

We then, changed our focus to providing a proof-of-concept implementation of VFDM. We started by identifying and providing possible solution to some of the common practical issues, such as for example, channel estimation. We identified operating parameters for VFDM, necessary for the subsequent proposal of VFDM transceiver. Finally, such a transceiver was implemented and tested on a platform.

## 7.1 Conclusions

The conclusions are divided into three parts which span the main macro divisions of this work, spread throughout chapters 2, 3, 4, 5 and 6.

### 7.1.1 Single-user VFDM

In this part we have concentrated on introducing VFDM as a technique for dynamic spectrum access (DSA) in cognitive radio networks. We have shown that VFDM can effectively share a band with a primary system on a cognitive interference channel. It behaves as an opportunistic radio system that makes use of the available free dimensions to transmit its own data at the cost of channel knowledge and extra processing power.

We showed that there exists a set of pre-coders which lie in the nullspace of the secondary-to-primary interfering channel, which are able to achieve our interference cancellation goals. Due to the particular structure of the frequency selective channel model adopted based on the Toeplitz matrix this nullspace can be easily found by constructing a specially built Vandermonde matrix based on the roots of a polynomial created from the interfering channel coefficients. We named this the Vandermonde-subspace.

We have shown that, since VFDM is dependent and limited to the available dimensions, restricting its performance. In fact the maximum spectral efficiency of VFDM will always be bounded by the ratio of  $L/N$ , in our numerical cases, usually 1/4 of the spectral efficiency of the primary system. Furthermore, we have seen that VFDM is still susceptible to interference coming from the primary transmitter, which further limits its performance.

Then we moved on to providing VFDM versions of the classical linear equalizers. We showed that the best receiver, the minimum mean square error (MMSE) lags behind by about 2 dB with respect to the optimal receiver, followed by the zero forcing (ZF) with a gap of about 4 dB and the matched filter (MF) which could not keep up with the others, saturating at 16 dB of signal to noise ratio (SNR).

Finally, we compared VFDM to a classical approach based on spectrum sensing, in which a secondary system can transmit at the same time and on the sensed unused carriers of the primary system. We saw that, if the spectrum sensing approach uses a similar proportion of carriers as VFDM (3/4 for the primary system against 1/4 for the secondary one), then VFDM can achieve even better results, improving the overall sum spectral efficiency by about 20% if no interference at the secondary system is present and by about 10% in the case of full interference  $\alpha = 1$  at the secondary system.

### 7.1.2 Multi-user VFDM

In this part, we have extended the work presented for the single user case, showing that the main concepts behind VFDM can be successfully be extended to a secondary user dealing with a primary long term evolution (LTE)/OFDMA multi-user system. We have derived

a solution using a weighted water-filling algorithm that allows a secondary cognitive-like system using VFDM to achieve a non-negligible rates, at the sole cost of perfect channel state information (CSI). As with the single user VFDM, this initial multi-user case is highly dependent on the available dimensions used.

Iterating on this initial multi-user VFDM scheme, we presented a full DSA technique, called multi-user Vandermonde-subspace frequency division multiplexing (MU-VFDM), that allows the use of multiple small-cells to operate along a primary system while generating no interference. By increasing the number of small-cells deployed inside the secondary system, and therefore the dimensionality of the problem, we have shown to enhance the overall sum rate. Network multiple input, multiple output (MIMO) effectively transformed a potentially interference limited system into a MIMO-broadcast channel (BC). Thanks to this fact, several linear precoding techniques involving cooperation between transmitters have been taken into account, underlining the inherent dimensionality constraint present in the structure of the pre-coder  $\mathbf{E}$ . The search for a performing scheme, brought us to the proposed flexible regularized inverse beamforming (RIBF) based approach presented in section 4.2.2. We have seen that, by increasing the number of transmitting dimensions while keeping the receiver layout, a viable to overcome the dimensionality problem can be found enhancing the performance of the small-cells. Such a system design, can be done by either adding extra antennas to the small-cells or by a denser small-cells deployment or even a flexible combination of both. MU-VFDM can, therefore, be considered a candidate technique for coexistence of future primary and secondary systems inside the same coverage area.

### 7.1.3 Practical Aspects and Implementation

In this part we aimed at ultimately producing a prototype of a VFDM transceiver. This prototype is to be the first step of a future full VFDM proof-of-concept, including a primary system.

We started off by identifying and discussing some of the main issues concerning a practical implementation of VFDM. We identified potential issues concerning channel estimation, synchronization and some system-level issues.

On channel estimation, we started by proposing a protocol that makes use of prior knowledge of the primary system to estimate all the required channels. We tested the protocol, providing the best ratio of pilots to data for a configuration inspired on the 802.11a system. We saw that, unlike the primary system, whose best pilots to data ratio was not constant for different SNRs, VFDM's one remains constant at about 0.04. Furthermore, we saw that VFDM performs best when a small amount of training is used. Its performance is thus highly dependent on the pre-log factor. Finally we briefly looked into the imperfect CSI case for the multi-user scenario. Imperfect CSI at the secondary transmitters, as expected, incur in a reduction in performance due to loss of orthogonality in the pre-coder structure. The best compromise between training and data symbols has been shown, for some SNR values.

On synchronization, we showed the amount of interference affecting the primary system due to an incorrect synchronization. We also discussed some ways in which the full synchronization (secondary transmitter to primary receiver and secondary receiver to secondary transmitter) procedure could be done.

On system level issues, we discussed some of the problems an operator would face when trying to install VFDM in a real network setting. A cell border problem was identified, and some solutions were proposed. Then we discussed about the influence of mobility on the ability of VFDM to stay within the coherence time, depending on the time it wastes on processing and briefly touched the subject of MU-VFDM small-cell subset selection, proposing criteria for the selection of the small-cells that will be part of the service pool.

## 7.2 Perspectives

The studies conducted within this work offer several possible perspectives for future work. Some of these perspectives follow:

- **Uplink.** The work herein focused on the downlink operation, but the uplink is necessary for duplex communications. The performance of the VFDM uplink needs to be characterized as well as the identification of suitable techniques to make it viable;
- **PAPR.** We saw that VFDM is plagued with a high peak to average power ratio (PAPR) problem. A better characterization of VFDM's PAPR will allow better appreciation of its impact on performance and the eventual proposal of solutions to deal with it;
- **Full VFDM implementation.** Now that the VFDM transceiver has been proven to work in a transmission platform, the next logical step is to include the primary system. Initially, a primary receiver must be included and we need to show that a negligible interference is perceived. This requires realtime operation to be able to feedback the channel estimations as fast as possible. Unfortunately, the current version of the SDR4all is not up to this task. In a second moment, the primary transmitter should be included and the whole setup must be shown to work. A new implementation of the full VFDM demonstrator has been started in GNU Radio, but it is still in the early stages;
- **VFDM-only CR scenario.** What would be the performance of a full small-cells environment based on VFDM? The future is pointing to a relaxation of the cellular paradigm, tending to a more chaotic environment in which small-cells cooperate to better serve the users. It would be interesting to take this step forward and see how VFDM performs as an enabling technology.
- **Level of cooperation.** It is known that we can not dispose of infinite capacity back hauls, as assumed in this work. It is important to determine what is the impact

of limited back hauls to the pre-coder construction and what is the least necessary level of interconnection to achieve a target performance;

- **Synchronization.** Although we touched lightly on the subject, synchronization remains an open issue and should be dealt with in a continuation of this work, to find practical algorithms that allow a over-the-air synchronization of the secondary system as a whole;
- **System level VFDM.** Propose a system level deployment strategy for VFDM, aggregating all the issues above into a full network version of VFDM. It will be necessary to also deal with issues such as inter-cell interference management, uplink, clustering of small-cells and mobility;
- **Multi-user.** A deeper investigation of MU-VFDM is required, through an analytical optimization of the achievable capacity. This will provide a better understanding of the technique and steer the research efforts into the future.



# Bibliography

- [1] J. Van Dijk, *The network society: Social aspects of new media*. Sage Publications Ltd, 2006.
- [2] L. Hoover. (2009, april) How social networking has changed society. [Online]. Available: [http://www.pcworld.com/article/162719/how\\_social\\_networking\\_has\\_changed\\_society.html](http://www.pcworld.com/article/162719/how_social_networking_has_changed_society.html)
- [3] E. Wheeldon. (2010, 04) A social society: The positive effects of communicating through social networking sites. [Online]. Available: <http://networkconference.netstudies.org/2010/04/a-social-society-the-positive-effects-of-communicating-through-social-networking-sites/>
- [4] M. Bunz. (2009, September) How social networking is changing journalism. [Online]. Available: <http://www.guardian.co.uk/media/pda/2009/sep/18/oxford-social-media-convention-2009-journalism-blogs>
- [5] S. Tarrow, *Power in movement: Social movements and contentious politics*. Cambridge Univ Pr, 2011.
- [6] Spectrum Efficiency Working Group - FCC, "Report of the spectrum efficiency working group," FCC, Tech. Rep., November 2002.
- [7] J. Peha, "Approaches to spectrum sharing," *Communications Magazine, IEEE*, vol. 43, no. 2, pp. 10–12, 2005.
- [8] FCC, "In the matter of unlicensed operation in the tv broadcast bands docket 04-186 incremental reform towards a broadcast underlay, and the radio traffic signal," FCC, Tech. Rep., November 2008.
- [9] IEEE, "Ansi/ieee standard 802.11," ANSI/IEEE, Tech. Rep., 1999.
- [10] J. Mitola and G. Maguire, "Cognitive radio: making software radios more personal," *Personal Communications, IEEE*, vol. 6, no. 4, pp. 13 –18, aug 1999.
- [11] S. Haykin, "Cognitive radio: brain-empowered wireless communications," *Selected Areas in Communications, IEEE Journal on*, vol. 23, no. 2, pp. 201–220, 2005.

- [12] E. Buracchini, “The software radio concept,” *Communications Magazine, IEEE*, vol. 38, no. 9, pp. 138–143, sep 2000.
- [13] H. Holma and A. Toskala, *WCDMA for umts: hspa evolution and lte*. wiley, 2010.
- [14] J. Mitola, “The software radio architecture,” *Communications Magazine, IEEE*, vol. 33, no. 5, pp. 26–38, may 1995.
- [15] R. Lackey and D. Upmal, “Speakeasy: the military software radio,” *Communications Magazine, IEEE*, vol. 33, no. 5, pp. 56–61, may 1995.
- [16] L. Cardoso, M. Debbah, S. Lasaulce, M. Kobayashi, and J. Palicot, *Cognitive Radio Networks: Architectures, Protocols and Standards*. Taylor&Francis Group, 2008, ch. Spectrum Sensing in Cognitive Radio Networks, unpublished.
- [17] P. Judge. (2011, June) Bt, bbc and microsoft in cambridge white space trial. [Online]. Available: <http://www.eweekurope.co.uk/news/bt-bbc-and-microsoft-back-cambridge-white-space-trial-32678>
- [18] J. Cox. (2011, April) First white spaces access point gives grandma the internet. [Online]. Available: <http://www.networkworld.com/news/2011/041911-whitespaces-superwifi-rice.html>
- [19] R. Tandra and A. Sahai, “Fundamental limits on detection in low SNR under noise uncertainty,” in *Wireless Networks, Communications and Mobile Computing, 2005 International Conference on*, vol. 1, 2005.
- [20] I. Akyildiz, W. Lee, M. Vuran, and S. Mohanty, “NeXt generation/dynamic spectrum access/cognitive radio wireless networks: a survey,” *Computer Networks*, vol. 50, no. 13, pp. 2127–2159, 2006.
- [21] C. Sun, W. Zhang, and K. Letaief, “Cluster-based cooperative spectrum sensing in cognitive radio systems,” in *In Communications, 2007. IEEE International Conference on Communications. ICC’07.*, 2007, pp. 2511–2515.
- [22] G. Ganesan and Y. Li, “Cooperative spectrum sensing in cognitive radio networks,” in *New Frontiers in Dynamic Spectrum Access Networks, 2005. DySPAN 2005. 2005 First IEEE International Symposium on*, 2005, pp. 137–143.
- [23] L. Cardoso, M. Kobayashi, Ø. Ryan, and M. Debbah, “Vandermonde frequency division multiplexing for cognitive radio,” in *Proceedings of the 9th IEEE Workshop on Signal Processing Advances in Wireless Communications (SPAWC’08)*, 2008, pp. 421–425.
- [24] A. Ghasemi and E. Sousa, “Fundamental limits of spectrum-sharing in fading environments,” *Wireless Communications, IEEE Transactions on*, vol. 6, no. 2, pp. 649–658, 2007.

- [25] D. Čabrič, A. Tkachenko, and R. Brodersen, "Spectrum sensing measurements of pilot, energy, and collaborative detection," in *Military Communications Conference, 2006. MILCOM 2006*, 2006, pp. 1–7.
- [26] X. Huang, N. Han, G. Zheng, S. Sohn, and J. Kim, "Weighted-Collaborative spectrum sensing in cognitive radio," in *Second International Conference on Communications and Networking in China, (CHINACOM, 2007)*, pp. 110–114.
- [27] Q. Zhao and B. Sadler, "A survey of dynamic spectrum access," *Signal Processing Magazine, IEEE*, vol. 24, no. 3, pp. 79–89, 2007.
- [28] A. Goldsmith, S. Jafar, I. Maric, and S. Srinivasa, "Breaking spectrum gridlock with cognitive radios: An information theoretic perspective," *Proceedings of the IEEE*, vol. 97, no. 5, pp. 894–914, 2009.
- [29] L. Dong, "Efficient power allocation for multiuser cognitive radio networks," *Wireless Personal Communications*, pp. 1–9, 2010, 10.1007/s11277-010-9926-6. [Online]. Available: <http://dx.doi.org/10.1007/s11277-010-9926-6>
- [30] P. Cheng, Z. Zhang, H. Huang, and P. Qiu, "A distributed algorithm for optimal resource allocation in cognitive ofdma systems," in *ICC 2008*, 2008.
- [31] Y. Ma, D. Kim, and Z. Wu, "Optimization of ofdma-based cellular cognitive radio networks," *IEEE Transactions on Communications*, vol. 58(8), pp. 2265–2276, 2010.
- [32] R. Menon, R. Buehrer, and J. Reed, "Outage probability based comparison of underlay and overlay spectrum sharing techniques," in *First IEEE International Symposium on New Frontiers in Dynamic Spectrum Access Networks*,, 2005.
- [33] N. Devroye, P. Mitran, and V. Tarokh, "Achievable rates in cognitive radio channels," *IEEE Transactions on Information Theory*, vol. 52, no. 5, pp. 1813–1827, 2006.
- [34] S. Perlaza, N. Fawaz, S. Lasaulce, and M. Debbah, "From Spectrum Pooling to Space Pooling: Opportunistic Interference Alignment in MIMO Cognitive Networks," *Arxiv preprint arXiv:0907.1255*, 2009.
- [35] W. Zhang and U. Mitra, "Spectrum shaping: A new perspective on cognitive radio (part i): Coexistence with coded legacy transmission," *IEEE Transactions on Communications*, vol. 58(6), pp. 1857–1867, 2010.
- [36] —, "Spectrum shaping: A new perspective on cognitive radio (part ii): Coexistence with uncoded legacy transmission," *IEEE Transactions on Communications*, vol. 58(10), pp. 2971–2983, 2010.
- [37] J. Hoydis, M. Kobayashi, and M. Debbah, "Green small-cell networks," *Vehicular Technology Magazine, IEEE*, vol. 6, no. 1, pp. 37–43, march 2011.
- [38] V. Chandrasekhar, J. Andrews, and A. Gatherer, "Femtocell networks: a survey," *Communications Magazine, IEEE*, vol. 46, no. 9, pp. 59–67, september 2008.

- [39] S. Kishore, L. Greenstein, S. Schwartz, and H. Poor, "Uplink user capacity of a multi-cell cdma system with hotspot microcells," in *Vehicular Technology Conference, 2002. VTC Spring 2002. IEEE 55th*, vol. 2, 2002, pp. 992 – 996 vol.2.
- [40] A. Doufexi, E. Tameh, A. Nix, S. Armour, and A. Molina, "Hotspot wireless lans to enhance the performance of 3g and beyond cellular networks," *Communications Magazine, IEEE*, vol. 41, no. 7, pp. 58 – 65, july 2003.
- [41] F. Cavalcanti and S. Andersson, *Optimizing wireless communication systems*. Springer Verlag, 2009.
- [42] L. Cardoso, F. Cavalcanti, M. Kobayashi, and M. Debbah, "Vandermonde-subspace frequency division multiplexing receiver analysis," in *PIMRC 2010*, September 2010.
- [43] L. Cardoso, M. Kobayashi, F. Cavalcanti, and M. Debbah, "Vandermonde-subspace frequency division multiplexing a feasible alternative for spectrum sharing," *Under preparation*, 2011.
- [44] L. Cardoso, M. Maso, M. ans Kobayashi, and M. Debbah, "Orthogonal lte two-tier cellular networks," in *To appear in proceedings of ICC 2011*, 2011.
- [45] M. Maso, L. S. Cardoso, M. Debbah, and L. Vangelista, "Orthogonal precoder for two-tiered networks," *IEEE Transactions on Wireless Communications (submitted)*, 2011.
- [46] L. S. Cardoso, R. de Larcera, P. Jallon, and M. Debbah, "Sdr4all a tool for making flexible radio a reality," in *Proceedings of COGnitive System with Interactive Sensors*, 2009.
- [47] H. Weingarten, Y. Steinberg, and S. Shamai, "The capacity region of the gaussian multiple-input multiple-output broadcast channel," *Information Theory, IEEE Transactions on*, vol. 52, no. 9, pp. 3936 –3964, September 2006.
- [48] G. Caire and S. Shamai, "On the achievable throughput of a multi-antenna gaussian broadcast channel," *IEEE Transactions on Information Theory*, vol. 49, pp. 1691–1706, 2003.
- [49] W. Rhee and J. Cioffi, "Increase in capacity of multiuser ofdm system using dynamic subchannel allocation," in *Vehicular Technology Conference Proceedings, 2000. VTC 2000-Spring Tokyo. 2000 IEEE 51st*, vol. 2, 2000, pp. 1085 –1089 vol.2.
- [50] H. Huh, H. Papadopoulos, and G. Caire, "Mimo broadcast channel optimization under general linear constraints," in *Information Theory, 2009. ISIT 2009. IEEE International Symposium on*, July 2009, pp. 2664 –2668.
- [51] A. Wiesel, Y. Eldar, and S. Shamai, "Zero-forcing precoding and generalized inverses," *Signal Processing, IEEE Transactions on*, vol. 56, no. 9, pp. 4409 –4418, Sep. 2008.

- [52] G. Golub and C. Van Loan, *Matrix Computations*. Johns Hopkins University Press, 1996.
- [53] C. Meyer, *Matrix analysis and applied linear algebra*. Society for Industrial Mathematics, 2000.
- [54] M. Kobayashi, M. Debbah, and S. Shamai, “Secured communication over frequency-selective fading channels: A practical vandermonde precoding,” *EURASIP Journal on Wireless Communications and Networking*, vol. 2009, p. 2, 2009.
- [55] D. Tse and P. Viswanath, *Fundamentals of wireless communication*. Cambridge University Press, 2005.
- [56] L. Rabiner and B. Gold, *Theory and application of digital signal processing*. Prentice-Hall, 1975.
- [57] S. Verdú, *Multiuser detection*. Cambridge University Press, 1998.
- [58] S. Haykin, *Digital communications*. Wiley, 1988.
- [59] S.-Y. Tu, K.-C. Chen, and R. Prasad, “Spectrum sensing of ofdma systems for cognitive radio networks,” *Vehicular Technology, IEEE Transactions on*, vol. 58, no. 7, pp. 3410–3425, September 2009.
- [60] TSG-RAN1, “3gpp tr 25.814, physical layer aspects for evolved utra, v.2.0.0,” 3GPP, Tech. Rep., 2006.
- [61] J. Wang, F. Adachi, and X. Xia, “Coordinated and distributed mimo,” *IEEE Wireless Communications*, vol. 17, pp. 24–25, 2010.
- [62] F. J. Ayres, *Theory and Problems of Matrices*. Mcgraw-Hill, 1967.
- [63] A. Goldsmith, *Wireless communications*. Cambridge University Press, 2005.
- [64] Q. Spencer, A. Swindlehurst, and M. Haardt, “Zero-forcing methods for downlink spatial multiplexing in multiuser MIMO channels,” *IEEE Transactions on Signal Processing*, vol. 52(2), pp. 461–471, 2004.
- [65] C. Peel, B. Hochwald, and A. Swindlehurst, “A vector-perturbation technique for near-capacity multiantenna multiuser communication (part i): channel inversion and regularization,” *IEEE Transactions on Communications*, vol. 53(1), pp. 195–202, 2005.
- [66] P. Viswanath, D. Tse, and R. Laroia, “Opportunistic beamforming using dumb antennas,” *IEEE Transactions on Information Theory*, vol. 48(6), pp. 1277–1294, 2002.
- [67] M. Sharif and B. Hassibi, “On the capacity of mimo broadcast channel with partial side information,” *IEEE Transactions on Information Theory*, vol. 51(2), pp. 506–522, 2005.

- [68] V. Stankovic and M. Haardt, "Multi-user mimo downlink precoding for users with multiple antennas," in *Proc. 12-th Meeting of the Wireless World Research Forum (WWRWF)*, 2004.
- [69] —, "Generalized design of multi-user mimo precoding matrices," *IEEE Transactions on Wireless Communications*, vol. 7(3), pp. 953–961, 2008.
- [70] G. Dimic and N. Sidiropoulos, "On downlink beamforming with greedy user selection: Performance analysis and simple new algorithm," *IEEE Transactions on Signal Processing*, vol. 53(10), pp. 3857–3868, 2005.
- [71] T. Yoo and A. Goldsmith, "On the optimality of multiantenna broadcast scheduling using zero-forcing beamforming," *IEEE Journal on Selected Areas in Communications*, vol. 24(3), pp. 528–541, 2006.
- [72] S. Shim, J. Kwak, R. Heath Jr., and J. Andrews, "Block diagonalization for multi-user MIMO with other-cell interference," *IEEE Transactions on Wireless Communications*, vol. 7(7), pp. 2671–2681, 2008.
- [73] F. Boccardi, F. Tosato, and G. Caire, "Precoding schemes for the mimo-gbc," in *International Zurich Seminar on Communication*, 2006.
- [74] M. Andrews, V. Capdevielle, A. Feki, and P. Gupta, "Autonomous spectrum sharing for mixed LTE femto and macro cells deployments," in *2010 INFOCOM IEEE Conference on Computer Communications Workshops*, 2010.
- [75] M. Biguesh and A. Gershman, "Training-based mimo channel estimation: a study of estimator tradeoffs and optimal training signals," *Signal Processing, IEEE Transactions on*, vol. 54, no. 3, pp. 884 – 893, march 2006.
- [76] Y. Li, "Optimum training sequences for ofdm systems with multiple transmit antennas," in *Global Telecommunications Conference, 2000. GLOBECOM '00. IEEE*, vol. 3, 2000, pp. 1478 –1482 vol.3.
- [77] B. Hassibi and B. Hochwald, "How much training is needed in multiple-antenna wireless links?" *IEEE Transactions on Information Theory*, vol. 49(4), pp. 951–963, 2003.
- [78] J. Hoydis, M. Kobayashi, and M. Debbah, "Optimal channel training in uplink network MIMO systems," *IEEE Transactions on Signal Processing*, vol. 59(6), pp. 2824–2833, 2011.
- [79] B. Sklar, "Rayleigh fading channels in mobile digital communication systems. i. characterization," *Communications Magazine, IEEE*, vol. 35, no. 7, pp. 90–100, 1997.
- [80] ETTUS. (2011, october) Ettus research llc. [Online]. Available: <http://www.ettus.com/>

- [81] E. Blossom, “Gnu radio: tools for exploring the radio frequency spectrum,” *Linux J.*, vol. 2004, pp. 4–, June 2004. [Online]. Available: <http://dl.acm.org/citation.cfm?id=993247.993251>
- [82] M. Golay, “Complementary series,” *IRE Transactions on Information Theory*, vol. IT-7, pp. 82–87, 1961.
- [83] *TS 101475 v1.2.2, Broadband Radio Access Networks (BRAN); HIPERLAN Type 2; Physical (PHY) layer*, ETSI Std.



# Appendix A

## OFDM Implementation

An orthogonal frequency division multiplexing (OFDM) transceiver chain scheme is currently available in the SDR4all (SDR4all) toolbox. It was constructed as a starting point for the implementation of the VFDM chain. The OFDM transceiver chain is able to transmit variable size frames, comprised of two parts as seen in figure A.1: *preamble* and *payload*. Two modes are available: data bearing and channel sounder. These modes will be detailed in the sequence. The preamble of size  $n_{pre}$  symbols is transmitted as binary phase shift keying (BPSK) ones (1,0) in time. It is used to assure correct detection of the frame and detect phase offset variations due to imperfections in the phase-locked loop (PLL) responsible for generating the carrier frequency at the chosen central frequency  $f_c$ .



Figure A.1: General OFDM transmission chain frame configuration.

Frame detection is achieved by means of a windowed energy detection of the form

$$E(t) = \sum_{i=1}^{\mathcal{M}} |S(t+i)|^2$$

for every  $t \in \{1, \dots, \mathcal{N}\}$ , where  $S(j)$  is the complex baseband received sample at instant  $j \in \{1, \dots, \mathcal{N}\}$ ,  $\mathcal{M}$  is the window energy detector window size (in our case is also the frame size) and  $\mathcal{N}$  is the total number of received samples. The frame is then decided to start at index

$$k = \underset{t \in \{1, \dots, \mathcal{N}-\mathcal{M}\}}{\operatorname{argmax}} (E(t)).$$

Although, maybe not the best frame detection technique, the energy detector is simple, computationally fast and provides rather robust results for the OFDM case.

Once the frame is detected, the phase offset estimation takes part. To estimate the phase offset we make use of the fact that the preamble is composed of same-phase symbols. Phase offset is estimated by

$$\hat{\phi} = \frac{1}{n_{pre}} \sum_{m=1}^{n_{pre}-1} (\angle[S(m+1)] - \angle[S(m)]),$$

where  $\angle(\cdot)$  is the complex angle function. Note that each subsequent phase offset calculation is averaged out to compensate for phase noise. This technique was chosen due to its simplicity. After the preamble, a silence gap of the same size of the preamble is inserted in order to allow for the estimation of the noise power. The phase offset of the whole frame is later corrected by

$$S_c(m) = \frac{S(m)}{e^{i\hat{\phi}m}}$$

for every  $m \in \{0, \dots, \mathcal{M}\}$ .

Still in the structure of the frame, a silent space is inserted between the preamble and the payload. This silence space is used for noise energy estimation for signal-to-noise ratio calculations.

As stated before, two OFDM modes can be used, each of which will configure the payload part of the frame differently. In the following we provide details on both modes.

### A.0.1 Data Bearing Mode

A data bearing mode can be used to transmit useful data. The frame structure for the data bearing mode is shown in figure A.3. It is capable of carrying packets of different sizes.

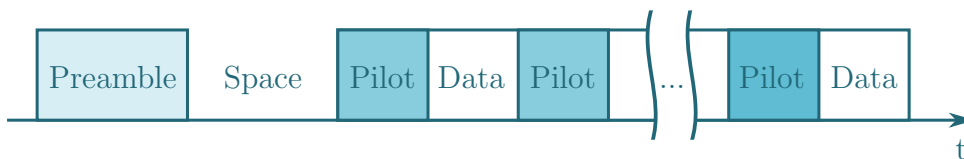


Figure A.2: OFDM frame structure for data bearing mode

The payload is composed of pilots and data sandwiched into the discrete Fourier transform (DFT)-modulated part of the frame. The number of carriers is of  $n_{FFT}$ , of which  $n_{zpad}$  carriers are reserved for zero-padding, leaving a total of  $N$  carriers for useful transmission. A total of  $n_{pilot}$  OFDM symbols are transmitted. These are a randomly-generated symbols sequence, known by both the transmitter and receiver. The pilots can be either modulated with a quadrature phase shift keying (QPSK) or be complex circularly symmetric. They are used to estimate the channel for subsequent equalization of the data symbols. The channel is estimated by

$$\hat{\mathbf{h}} = \mathbf{r}\mathbf{p}^{-1} \tag{A.1}$$

where  $\hat{x}$  is  $x$  and  $\hat{y}$  is  $y$ , averaged over all  $n_{pilot}$  pilot symbols to smooth out the noise imperfections.

Following the pilot symbols,  $n_{data}$  data symbols are bitmapped to a QPSK constellation and transmitted. The sequence: pilot-data is repeated until all the data to be transmitted is inside the payload. At reception the data is equalized by

$$\hat{\mathbf{d}} = \mathbf{y}$$

where  $\hat{x}$  is  $x$  and  $\hat{y}$  is  $y$ . Each data block is equalized by the channel estimation from its preceding pilot block. The parameters for the data bearing mode are summarized in table A.1. All parameters therein are selectable.

parameter	value
$f_c$	flexible inside the ISM band
base band rate	1 MHz
$n_{pre}$	1000 syms
$n_{FFT}$	64
$n_{zpad}$	16 (8 at each end)
$N$	48 carriers
$n_{pilots}$	30
$n_{data}$	30
pilot structure	QPSK

Table A.1: Parameters for the data bearing mode.

## A.0.2 Channel Sounder Mode

The OFDM chain also has a channel sounder mode, which is used to provide channel analysis. The frame structure for the channel sounder mode is shown in figure A.3.

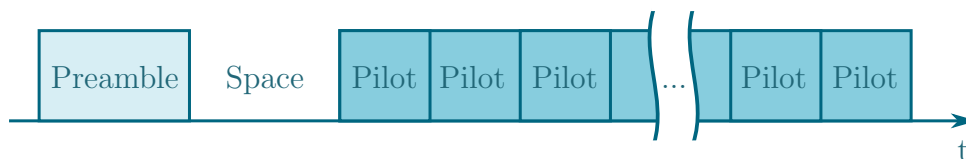


Figure A.3: OFDM frame structure for channel sounder mode

In this mode, the payload is composed of pilots only. Similar to the data bearing mode, the FFT size of the packet is of  $n_{FFT}$ , of which  $n_{zpad}$  carriers are reserved for zero-pad purposes, leaving a total of  $N$  carriers of useful symbols for channel estimation. A total of  $n_{pilot}$  OFDM symbols are transmitted in each pilot block. Again, these pilots symbols can be either modulated with a QPSK or be complex circularly symmetric, known by both the transmitter and receiver. Channel estimation is carried out as in (A.1).

The parameters for the data bearing mode are summarized in table A.2. Again, all parameters therein are selectable.

parameter	value
$f_c$	flexible inside the ISM band
base band rate	1 MHz
$n_{pre}$	1000 syms
$n_{FFT}$	64
$n_{zpad}$	16 (8 at each end)
$N$	48 carriers
$n_{pilots}$	30
$n_{data}$	30
pilot structure	QPSK

Table A.2: Parameters for the channel sounder mode.

### A.0.3 Reception Trigger

Due to its non real-time constraint, the receiver can not de decode the transmitted stream on the fly to detect the signal. That would require much more processing power and memory than Matlab can cope with at the base-band rate. Thus, a triggering system was implemented to initiate the reception, to minimize the number of samples processed so that the detection of the packet can take place. To that end, the transmission control protocol / internet protocol (TCP/IP) network was adopted as a triggering bearer. In the absence of a wired network, the wireless network can be used. In the case of a frequency superposition, the transmission/reception takes places one full second after the trigger has been sent to guarantee that the wireless network will not interfere with the toolbox packet transmission.

## A.1 Metrics and Outputs

One of the best advantages of SDR4all relies on the fact that it processes actual base-band symbols. This allows for the creation of well tailored kinds of results and metrics, useful for either demonstrating the inner workings of the physical layer or for assessing the performance of an algorithm. In particular, this flexibility can be very useful for teaching and research scenarios. Nevertheless, with access to the transmission/reception chain code, the user can also implement new metrics that suits his needs.